Polymères neutres solubles dans l'eau : Origine et signatures de la dépendance en concentration du paramètre de Flory chi

Vladimir Baulin

Thèse

présentée pour obtenir le titre de

Docteur de l'Université Joseph Fourier – Grenoble I

Spécialité: Physique

(arrêté du 30 mars 1992)

par

Vladimir A. BAULIN

sur le sujet

Polymères neutres solubles dans l'eau : Origine et signatures de la dépendance en concentration du paramètre d'interaction de Flory χ

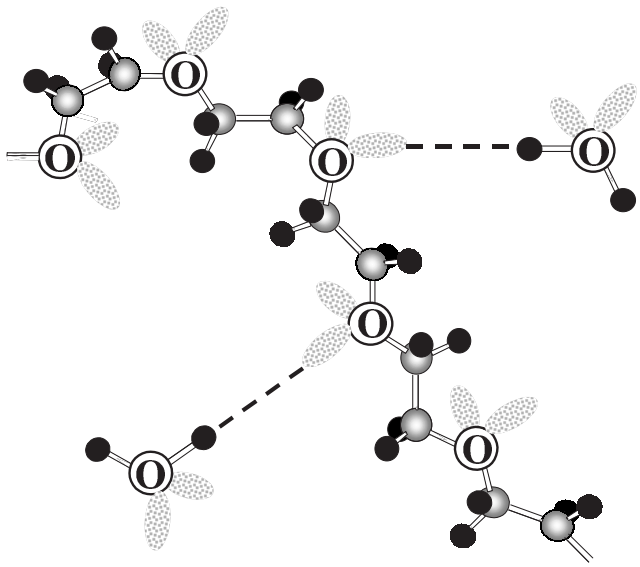

soutenue publiquement le 6 octobre 2003 devant le Jury composé de

M. Marcel VALLADE	Président du Jury
M. Mohamed DAOUD	Rapporteur
M. Albert JOHNER	Rapporteur
M. Loïc AUVRAY	Examinateur
M. Avi HALPERIN	Directeur de Thèse

Ph.D. Thesis

presented to obtain the degree of

Doctor of the University Joseph Fourier – Grenoble I

Speciality: Physics

(decision of March 30, 1992)

by

Vladimir A. BAULIN

entitled

Neutral water-soluble polymers: Origin and signatures of concentration dependent Flory interaction χ-parameter

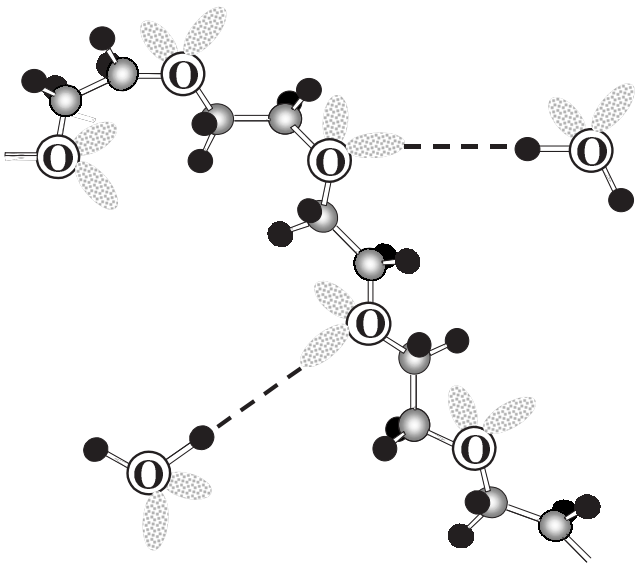

defended on October 6, 2003 in front of the Jury composed of

M. Marcel VALLADE	president of the jury
M. Mohamed DAOUD	Referee
M. Albert JOHNER	Referee
M. Loïc AUVRAY	member of the jury
M. Avi HALPERIN	Thesis promotor

Acknowledgments

First of all I wish to express my profound gratefulness to my scientific supervisor Avi Halperin for three years of his life that he devoted to me during the PhD thesis, for his knowledge and experience which he kindly shared with me all this time. I appreciated the most his pedagogical style of work and his talent to formulate problems in the simplest possible way. I am grateful to Avi for his exceptional accessibility. I could always visit him even at home with my questions and problems and get a wise advise. Weekends and holidays do not exist for that. I shall never forget these long discussions which have always led to a serious progress.

I would also like to thank Eketerina B. Zhulina for introducing me in the Self-Consistent Field theory, for useful comments and numerous advises. It was a great pleasure to work with her. Special thanks to Olaf Evers for teaching me computer methods in general and numerical SCF in particular. Sincere thanks for his hospitality during my stay in Germany.

I am grateful and indebted to Mohamed Daoud and Albert Johner who accepted to referee my thesis and for their kind reports. I also thank Loïc Auvray and Marcel Vallade for their active participation in the defence as members of the jury.

I wish to thank Jean-François Legrand for the particular atmosphere of goodwill and kindness in his laboratory. It was always a pleasure to be there. I am also grateful to Bertrand Fourcade for excellent conditions of work in the theory group.

Sincere thanks to Miguel Aubouy, Ferdinand Volino, Arnaud Buhot for numerous discussions and advises. I am very grateful to Martin Castelnovo for small corrections of my French in the French parts of the thesis.

Special thanks to Nicole Fanjas for the real help in the organizing of the "pot de thèse" and for kind attitude and support during three years.

Thanks to my officemate Manoel Manghi with whom I spent two years shoulder to shoulder in my office. Also thanks to Laurent, Gilles, Laurence, Alice for various help and support.

I cannot express all my gratefulness to my mother Galina who felt deeply even at distance all events of my life.

As a last remark, I regret that this period of my life is finished. Many plans were not realized. Not everything was included in this thesis, but I hope, it will be reflected in future works.

To my mother

Galina

with tenderness

Contents

Theory is the best guess

Richard Feynmann

Introduction

Les polymères neutres solubles dans l'eau sont employés dans les diverses applications industrielles telles que les formulations de peintures, la suppression de l'adsorption des protéines, la livraison des médicaments, etc. Bien que les structures chimiques de ses polymères soient différentes, il y a certains traits distinctifs qui sont similaires pour beaucoup d'entre eux: (i) les polymères hydrosolubles forment des liaisons hydrogènes entre monomères et molécules d'eau [1, 2, 3, 4, 5], (ii) certains d'entre eux possèdent une structure secondaire (par exemple la structure d'hélice) [6] qui implique que les monomères existent dans plus qu'un seul état [7, 8, 9, 10], (iii) les diagrammes de phase des polymères neutres solubles dans l'eau sont beaucoup plus riches que ceux de polymères solubles dans les solvants organiques : à côté des diagrammes de phase habituels de type UCST avec la séparation de phases à la diminution de température, il existe aussi des diagrammes de phase de type LCST (séparation à l'augmentation de température) ou celles en boucle [11] ou en sablier.

La plupart de ses phénomènes ne peuvent pas être décrit par la théorie standard de Flory [12, 13, 14, 15, 16] qui donne la plus simple description de polymères en solution. On pourrait envisager deux possibilités pour résoudre ce problème. Pour décrire de tels polymères de la façon la plus directe on pourrait développer un modèle moléculaire spécifique pour chacun de ses polymères, tenant compte de toutes les caractéristiques distinctives du système en question. Bien qu'un tel modèle puisse fournir une description rigoureuse d'un système particulier, ce modèle ne peut pas être appliqué à un autre système possédant des propriétés similaires. Par contre, une approche alternative impliquant une description phénoménologique

permettrait de relier les phénomènes inhérents même sans spécification exacte de leurs origines moléculaires. La force de cette méthode est la possibilité de décrire plusieurs systèmes à l'aide d'une seule approche unifiée. La faiblesse est l'absence d'interprétation microscopique.

Pour étudier les polymères neutres solubles dans l'eau nous ferons l'hypothèse que la variété de diagrammes de phase est le résultat d'un seul mécanisme, à savoir l'interconversion entre deux états différents d'un monomère (sans la spécification explicite des états). Cette idée était utilisée dans les années 30 [17] pour analyser le comportement de phase des solutés à faible masse moléculaire. Ensuite elle a inspiré une série de modèles moléculaires consacrés à l'explication de comportement de phase des polymères hydrosolubles [18, 19, 20, 21, 22, 23, 24].

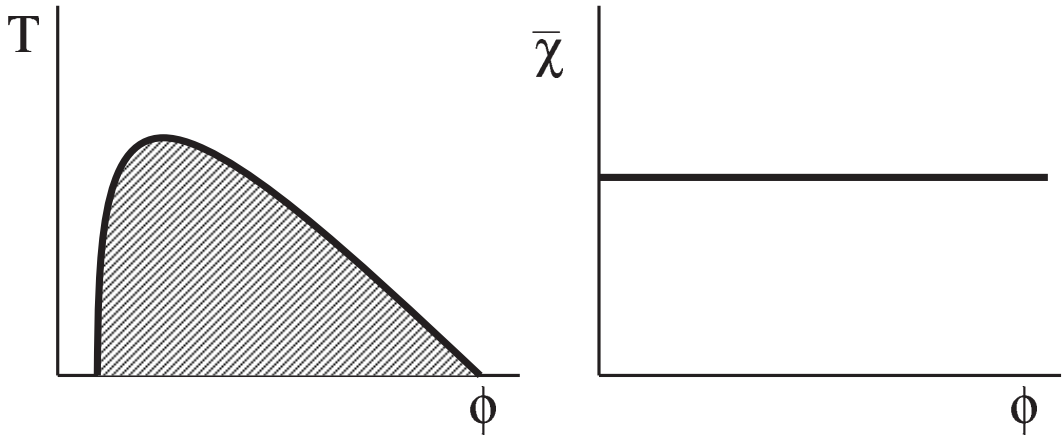

Figure 1: *Diagramme de phase typique et paramètre de Flory χ des polymères " normaux " décrits dans les manuels. La région de séparation de phase est hachurée.*

Une autre observation expérimentale concernant les polymères neutres solubles dans l'eau implique le paramètre d'interaction de Flory χ. Typiquement, il est supposé que χ ne dépend que de la température, $\chi = \chi(T)$ [12, 13, 14, 16]. Les polymères décrits par la théorie de type de Flory ont le diagramme de phase UCST, c'est-à-dire qu'ils précipitent avec la baisse de la température. (cf. Figure 1).

Lorsque les données thermodynamiques sont analysées dans les termes de l'éner-

gie libre de Flory, il est souvent nécessaire de remplacer $\chi\phi(1-\phi)$ par $\chi_{eff}\phi(1-\phi)$, c'est-à-dire χ_{eff} qui est une fonction de T et ϕ, $\chi_{eff} = \chi_{eff}(T,\phi)$ [1, 12, 25, 26, 27, 28, 29, 30]. L'introduction de $\chi_{eff}(T,\phi)$ exige la modification de la discussion de qualité du solvant. On va montrer, que la qualité " globale " du solvant pour un système de densité uniforme est caractérisée par $\overline{\chi}(\phi) = \chi_{eff} - (1-\phi)\partial\chi_{eff}/\partial\phi$ au lieu de $\chi_{eff}(\phi)$. Cependant les données expérimentales montrent que le paramètre χ pour les polymères neutres solubles dans l'eau n'est pas constant. Le paramètre $\overline{\chi}(\phi)$ qui peut aussi bien augmenter avec la concentration [25, 31] que diminuer [32]. Quant aux diagrammes de phase, il est soupçonné [33], que la diversité des diagrammes de phase observés pour les polymères hydrosolubles peut être résumée dans un seul graphe (Figure 2). Selon la position de la température d'ébullition et la température de congélation, ce graphe peut représenter la plupart des types connus de diagrammes de phase.

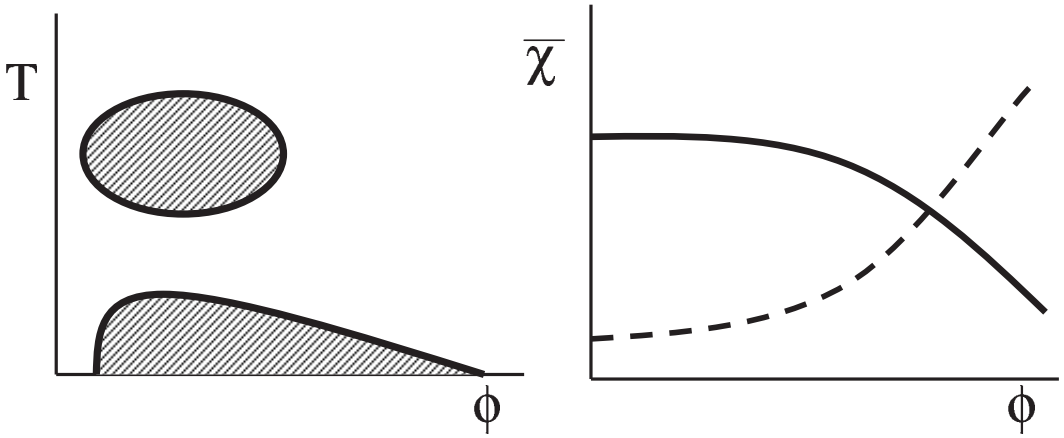

Figure 2: *Diagramme de phase et paramètre d'interaction de Flory χ pour les polymères neutres solubles dans l'eau. La région de séparation de phase est hachurée.*

Le objectif principal de ce travail est (i) la clarification de la question des origines moléculaires de la dépendance en concentration de $\chi_{eff}(T,\phi)$ et (ii) l'exploration des conséquences de $\chi_{eff}(T,\phi)$ pour les polymères dans les géométries différentes: des polymères dans la solution, des chaînes isolés et des brosses de polymère. Il sera aussi

montré que $\chi_{eff}(T, \phi)$ peut servir comme une mesure de l'exécution de différentes modèles moléculaires [34].

Nous commençons notre discussion avec la description de l'eau liquide (chapitre 1). Nous y discutons la structure particulière de molécule d'eau qui permet l'auto-association des molécules d'eau par la formation des liaisons hydrogènes. Des liaisons hydrogènes sont l'ingrédient principal à la compréhension de la structure de l'eau liquide. Ensuite, nous exposons la structure et les propriétés de trois exemples particuliers de polymères neutres solubles dans l'eau : poly(oxyéthylène), poly(N-vinylpyrrolidone) et poly(N-isopropylacrylamide). Nous montrons que la formation des liaisons hydrogènes est l'origine de leur solubilité dans l'eau.

Le comportement de phase de polymères hydrosolubles peut être décrit dans le cadre des modèles à deux états. Dans le chapitre 2 nous comparons différents modèles à deux états qui étaient conçus pour expliquer le diagramme de phase en boucle fermé de POE dans l'eau basés sur la courbure expérimentale de $\overline{\chi}(\phi)$. Cette dépendance nous permettra de distinguer entre les différents modèles et tester la pertinence des paramètres impliqués.

Dans le chapitre 3 nous discutons les modèles moléculaires à un seul état qui mènent à $\overline{\chi}(\phi)$. Ces modèles peuvent être appliqués aux polymères solubles dans l'eau de même qu'aux polymères dans les solvants non aqueux.

Le chapitre 4 est consacré à la description des signatures de la dépendance $\overline{\chi}(\phi)$ dans les systèmes à densité uniforme. Il s'agit de gonflement des pelotes isolées et des brosses de chaînes greffées.

La théorie de champ auto-cohérent de brosses planes avec $\overline{\chi}(\phi)$ est présenté dans le chapitre 5. Nous y montrerons que $\overline{\chi}(\phi)$ qui croît avec ϕ peut mener à la séparation de phase verticale dans la brosse de polymères. La séparation de phase verticale peut être provoquée aussi par la compression.

Nous illustrons dans le chapitre 6 l'application de $\overline{\chi}(\phi)$ sur l'exemple de Poly(N-isopropylacrylamide) (PNIPAM). $\overline{\chi}(\phi)$ obtenu à partir de données thermodynamiques sur la séparation de phase des chaînes linéaires de PNIPAM dans la solution nous permettra d'indiquer les conditions pour la séparation de phase verticale dans

les brosses de PNIPAM.

Le dernier chapitre résume les résultats obtenus.

Introduction

Neutral water-soluble polymers are used in many industrial applications such as formulations of paints, suppression of the protein adsorption, drug delivery, *etc.* Despite different chemical structures many of them have similar properties: (i) neutral water-soluble polymers can form hydrogen bonds with water [1, 2, 3, 4, 5], (ii) some of neutral water-soluble polymers can have a secondary structure (*e.g.* helix structure) [6] and a monomer unit can have more than one rotational state [7, 8, 9, 10], (iii) apart from an upper critical point, neutral water-soluble polymers can exhibit phase diagrams with a lower critical solution point [33, 35, 36], hourglass phase diagrams or miscibility loops [11].

Most of the listed phenomena do not follow from the standard Flory-type description of polymer solutions [12, 13, 14, 15, 16], which gives the simplest unified description of polymers in a solution. The straightforward way to describe such polymers is to develop a particular molecular model for each particular polymer – solvent system, taking into account all distinctive features of the system in question. Although such a model may furnish a rigorous description of a particular system, such a model may not be applicable to another systems, even with similar properties. An alternative approach involves a phenomenological description, which allows to relate the inherent phenomena to each other even without specifying their explicit molecular origin. The strength of this method is the possibility to describe a wide range of systems in terms of a single unified approach. The weakness is a luck of microscopic interpretation.

To describe neutral water-soluble polymers we shall use the idea that the variety

of phase diagrams observed for such polymers can be a consequence of a single mechanism, namely the interconversion between two different states of a monomer (without explicit specification of the states). This idea was first used in the 30'es [17] to describe the phase behavior of low molecular solutes. Afterwards it inspired a series of molecular models devoted to explanation of phase behavior of water-soluble polymers [18, 19, 20, 21, 22, 23, 24].

Another experimental observation concerning neutral water-soluble polymers involves the interaction Flory χ-parameter. Typically, it is assumed that χ depends only on temperature, $\chi = \chi(T)$ [12, 13, 14, 16]. Polymers described by the Flory theory has an upper critical solution temperature, i.e. they precipitate upon cooling. The χ-parameter and a typical phase diagram in the Flory theory is shown in Figure 3.

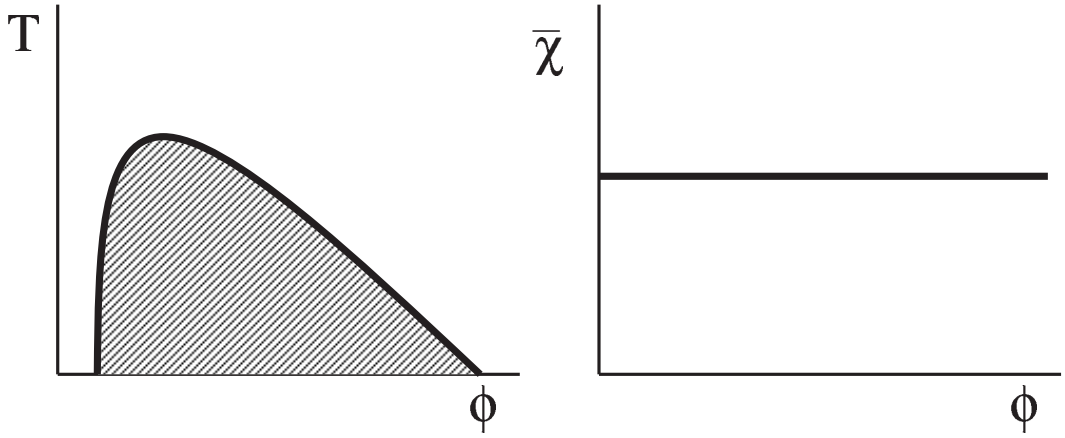

Figure 3: *Typical phase diagram and the interaction Flory χ-parameter for usual polymers described in textbooks. The phase separation region is hatched.*

However when thermodynamic data are analyzed in terms of the Flory free energy, it is often necessary to replace $\chi\phi(1-\phi)$ by $\chi_{eff}\phi(1-\phi)$ where χ_{eff} is a function of both T and ϕ *i.e.*, $\chi_{eff} = \chi_{eff}(T,\phi)$ [1, 12, 25, 26, 27, 28, 29, 30]. In turn, the introduction of $\chi_{eff}(T,\phi)$ requires modification of the discussion of solvent quality. As we shall discuss, the global solvent quality for system with uniform

density is characterized by $\overline{\chi}(\phi) = \chi_{eff} - (1-\phi)\partial\chi_{eff}/\partial\phi$ rather than by $\chi_{eff}(\phi)$.

$\overline{\chi}(\phi)$ for neutral water-soluble polymers can be both increasing [25, 31] and decreasing [32] function. It is believed [33], that diverse phase diagrams observed for neutral water-soluble polymers can be summarized in a single plot (Figure 4). Depending on the position of the temperature range of experimental measurements as well as the position of boiling and freezing temperatures, this plot can represent most of known types of phase diagrams.

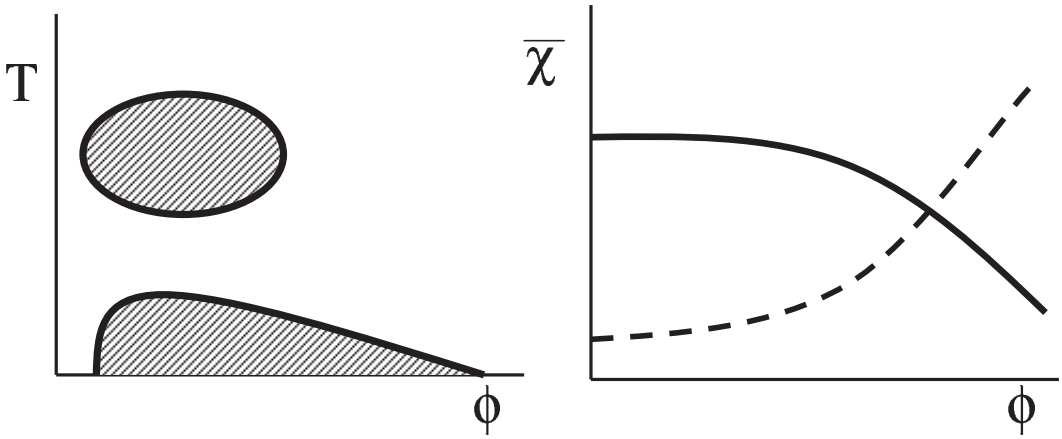

Figure 4: *Typical phase diagram and the interaction Flory χ-parameter for neutral water-soluble polymers. The phase separation region is hatched.*

The present thesis is aimed (i) to clarify the issue of possible molecular origins of the concentration dependence of $\chi_{eff}(T,\phi)$ and (ii) to explore the consequences of $\chi_{eff}(T,\phi)$ for polymers in different geometries: bulk solution of polymers, isolated coils and polymer brushes. It will also be shown that the concentration dependent $\chi_{eff}(T,\phi)$ can serve as a measure of the performance of different molecular models [34].

We start our discussion with the description of liquid water in chapter 1. The particular structure of water molecule allows for self-association of water via hydrogen bonds. In this chapter we discuss the hydrogen bonding, the key ingredient to the understanding the structure of liquid water. Then we discuss the structure and prop-

erties of three particular examples of neutral water-soluble polymers: poly(ethylene oxide), poly(N-vinylpyrrolidone) and poly(N-isopropylacrylamide). The formation of hydrogen bonds is the origin of their solubility in water.

Possible description of phase behavior of neutral water-soluble polymers can be made within the framework of two-state models. In chapter 2 we compare different two-state models designed to explain closed loop phase diagram of PEO in water on the basis of experimentally attained $\overline{\chi}(\phi)$. This dependence allows to distinguish between different models and to test involved parameters.

In chapter 3 we discuss non "two-state" molecular models leading to $\overline{\chi}(\phi)$. These models can be applied to polymers soluble in water as well as to polymers in non-aqueous solvents.

Chapter 4 is devoted to the description of signatures of the dependence $\overline{\chi}(\phi)$ in the Flory-type theory. It concerns the swelling behavior of isolated coils and of brushes of terminally anchored chains.

The self-consistent field theory of planar brushes with concentration dependent $\overline{\chi}(\phi)$ is given in chapter 5. It will be shown that the increasing $\overline{\chi}(\phi)$ can lead to the vertical phase separation in the brush. This phase separation can manifest itself in the minimum in the plot of the average thickness of the brush vs. grafting density. The vertical phase separation can also be induced by the compression.

In chapter 6 we illustrate the application of $\overline{\chi}(\phi)$ for the case of Poly(N-isopropylacrylamide) (PNIPAM). Extracting $\overline{\chi}(\phi)$ from thermodynamic data on bulk phase separation of PNIPAM linear chains we can indicate the conditions for the vertical phase separation in PNIPAM brushes.

The last chapter summarizes the obtained results.

Chapter 1

Water and Polymers Soluble in Water

1.1 Résumé

La solubilité de polymères neutres solubles dans l'eau est attribuée à la formation de liaisons hydrogènes avec l'eau. Nous discutons les propriétés de liaisons hydrogènes, l'architecture de l'eau liquide, les théories de l'eau ainsi que la structure de trois polymères particulières: Poly(oxyéthylène), Poly(N-vinylpyrrolidone) et Poly(N-isopropylacrylamide).

1.2 Introduction

Water is a substance of great importance in both the physical world and biological world. Water is a necessary ingredient of all living organisms, which usually contains over 80% of H_2O.

Water deviates strongly from simple liquids in almost every respect [37, 38]. The unusual properties, which mark it out among other liquid substances [38] are: high dielectric constant, $\varepsilon \sim 80$; anomalously high melting, boiling and critical temperatures. Water has a maximum density in the normal liquid range (4°C). The

isothermal compressibility passes through the minimum in the normal liquid range, 45^oC (the same behavior is found for the heat capacity for the constant pressure).The melting is accompanied by the decrease of volume, water shrinks by about 11% in the melting process, while the density of most liquids increases as they melt. Water has several polymorphs of crystal phase.

These unusual properties are strongly related to the particular structure of water. The key ingredient of the water structure is the formation of the three-dimensional network of hydrogen bonds. Thus, modelling of phenomena such as water solubility, solvation or the hydrophobic effect should allow for the hydrogen bonding.

This chapter is aimed to summarize the relevant information on the molecule of water, the structure of liquid water, the definition and properties of hydrogen bonds and their possible arrangement in water. Finally the structure and properties of neutral polymers soluble in water will be discussed.

1.3 Water Molecule

1.3.1 Structure of a Water Molecule

Two hydrogens atoms of water molecule are covalently bound to the oxygen atom. The covalent O–H bond length is 0.96 Å[39]. The bound angle between two hydrogens and oxygen of free H_2O molecule is about 104.7^o. Asymmetrical distribution of electrons in a water molecule has two important consequences. (i) A water molecule has a strong dipole moment, $\mu_d \approx 1.8$ Debye [40]. The dipole moment plays an important role in the formation of hydrogen bonds. (ii) The sp^3 hybridization [41] of $2s$ with two $2p$ oxygen's orbitals leads to the formation of two additional lobes in the perpendicular to the $y-z$ plane [39]. The lobes are symmetrically located above and below the $y-z$ plane away from the hydrogen atoms (see Figure 1.1). They called lone-pair hybrids. The angle between the lone-pair hybrids is 120.2^o. It is these lobes that are responsible for the formation of hydrogen bonds and the *tetrahedral coordination* of water molecules in ice and liquid water.

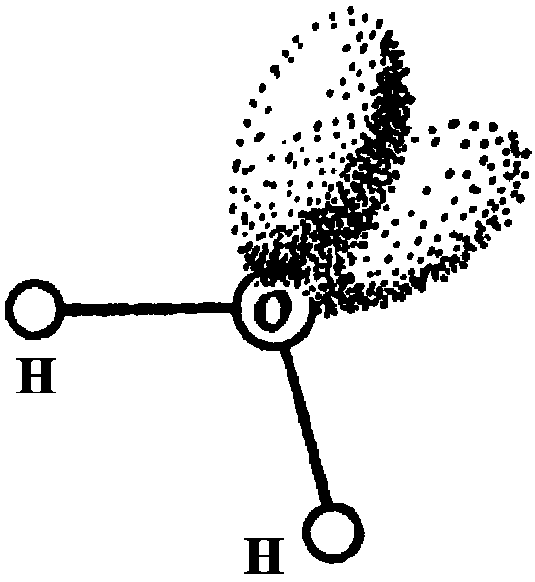

Figure 1.1: *Water molecule. Two O–H covalent bonds and two lone-pair hybrids (lobes) which arise from the sp^3 hybridization of $2s$ orbital of oxygen atom with two orbitals forming covalent bonds. The lobes are located in the plane perpendicular to the H–O–H plane (Redrawn from [40]).*

Lone-pairs allows for an oxygen atom of a water molecule to bind one or two hydrogens of another molecules. In this case, electrons of the oxygen atom can be shared between two molecules. The formation of such bond is called hydrogen bonding. The energy of the hydrogen bond (and thus, its lifetime) is lower than the energy of a covalent bond, but higher than the energy of the van der Waals interactions. Figure 1.2 represents two water molecules forming a hydrogen bond. A typical length of a hydrogen bond in water (the distance between two oxygen atoms) is around 3 Å. This length depends on the angle of hydrogen bond ϑ, the angle between O–H line of one molecule and the H–O–H plain of another molecule.

Due to its particular structure and geometry, a water molecule can act as a donor and an acceptor of hydrogen bonds at the same time. This favours the formation of a three-dimensional tetrahedral network of water molecules connected by hydro-

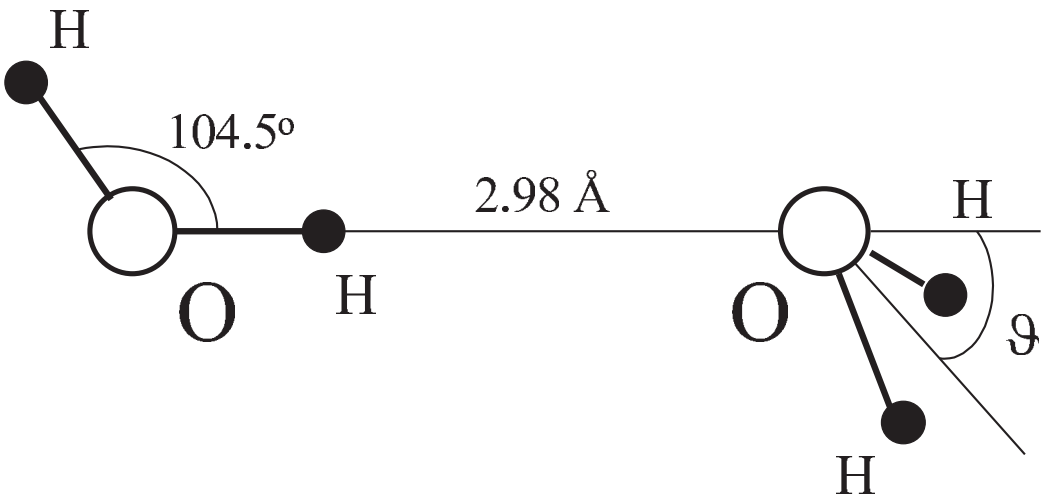

Figure 1.2: *Two water molecules forming a hydrogen bond (linear dimer). The strength of the hydrogen bond depends on the distance between two oxygen atoms and the angle ϑ. The optimal distance for the hydrogen bond is* 2.98 *Å and the optimal angle* $\vartheta = 57^o$.

gen bonds. The hydrogen bond network structure gives rise to many exceptional properties of water.

1.3.2 Energetics of a Water Molecule

The table 1.1[1] represent the energy scales of a water molecule. The energy of a molecule formation is almost two times larger than the dissociation energy of H–O bond. The energy of a covalent H–O bond is much larger than the energy of a hydrogen bond, which in turn is much larger than a typical energy of van der Waals interactions. The energy of van der Waals interactions is of the order of energy changes associated to the phase transitions: melting and evaporating at the boiling point which are relatively small.

The energies in the Table 1.1 can be presented in units of the energy of thermal

[1] All energies in the Table 1.1 should be considered with the sign minus, since they represent the energy gain due to corresponding processes.

Energy of formation at 25^o C	221.6 kcal/mol
Dissociation energy of H–O bond	101.5 kcal/mol
Energy of a hydrogen bond	2–10 kcal/mol
Energy of van der Waals interactions	0.28 kcal/mol

Table 1.1: *Molecular energies of water in kcal/mol showing different energy scales of a water molecule (on the basis of refs. [39], [42] and [38]).*

fluctuations kT at room temperatures, $T \sim 300$ K. For example, the energy of H–O covalent bond is $\sim 150\ kT$, while the energy of a hydrogen bond is of the order of $5 - 10\ kT$.

Since the energy of the hydrogen bond has an intermediate position between the energy of a covalent bond and the energy of van der Waals interactions, the hydrogen bond possesses properties both a bond and a weak interaction.

1.4 Hydrogen Bond

This section describes the hydrogen bonding, the conditions necessary for the formation of the hydrogen bond and the specific properties of hydrogen bonded substances.

1.4.1 Single Hydrogen Bond

If one hydrogen atom of a water molecule come close to one of two lone-pair hybrids of another water molecule, two water molecules can form a hydrogen bond. The hydrogen bond posses properties of a covalent bond, *i.e.* two hydrogen bonded molecules behave rather like a complex than a separate units. In this case the electron of the hydrogen atom can be "shared" between the oxygen of its own molecule and the oxygen of another molecule. This situation is schematically depicted in Figure 1.3. The hydrogen bond between hydrogen atom H and other atom A is denoted as H$\cdots$A.

Hydrogen bonds are strongly *directional* and they depend on the configuration of two molecules participating in the hydrogen bond. There are two main factors which determine the energy of a hydrogen bond between two water molecules: the distance between two oxygen atoms participating in the bond and the angle between O–H group of one molecule and H–O–H plain of another molecule.

Indirect evidence of the existence of the hydrogen bond give X-ray and neutron diffraction experiments. They provide the information concerning the relative positions of atoms and indicate that hydrogen atoms are at the bonding distance to another atom.

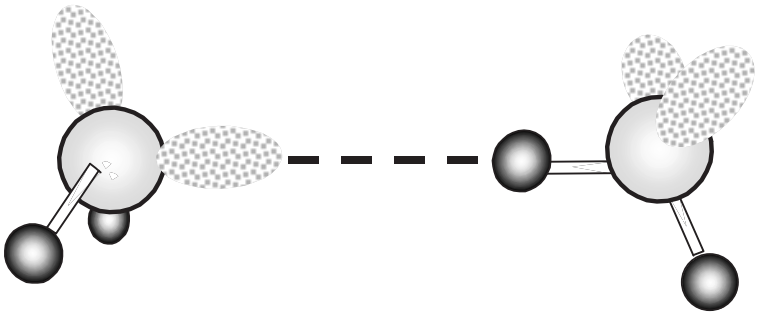

Figure 1.3: *Hydrogen bond between two water molecules. Two lobes of a water molecule designate two lone-pairs. By definition, the hydrogen atom is a donor and one of the lone-pairs is an acceptor.*

The hydrogen bond between two atoms is said to be *intra*-molecular if they belong to the same molecule and *inter*-molecular, if the two atoms belong to different molecules. The inter-molecular association is divided in *self*-association, then the complexioned molecules are of the same type and *mixed* association, then molecules are of different types. According to this notation, water is a self-associating liquid.

Self-association of two water molecules (dimer) may comprise of one hydrogen bond or two. One of possible conformations of water dimer is open or chain dimer as shown in Figure 1.3 contains one hydrogen bond. However, there is an experimental evidence that *isolated* dimers of water (for example in solid nitrogen [40]) contain two hydrogen bonds (Figure 1.4).

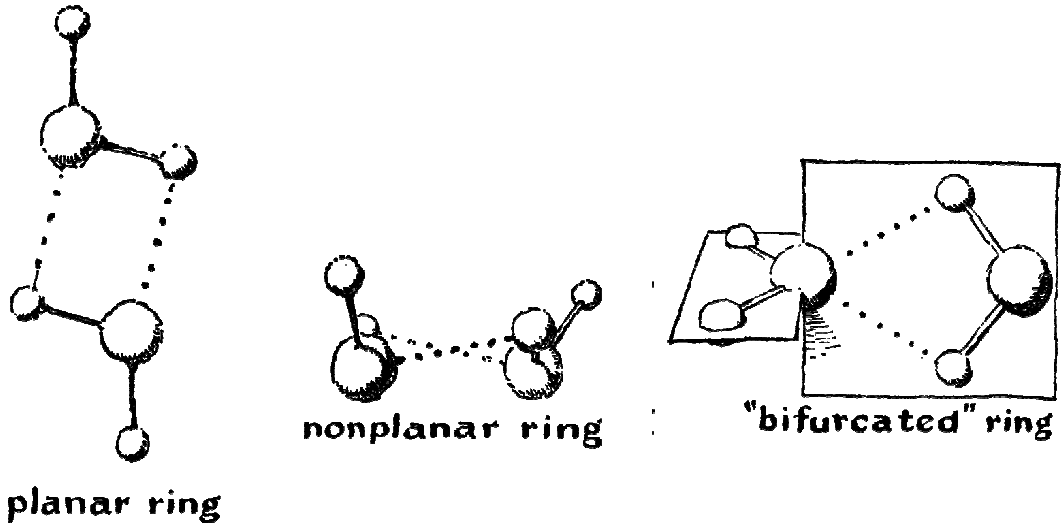

Figure 1.4: *Possible conformation of two water molecules bounded by two hydrogen bonds. Redrawn from Ref. [40].*

Since the energies of hydrogen bonds are rather low, lifetimes of a hydrogen bond is also small. The lifetime corresponding to the hydrogen bond is about $\tau \sim 0.001$ ps. Thus, even thermal motion and molecular or electrostatic interactions can strongly affect the hydrogen bonding.

1.4.2 Hydrogen Bonded Substances

The hydrogen bonded substances usually contain hydrogen bonds involving *electronegative* atoms. The atoms most frequently forming hydrogen bonds are: oxygen, nitrogen, fluorine and chlorine [40]. Thus, compounds containing these atoms may form hydrogen bonds.

There are some examples of well recognized substances forming hydrogen bonds: water, HF, alcohols, phenols, carboxylic acids, amides, amines, ketones, ethers, esters, ammonia, pyrrole [40]. Some of them are presented in Figure 1.5. However, there are some other substances for which the formation of hydrogen bonds is not obvious but possible: chloroform, acetylene, some aromatics, boranes, etc.

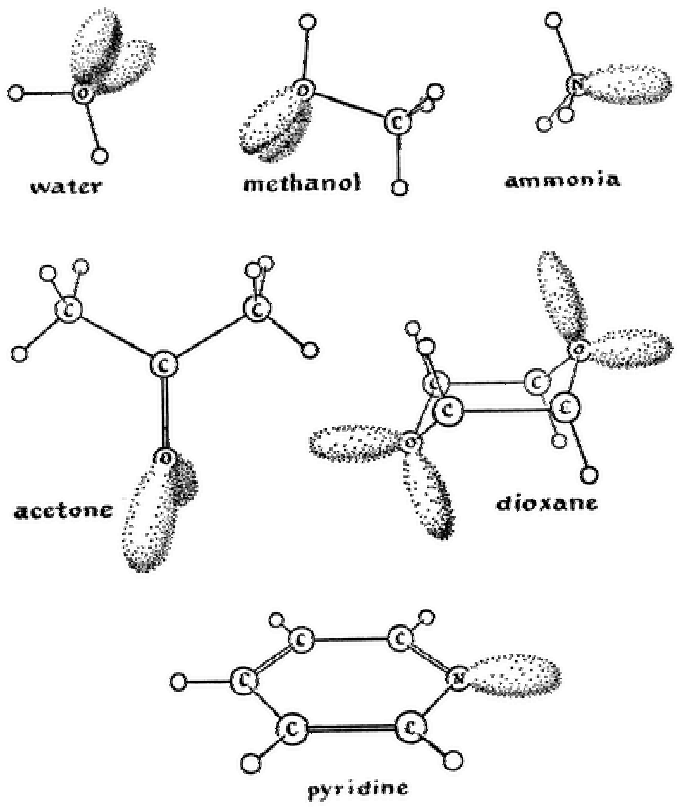

Figure 1.5: *Examples of hydrogen bonded substances. Two lobes represent schematically lone-pairs which can form hydrogen bonds with water. Redrawn from Ref. [40]*

1.4.3 Properties of Systems Involving Hydrogen Bonds

Formation of hydrogen bonds in a system modifies its physical and chemical properties: the hydrogen bonding alters size, shape, arrangement of atoms and the electronic structure of the functional groups, freezing and boiling points, electrical conductivity and dielectric properties of substances. It influence some physical properties as molar volume, viscosity, heat and sound velocity, etc. [40].

In the following chapters we will focus on another important property which is strongly influenced by the hydrogen bonding, namely, the solubility of neutral water-soluble polymers. It is due to the formation of hydrogen bonds between polymer

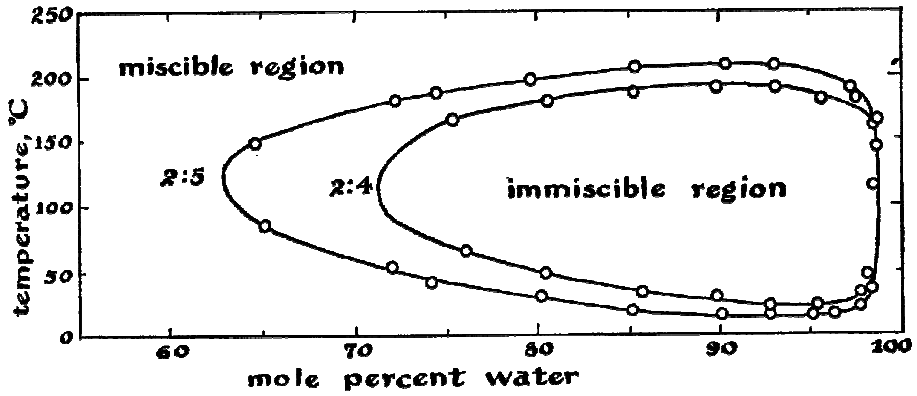

Figure 1.6: *Closed loop phase diagram for 2,4- and 2,5-dimethyl pyridine in water (after [40]).*

and water that the hydrogen bonded substances become highly soluble in aqueous media. The hydrogen bonding is responsible for the closed loop phase diagrams observed for such systems. For example, this is the case for dimethyl pyridine in water. The phase diagram is depicted in Figure 1.6. Closed loops phase diagrams of high molecular weight solutes will be discussed in the next chapter.

Most of the listed phenomena are closely related to the changes in the molecules which participate in hydrogen bonds. For example, high freezing and boiling points for pure hydrogen bonded substances are due to strong intermolecular forces because of the formation of hydrogen bonds.

1.5 Structure of Liquid Water

The hydrogen bonding between water molecules is responsible for the numerous water anomalies discussed in the previous section. The formation of a hydrogen bond is also the key ingredient in the understanding of liquid water. In this section we focus on the structure of liquid water.

1.5.1 Cooperativity of Hydrogen Bonding

We formulated the basic definition of a *single* hydrogen bond in section 1.4.1. However, if a water cluster contains more than one hydrogen bond, the existing hydrogen bonds in the aggregate can strongly influence the formation of the consequent hydrogen bonds. In other words, the formation of hydrogen bonds is not additive. This property of hydrogen bonding is called the *cooperativity* of hydrogen bonds [37, 38, 43, 44].

Quantum mechanical studies support the idea that the energy of the hydrogen bond depends on the number of hydrogen bonds in the aggregate [38]. After forming a first hydrogen bond the charge in the cluster distributes in such a way that the formation of another hydrogen bond becomes even more favorable than the first one. So, the system can form a stronger second bond because of the presence of the first bond. The described cooperative reinforcement of hydrogen bonds favors the formation of hydrogen bonds with a mean bond energy larger than that of the cluster with a single hydrogen bond.

This effect has strong consequences. (i) It leads to the shortening of H$\cdots$O hydrogen bonds in large clathrate hydrates reducing the overall distance between oxygen atoms participating in the hydrogen bond. (ii) Closed structures such as rings and pentagons are energetically more favorable than any open structures like chains and stars. (iii) The hydrogen bond energy for which the particular clathrate hydrate still exists depends on the number of hydrogen bonds in it.

The cooperativity of hydrogen bonds leads, for example, to the fact that hydrogen bonding energies in a water pentamer are almost twice as strong as the hydrogen bond in a linear dimer [37].

1.5.2 Operational Criterion of a Hydrogen Bond

One of possibilities to study hydrogen bonds is computer simulations. It seems to be the only source of information concerning the structure of water and the topology of hydrogen bond network. However, it is rather difficult to incorporate directly the

cooperativity of hydrogen bonds into computer simulations.

To describe hydrogen bonded aggregates in water, it was proposed to introduce the criterion based on the minimal[2] energy of a hydrogen bond. According to refs. [38, 43, 45, 46] the pair of one hydrogen atom H and another atom A is hydrogen bonded if the energy of this bond is higher than some preassigned limit, V_{HB}. Otherwise the pair is regarded as not hydrogen bonded. Thus, V_{HB} defines the minimal energy of hydrogen bond. With this definition the hydrogen bonds may unambiguously be identified in any given arrangement of water molecules, though it depends on the particular choice of the preassigned limit V_{HB}. If V_{HB} is selected to be too small, than the number of hydrogen bonds per molecule would be very large. Many of them would represent weakly interacting and widely separated pairs. In the opposite limit of large V_{HB}, the hydrogen bonds will become rare [43]. As V_{HB} moves up, it becomes more and more difficult to satisfy this criteria in large aggregates. As a result, dimers, triangles will be eliminated first, than quadrilaterals, pentagons, hexagons, *etc.* [43].

The proposed choice of the intermediate regime of the minimal energy in the range $1.6 < V_{HB} < 4.6$ kcal/mol [43][3], selects a certain number of clathrate structures, corresponding to that range [46]. It is possible to investigate the shape and the abundance of these crystal structures in water. Although this definition of hydrogen bonds is not unique, it turned out to be very useful in computer simulations.

1.5.3 Architecture of Liquid Water

At present, there are no possible experiments which allow to determine directly the topology of hydrogen bonds and the structure of liquid water. Experimental methods such as X-rays diffraction and the diffraction of neutrons give the distribution of distances and relative positions of hydrogen-oxygen pairs in water. In turn, computer simulations can generate a set of configurations of hydrogen bonds for a small region containing limited number of water molecules [38]. Thus, the only way to asses

[2] Here and below we assume *absolute* values of energies of hydrogen bonds, which are negative.
[3] This corresponds approximately to the energy range $3 \div 8\ kT$ at room temperature.

hydrogen bond geometrical structures in water is computer simulations [45, 47].

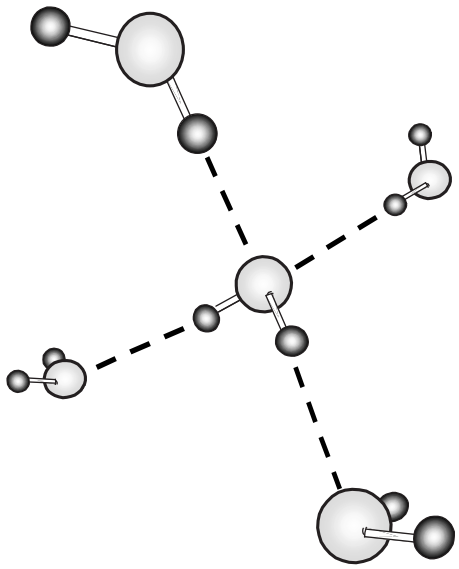

Figure 1.7: *Tetrahedral structure of water. Each water molecule form four hydrogen bonds with its neighbours.*

The experimental data indicate the persistence of 3- and 4- coordinate order in liquid water [38]. Each oxygen of a water molecule can form two hydrogen bonds with hydrogen atoms of nearby water molecules, which can come into close contact with its two lone pairs (Figure 1.3). In turn, two hydrogens of the water molecule can form two hydrogen bonds with oxygen atoms of neighboring molecules [37, 39]. As a result, two hydrogens of a water molecule can act as acceptors and two lone pairs as donors. The tetrahedral configuration of water molecules is presented in Figure 1.7.

Substantial disorder in liquid water disturb the tetrahedral network structure. Computer simulations model liquid water as 3- or 4-coordinate weakly hydrogen bonded statistical network (Figure 1.8).

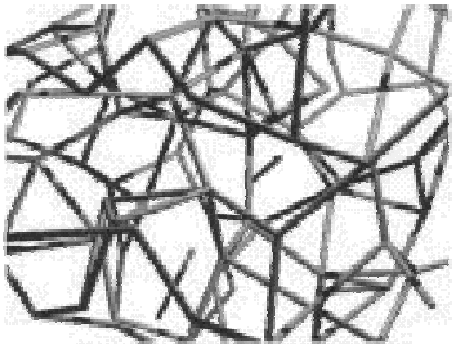

Figure 1.8: *Hydrogen bonded network of liquid water. Snapshot from molecular dynamics simulations [37].*

1.5.4 Theories of Liquid Water

The theories of liquid water can be split into two broad categories: (i) mixture/interstitial models [39], and (ii) continuum or distorted hydrogen bond models. The last category includes water models based on hydrogen bonded network picture [43, 46, 47, 48, 49, 50, 51].

Mixture models describe liquid water composing of a small number of different distinguishable molecular species. Interstitial models are the class of mixture models in which one of the hydrogen bonds form a hydrogen-bonded network and the other species reside in the cavities of the network. The distinction between the species in mixture models is made between a population of "intact" and "broken" hydrogen bonds. Each of the species occupies one of the discrete energy levels. In equilibrium the species can transform one to another by breaking and forming hydrogen bonds. The main assumption of mixture models is that hydrogen bonded molecules in species are distinctly different from the non-hydrogen bonded molecules [39]. Such description of liquid water was incited by the cooperativity effect of hydrogen bonds (Section 1.5.1). Formation of one hydrogen bond favours formation of another in its vicinity. In turn, breaking a hydrogen bond promotes breaking neighboring hydrogen bonds [39]. This picture suggests the equilibrium mixture of permanently

transforming one into another species.

In contrast to mixture models, continuum models assume that hydrogen bonds in water are not broken, but distorted. From this point of view most of water molecules are hydrogen bonded, but with the different energies of hydrogen bond. The mobility of water molecules is described by continuum modification of the topology of the hydrogen bonded network rather when the discrete disruption and formation of hydrogen bonds [37].

The distinction between two categories of theories of liquid water brings us again to the question of the definition of a hydrogen bond (Section 1.5.2). If we define a hydrogen bond by a *high* energy limit, V_{HB}, then only a small number of water molecules structures could be considered as hydrogen bonded. Hereby we get the mixture models limit. On the other hand, allowing for low energy hydrogen bonds, *i.e.* establishing *low* V_{HB}, we get the limit of continuum models, where all water molecules are connected in the hydrogen bonded network.

1.6 Structure of Polymers Soluble in Water

Addition of solute molecules in water disrupt the local structure of hydrogen bonds. The solute molecules induce a new order and new forms of water structure in the places of the insertion. "Hydrophobic" solutes enforce local rearrangement of hydrogen bonded structure of water around them in the so-called *cage-like* structure. The hydrogen bonds in such structure is even stronger than in bulk water [2]. Disruption of local structure and the formation of the cage-like structure leads to the increase of the free energy. This gives rise to an effective attraction between hydrophobic solutes. The effective attraction of hydrophobic solutes in aqueous media is called *hydrophobic effect*. This effect becomes stronger as the temperature rises up, since increasing temperature breaks hydrogen bonds and the formation of the cage-like structure becomes less favorable. In contrast, "hydrophilic" solutes form hydrogen bonds with water and thus, compensate, at least partially, the broken hydrogen bonds in water network induced by their insertion.

Water-soluble polymers usually have hydrophobic and hydrophilic groups at the same time. The sequence of hydrophobic and hydrophilic groups as well as their spatial orientation between each other plays the major role in the formation of hydrogen bonds and the solubility of neutral water-soluble polymers.

In this section we describe the structure of three common neutral water-soluble polymers: Poly(ethylene oxide), Poly(N-vinylpyrrolidone) and Poly(N-isopropylacrylamide) focusing on the essential properties which govern their solubility in water.

1.6.1 Poly(ethylene oxide)

Poly(ethylene oxide) or PEO[4] is one of the simplest structure of water-soluble polymers (Figure 1.9).

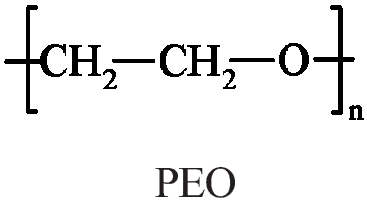

PEO

Figure 1.9: *Chemical structure of PEO.*

A repeated unit contains two CH_2 groups followed by an oxygen atom. The oxygen atom is able to form hydrogen bonds with water, while two CH_2 groups allow for some rotational degree of freedom for the oxygen atom in order to provide an optimal angle for the hydrogen bonding. The spatial structure of a repeated unit is shown in Figure 1.10. Such chemical structure of PEO allows for the solubility both in aqueous solutions and in a variety of organic liquids at room temperatures. Addressing the question of solubility of PEO in water, we should note, that two CH_2

[4]The abbreviation PEO is usually used for high molecular weight polymers and PEG for low molecular weight polymers. Short chains are usually terminated by CH_3 groups, while end groups of long chains are usually not saturated [2].

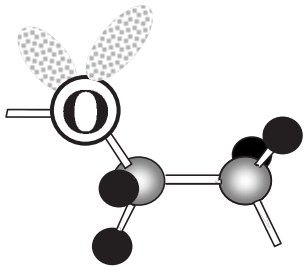

poly(ethylene oxide)

Figure 1.10: *Spatial structure of a repeated unit of PEO. Two lone-pairs can participate in the hydrogen bond formation.*

groups in the PEO chemical structure mark it out among other polyethers having an oxygen atom in the main chain. The polymer with only one CH_2 group followed by an oxygen atom, poly(oxymethylene), as well as the polymer with three CH_2 groups, poly(trimethylene oxide), are insoluble in water.

Although PEO is soluble not only in water, the phase behavior of PEO in water differs significantly from that of in organic liquids [2]. Aqueous solutions of PEO *phase separate upon heating*. Further increase of temperature leads again to dissolution of polymer in a solvent. The phase diagram of aqueous solutions of PEO has a closed loop form, similar to that of highly hydrogen bonded low molecular solutes like nicotine or dimethyl pyridine (Figure 1.6). In contrast, nonaqueous solutions of PEO shows normal upper critical solution temperature behavior [13, 14, 15, 16], *i.e.* it phase separates upon cooling and dissolves on heating like most of synthetic polymers in nonaqueous solutions.

1.6.2 Poly(N-vinylpyrrolidone)

Another example of a neutral water-soluble polymer is poly(N-vinylpyrrolidone) or PVP. The chemical structure is shown in Figure 1.11.

A repeated unit of PVP contains a highly polar amide group which is responsible

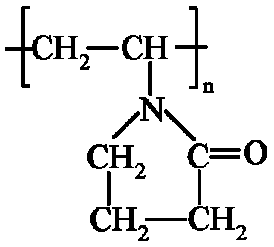

PVP

Figure 1.11: *Chemical structure of PVP.*

for the amphiphile properties and also apolar methylene and methine groups and the ring which gives hydrophobic properties [2]. The three dimensional structure of the repeated unit is given in Figure 1.12.

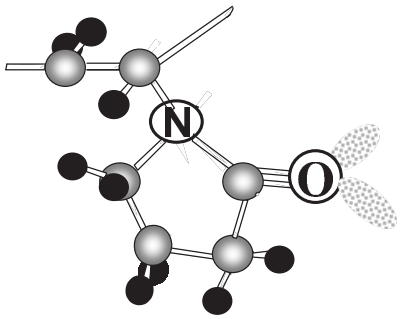

poly(N-vinylpyrrolidone)

Figure 1.12: *Spatial structure of a repeated unit of PVP. The oxygen end is exposed and is able to form hydrogen bonds, while nitrogen is surrounded by methylene and methine groups.*

PVP is soluble in water in the temperature range from 0 to 100^o C. However, decreasing intrinsic viscosity and shrinking of cross-linked polymers with increasing temperature suggest that the solvent quality of PVP in water decreases as temperature increases [2]. This indicates that PVP in water has lower critical solution temperature above 100^o C, *i.e.* PVP in aqueous solvents should *precipitate upon*

heating. Addition of salts decreases the critical point, so aqueous solutions of PVP in the presence of salts exhibit phase diagrams with lower critical solution temperature (precipitation upon heating). In that sense, the phase behavior of aqueous solutions of PVP is qualitatively similar to the phase behavior of PEO in water.

1.6.3 Poly(N-isopropylacrylamide)

Poly(N-isopropylacrylamide) or PNIPAM is one of highly studied thermo-sensitive water-soluble polymer [35, 36, 52, 53, 54, 55, 56, 57, 58, 59, 60, 61, 62, 63, 64, 65, 66, 67, 68, 69]. PNIPAM is soluble in water below 25^o C. It has a LCST phase behavior [52]. PNIPAM exhibit rather sharp coil-globule transition [53, 64, 65, 67, 68]. Addition of surfactants can shift the temperature of coil-globule transition by several degrees [53]. The transition temperature lies in the biological temperature range. This property can be used in several biological applications such as thermo-sensitive capsules for drug delivery.

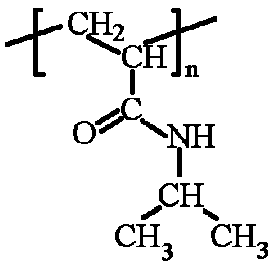

PNIPAM

Figure 1.13: *Chemical structure of PNIPAM.*

The chemical structure of PNIPAM is shown in Figure 1.13. The main chain of PNIPAM is highly hydrophobic (methine groups) as well as the end of the side chain containing two CH_3 groups. The oxygen atom in the middle of the side chain is able to form hydrogen bonds with water. The hydrogen bonding is the origin of the solubility at low temperatures. The three dimensional picture of the repeated

unit is presented in Figure 1.14.

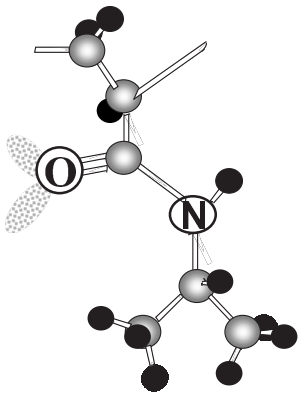

Poly(*N*-isopropylacrylamide)

Figure 1.14: *Spatial structure of a repeated unit of PNIPAM. Hydrophobicity of the main chain and two methylene groups at the end of the side group is compensated by the oxygen atom which can form hydrogen bonds with water.*

PNIPAM *phase separates upon heating* similarly to PEO and PVP in water. However, the experimental data concerning the phase diagram of PNIPAM in water are rather controversial. The phase diagram first measured by M. Heskins and J. E. Gillet [52] suggests that the polymer has the lower critical point around 31^o C and $\phi_c \simeq 0.16$. A recent investigation by Afroze *et al* [36] led to different results: depending on N, the LCST occurs around $T_c \simeq 27 - 28^o$ C and $\phi_c \simeq 0.43$. For high molecular polymers the critical concentration ϕ_c does not tend to zero. This observation suggests, that in the limit of $N \to \infty$ PNIPAM has the phase diagram with the minimum at non-vanishing ϕ. It indicates on the possibility of the existence of the temperature range where infinitely long polymer phase separates on dense and dilute phase with nonzero concentration. We shall discuss the manifestation of this effect, namely a vertical phase separation in polymer brushes in chapters 5 and 6.

Chapter 2

Two-state polymers: Concentration Dependent χ_{eff}-Parameter

2.1 Résumé

La dépendance en concentration de $\overline{\chi} = \chi_{eff} - (1-\phi)\partial\chi_{eff}/\partial\phi$, obtenu des propriétés colliquatives, fournit une mesure utile pour l'exécution des modèles théoriques et ses paramètres. Trois versions du modèle à deux état [21, 23, 70] proposés pour polymères neutres soluble dans l'eau mènent à $\overline{\chi}(\phi)$. Cette dépendance permet de distinguer qualitativement entre eux: (i) le modèle K [21] donne $\partial\overline{\chi}/\partial\phi > 0$ pendant que les modèles MB [23] et D [70] permettent aussi $\overline{\chi}(\phi)$ décroissant. (ii) $\overline{\chi}(\phi)$ calculé à partir de modèles K et D, en utilisant les paramètres originaux qui étaient employé pour ajuster le diagramme de phase de POE dans l'eau, concorde semiquantitativement avec la courbe expérimentale. En revanche, $\overline{\chi}(\phi)$ obtenu du modèle MB diffère qualitativement des résultats mesurés.

2.2 Introduction

As we discussed, the solubility of neutral water-soluble polymers is attributed to the formation of hydrogen bonds with water (Figure 2.1). We shall describe the

solubility of neutral water-soluble polymers on the basis of a *two-state model* wherein the monomers of the chain can exist in two distinct and interconverting states [18, 21, 23, 24, 71].

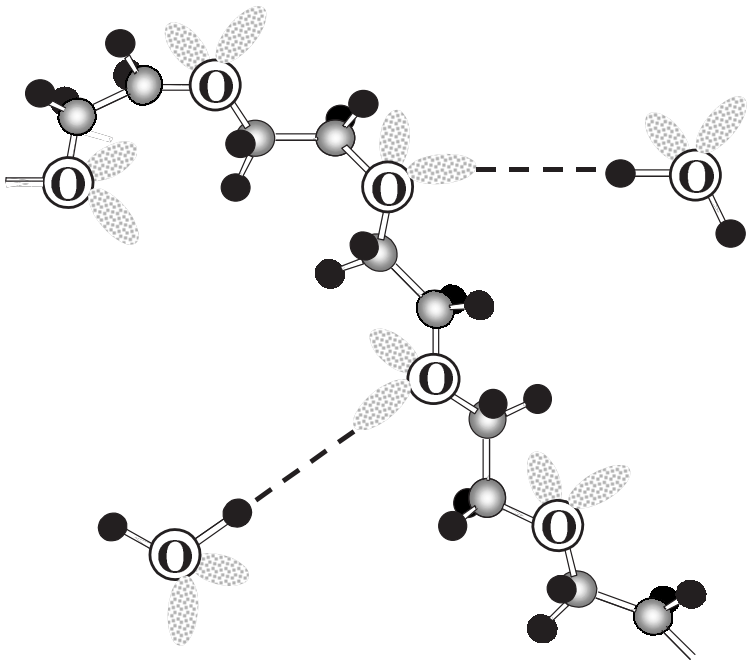

Figure 2.1: *PEO chain forming hydrogen bonds (- - -) with water molecules.*

In this chapter we demonstrate that various "two-state" models yield $\chi_{eff}(\phi)$ and analyze the ϕ dependence of the resulting χ_{eff}. Our discussion is concerned with three models: The one proposed by Karlstrom (K model) [21], the model of Matsuyama and Tanaka [71] as formulated by Bekiranov, Bruinsma and Pincus (MB model) [23] and the model of Dormidontova (D model) [24] which is in fact identical to the model of Veytsman [72]. The different versions of two-state model yield, as we shall see, χ_{eff} that depends on both T and ϕ. The original papers proposing theses models [21, 23, 24, 71] focused on the phase behavior while overlooking the emergence of $\chi_{eff}(\phi)$[1].

[1]Bekiranov *et al* actually conclude that their model does not yield a ϕ dependent χ_{eff}. This

The main purposes of this chapter is to obtain explicit expressions for $\chi_{eff}(\phi)$ for all three models, analyze the ϕ dependence and compare the results to experimental data. Note, that by allowing for the internal degrees of freedom of the monomers, the two-state models can rationalize the observed $\chi_{eff}(\phi)$ while retaining the main approximations of the Flory-Huggins theory such as incompressibility, monomers and solvent molecules of identical size and shape.

Aside from the fundamental interest in the origin of the ϕ dependence of χ_{eff} this analysis underlines the utility of $\chi_{eff}(\phi)$ as a criterion for the *performance* of the models. While all three models recover the observed phase diagram of PEO in water, only the K model and D model yields a qualitatively correct increasing $\overline{\chi(\phi)}$. On the other hand, in the case of the decreasing $\overline{\chi(\phi)}$ for PVP in water [32], the K model is inherently incapable of reproducing the experimental results while MB model and D model do allow for a similar behavior.

2.3 $\chi_{eff}(\phi)$: What Is Measured in Experiments?

All three models are of the Flory-type and the free energy per lattice site can be written in the form

$$\frac{F}{kT} = \frac{\phi}{N}\ln\phi + (1-\phi)\ln(1-\phi) + \chi_{eff}(\phi)\phi(1-\phi) \tag{2.1}$$

where $\chi_{eff}(\phi)$ incorporates the specific features of a particular model. Thus, we choose to analyze $\chi_{eff}(\phi)$ and compare it with available experimental data. Our analysis is mostly concerned with the concentration dependence of

$$\overline{\chi} = \chi_{eff} - (1-\phi)\frac{\partial\chi_{eff}}{\partial\phi} \tag{2.2}$$

We focus on $\overline{\chi}$ because measurements of colligative properties, such as vapor pressure and osmotic pressure, yield $\overline{\chi}$ rather than χ_{eff} [25, 29]. As a result, it is the $\overline{\chi}$ values that are usually reported in the literature [25, 29, 73]. Furthermore, it

conclusion is however obtained in the limit of $\phi \to 0$.

turns out that the ϕ dependence of $\overline{\chi}(\phi)$ is simpler to analyze. Note, that χ_{eff} and $\overline{\chi}$ coincide only in the case when there is no dependence on ϕ.

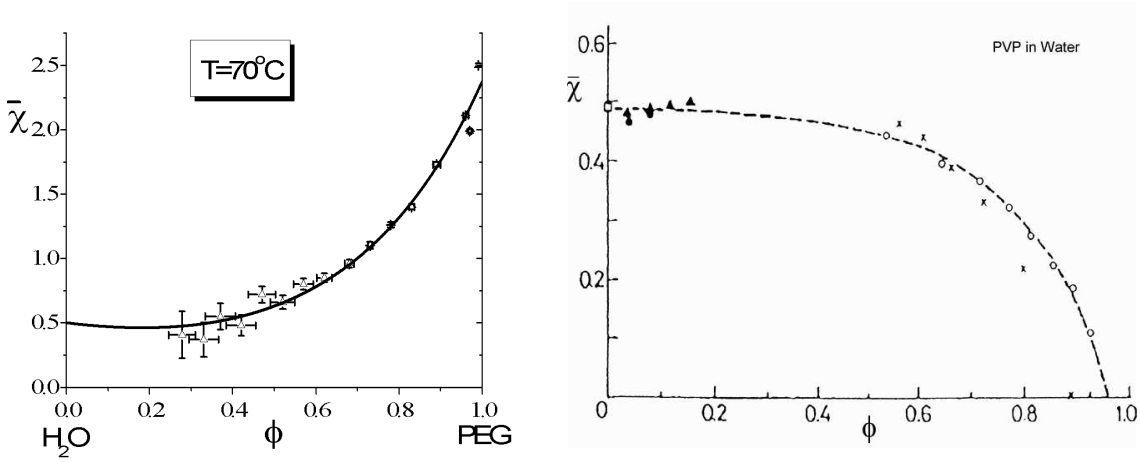

Figure 2.2: *Plots of measured* $\overline{\chi} = \chi_{eff} - (1-\phi)\partial\chi_{ef}/\partial\phi$ vs. ϕ *for aqueous solutions of the neutral water-soluble polymers PEO* $M_w = 6000$, $T = 70^o$ *C (full circle, after [74]) and PVP at* $T = 22^o$ *C after [32].*

Experimentally obtained $\overline{\chi}(\phi)$ for PEO in water and PVP in water are shown in Figure 2.2. For PEO $\overline{\chi}(\phi)$ is an increasing function, while for PVP $\overline{\chi}(\phi)$ decrease with concentration.

Since the different versions of the two-state model aimed to rationalize the phase behavior of aqueous solutions of PEO, the parameters involved were chosen with view of recovering the known phase diagram. However, two-state models are in fact suitable candidates for the description of aqueous solutions of neutral water-soluble polymers *in general*. With this in mind we consider the two-state model as a generic model for such systems rather than as a specific model for PEO. Accordingly, we make no specific assumptions regarding the choice of the various parameters involved.

2.4 Two-State Models

2.4.1 Definition of Two States

In the "two-state" models for neutral water-soluble polymers the monomers of the chain may assume two interconverting forms characterized by different interaction energies. Three models differ, as we shall discuss, in the precise identification of the monomeric states. In all the cases it is assumed that one monomeric state, A, is "hydrophilic" while the other, B, is "hydrophobic" (Figure 2.3). As a result, a binary solution of a polymer in water behaves in fact as a *reactive ternary system.* In particular, the fraction of A monomers, p, depends on both T and ϕ.

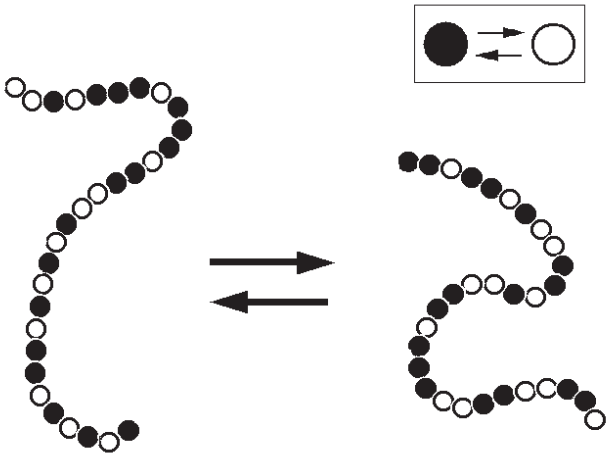

Figure 2.3: *A schematic representation of the dynamic equilibrium in two-state polymers where the monomers exist in two interconverting states (inset), A (empty circle) and B (full circle).*

The K, MB and D models differ with respect to the underlying physics. The K model [21] focuses on molecular rotations giving rise to monomeric states of different polarities. The state endowed with a strong dipole moment is identified as the hydrophilic species, A, while the less polar state is identified as the hydrophobic state, B. Within this model the interconversion is a unimolecular reaction, $A \rightleftarrows B$, and the mass action law is

$$\frac{p}{1-p} = K_K \tag{2.3}$$

Here p is the fraction of monomers in a hydrophilic A state and K_K is the corresponding equilibrium constant (Figure 2.3). The explicit form of K_K, to be given in section 2.5, is irrelevant at this point. The MB model [23] focuses on the role of polymer– water hydrogen bonds but ignores the hydrogen bonding in water. In particular, a monomer that forms a hydrogen bond with water is considered, in effect, as hydrophilic while a monomer that does not form such bond is hydrophobic. This model distinguishes between free water molecules (S) and water molecules that are bound to the polymer chain. This distinction has no counterpart in the K model. Accordingly the interconversion reaction is a bimolecular reaction, $B + S \rightleftarrows A$, and the chemical equilibrium is specified by

$$\frac{p}{(1-p)\phi_0} = K_{MB} \tag{2.4}$$

where ϕ_0 is the volume fraction of water. The explicit expression for K_{MB}, to be given in section 2.6, is not required for the present discussion. Thus, in the K model

$$\phi_0 = 1 - \phi \tag{2.5}$$

while in the MB model

$$\phi_0 = 1 - \phi - p\phi \tag{2.6}$$

where p is the fraction of monomers that form hydrogen bonds and $p\phi$ is the volume fraction of bound water.

The D model allows for water–water association in addition to PEO–water hydrogen bonds. To account for water structure it uses the approach similar to that in ref. [72]. Each water molecule has two hydrogen atoms which can be proton donors for both water–water and PEO–water hydrogen bonds. Each oxygen atom of water molecules and PEO backbone can participate in two hydrogen bonds as proton accepter. The D model is an extension of the MB model to allow for the association in water. The water–water hydrogen bonding leads to the additional interconversion reaction and equilibrium condition

$$\frac{p}{(1-p)2\phi_0} = K_D^{(p)} \tag{2.7}$$

$$\frac{q}{(1-q)2\phi_0} = K_D^{(q)} \tag{2.8}$$

where p is the average fraction of hydrogen bonds between PEO and water and q is the average fraction of association in water. ϕ_0 is the volume fraction of water which does not form hydrogen bonds ("free" water)

$$\phi_0 = (1-q)(1-\phi) - p\phi\omega \tag{2.9}$$

The factor 2 in the equilibrium conditions accounts for the fact that a water molecule can participate in two hydrogen bonds as an acceptor and two hydrogen bonds as a donor. ω accounts for the different size of a lattice site occupied by a solvent and a monomer. For PEO in water $\omega = 1/3$. This model will be described in section 2.7.

Different models involve different reference states. In particular, the melt state, $\phi = 1$, in the K model is characterized by

$$p(\phi = 1) = p_* \geq 0 \tag{2.10}$$

while in the MB and D models

$$p(\phi = 1) = 0 \tag{2.11}$$

In the opposite limit, pure water state, $\phi = 0$, only the D model has an extra contribution to the free energy which is due to association in pure water

$$q(\phi = 0) = q_0 \geq 0 \tag{2.12}$$

where q_0 is the average fraction of water–water hydrogen bonds in pure water.

In the following we first compare the K and MB models and then point out the differences between the MB and the D models. Both, the K and the MB, models utilize a Flory-type approach to obtain the thermodynamics of the solution. In

particular, random mixing is assumed and the energy per site of a polymer–water solution inscribed on a lattice is written as

$$\begin{aligned}\frac{E}{kT} &= \phi\left[p\frac{z\epsilon_{AA}}{2kT} + (1-p)\frac{z\epsilon_{BB}}{2kT}\right] + (1-\phi)\frac{z\epsilon_{SS}}{2kT} + \\ &\quad \phi(1-\phi)\left[p\chi_{AS} + (1-p)\chi_{BS}\right] + \phi^2\chi_{AB}p(1-p) \qquad (2.13)\end{aligned}$$

Here z is the coordination number of the lattice and k is the Boltzmann constant. ϵ_{AA}, ϵ_{BB} and ϵ_{SS} denote respectively the energies of A, B and solvent molecules in a pure bulk phase. χ_{AB}, χ_{AS} and χ_{BS} denote the Flory interaction parameters corresponding respectively to AB, AS and BS interactions (where $\chi_{AS} = \epsilon_{AS} - (\epsilon_{AA} + \epsilon_{SS})/2$, *etc.*). The first term allows for the energy of the A and B in a hypothetical pure bulk phase while the second reflects the energy of the solvent molecules in a pure bulk state. The interactions between the two monomeric states and the solvent gives rise to the third term while the last term allows for the AB interactions. For future reference it is convenient to define a dimensionless parameter

$$\Delta\epsilon = z\frac{\epsilon_{AA} - \epsilon_{BB}}{2kT} \qquad (2.14)$$

characterizing the difference between the energies of the two monomeric states. This expression reduces to the familiar Flory form when $p = 1$ or $p = 0$ that is, when the monomers have only one state. In the K and MB models the energy E is supplemented by two entropy terms. One allows for the different possible sequences of A and B states along the chain, leading to an entropy per lattice site of

$$\frac{S_{AB}}{k} = -\phi\left[p\ln p + (1-p)\ln(1-p)\right] \qquad (2.15)$$

while the second reflects the translational entropy of the chains

$$\frac{S_{trans}}{k} = -\frac{\phi}{N}\ln\frac{\phi}{N} - \phi_0\ln\phi_0. \qquad (2.16)$$

The S_{AB} term is distinctive to the two-state models. It vanishes when the monomers exist in a single state i.e., $p = 1$ or $p = 0$. As expected, S_{trans} is identical in form to the entropy term in the Flory free energy. Altogether, the free energy of the solution

is $F = E - T(S_{AB} + S_{trans})$ and the mixing free energy is

$$F_{mix} = F(\phi, p) - \phi F(\phi = 1) - (1 - \phi)F(\phi = 0) \tag{2.17}$$

Both models neglect the fluctuations in the number of A monomers per chain, m. Strictly speaking, chains with different m are distinguishable and should be treated as different chemical species [71]. Rather than allow for this multiple equilibria the K and MB models consider a single polymer species characterized by an average $\overline{m} = pN$ where N is the polymerization degree. This approximation is justified because the m values are described by a sharply peaked Gaussian distribution [23]. While the two models lead to similar free energies, the free energies invoked in the K and in the MB models differ in two respects. In the MB model (i) The translational entropy is p dependent because of the $\phi_0 \ln \phi_0$ term and, (ii) since $p(\phi = 1) = 0$, F_{mix} does not reflect contributions due to $p(\phi = 1) = p_* \geq 0$ that appears in the K model.

Finally, it is helpful to note certain additional differences between the models as described in the original papers [21, 23]. While the physical content of these is minor in comparison to the differences discussed above, they are of interest for comparison purposes. Thus, the analysis of Bekiranov *et al* focused on the particular case of $\chi_{AB} = 0$, $\chi_{AS} = \chi_{BS} = \chi = 2.885 - 0.0036T$ and $\Delta\epsilon = 6.38 - 2408/T$ while in the K model $\chi_{AS} = 80.0/T, \chi_{BS} = 684.5/T$, $\chi_{AB} = 155.6/T$ and $\Delta\epsilon = -625.2/T + \ln 8$. The temperature dependence of the χ parameters in the two papers is somewhat different. Bekiranov *et al* assume $\chi \sim a + bT$ while in the K model $\chi \sim b/T$. In both models $\Delta\epsilon \sim a + b/T$. In the model of Bekiranov *et al* this follows from the identification of $\Delta\epsilon$ with $\Delta F_0/kT$ where $\Delta F_0 = \Delta E_0 - T\Delta S_0$ is the free energy change associated with the formation of hydrogen bond. The $a + b/T$ dependence in the K model is a consequence of the degeneracy of the monomeric states. It assumed that each of the two monomeric forms can exist in a number of equivalent states and the resulting entropy gives rise to a. The analysis of Bekiranov *et al* allows for the effect of pressure. This is attributed to the existence of a preferred volume for a hydrogen bond [19]. The application of pressure is assumed to introduces a geometric

constraint resulting in a lower number of bound water molecules. This argument yields a semiquantitative agreement with experimental results on the phase diagram of PEO. Note that this coupling mechanism can only operate within the MB model and can not be used in the K model. Furthermore, it is not fully consistent with the incompressibility assumption invoked by Bekiranov *et al.*

As we noted before, the D model is the extension of the MB model in the sense that it allows for the water–water hydrogen bonds. Thus, instead of single energy parameter characterizing the PEO–water hydrogen bonds, eq. (2.14), the D model has two energy parameters: the energy difference due to formation of PEO–water hydrogen bonds, $\Delta\varepsilon_p$ and that of water–water hydrogen bonds, $\Delta\varepsilon_w$. Moreover, the D model takes into account the different sizes of PEO monomer and water molecule. The ratio of molecular volumes of PEO and water is $\omega = 1/3$. It also assumes that a PEO monomer can form *two* hydrogen bonds in contrast to MB models assuming one hydrogen bond per monomer. This leads to the additional factor, 2ω, in the first term of eq. (2.13) and in the eq. (2.15).

Another distinctive feature of the D model reflects the interconversion reaction of hydrogen bonds in water (2.8). In addition to the entropy of hydrogen bonds along the chain, S_{AB}, the D model includes the entropy of water–water hydrogen bonds,

$$\frac{S_w}{k} = -2\omega(1-\phi)\left[q\ln q + (1-q)\ln(1-q)\right] \tag{2.18}$$

Finally, there is an extra entropy term due to water–water hydrogen bonds which we shall discuss in section 2.7. In analogy to the MB model, the D model assumes $\chi_{AB} = 0$, $\chi_{AS} = \chi_{BS} = \chi$. However, the temperature dependence of χ differ from the MB model: while χ depends linearly on T in the MB model, it has an inverse temperature dependence in the D model, $\chi \sim a + b/T$. For PEO, the D model uses $\chi = -0.211 + 93.5/T$, $\Delta\varepsilon_p = 4.35 - 2000/T$ and $\Delta\varepsilon_q = 3.25 - 1800/T$ [24]. The energies of hydrogen bonds, $\Delta\varepsilon_{p,q} \sim a + b/T$ have the same temperature dependence as in the K and the MB models.

2.4.2 $\chi_{eff}(\phi)$ Within Two-State Models

Before we proceed to analyze the ϕ dependence of $\overline{\chi}$ within the two "two-state" models, it is helpful to summarize the thermodynamic relationships that apply when $\chi = \chi(T)$ is replaced by $\chi_{eff} = \chi_{eff}(T, \phi)$ [25]. The Flory like mixing free energy per site, F_{mix}, consists then of two terms. One is an interaction free energy that is the counterpart of the mixing energy $\chi\phi(1-\phi)$

$$\frac{F_{int}}{kT} = \chi_{eff}(\phi)\phi(1-\phi). \tag{2.19}$$

The second is the translational free energy

$$\frac{F_{trans}}{kT} = \frac{1}{N}\phi\ln\phi + (1-\phi)\ln(1-\phi). \tag{2.20}$$

The chemical potential of the solvent is $\mu_s = \mu_s^o(p,T) - \pi a^3$ while the osmotic pressure $\pi a^3 = \phi^2\frac{\partial}{\partial\phi}(\frac{F_{mix}}{\phi})$ is

$$\frac{\pi a^3}{kT} = \frac{\phi}{N} - \phi - \ln(1-\phi) - \overline{\chi}\phi^2 \tag{2.21}$$

where $\overline{\chi} = \chi_{eff} - (1-\phi)\frac{\partial\chi_{eff}}{\partial\phi}$ replaces χ. Since μ_s determines the colligative properties of the solution, measurements of such properties yield $\overline{\chi}$ rather than χ_{eff}. In turn, $\overline{\chi}$ is obtainable from F_{int} via

$$\overline{\chi} = -\frac{\partial}{\partial\phi}\frac{F_{int}}{kT\phi} \tag{2.22}$$

In the next two sections we will utilize equation (2.22) to obtain $\overline{\chi}$ from $F_{int} = F_{mix} - F_{trans}$. This equation also shows that terms of the form $const'\phi$ in F_{int} do not contribute to $\overline{\chi}$. This will allow us to ignore such linear terms that arise because of the choice of the reference state.

2.5 Karlstrom Model

2.5.1 Free Energy

Within the K model the mixing energy per lattice site, E_{mix}, is

$$\begin{aligned}\frac{E_{mix}}{kT} &= \phi p\Delta\epsilon + \phi(1-\phi)[p\chi_{AS} + (1-p)\chi_{BS}] + \phi^2\chi_{AB}p(1-p) \\ &\quad +\text{terms linear in } \phi \end{aligned} \tag{2.23}$$

The first term measures the difference in the energy of isolated A and B monomers. The second term accounts for the interactions between the monomers and the solvent. It is a generalization of the $\chi\phi(1-\phi)$ term in the Flory free energy for a binary solutions. The third term allows for the interaction between A and B monomers. The mixing entropy is

$$\begin{aligned}\frac{S_{mix}}{k} &= -\phi[p\ln p + (1-p)\ln(1-p)] - \left[\frac{\phi}{N}\ln\phi + (1-\phi)\ln(1-\phi)\right] \\ &\quad +\text{terms linear in } \phi \end{aligned} \tag{2.24}$$

The first term allows for the AB mixing within the chains and the second for the translational entropy of the chains. In both expressions, the terms linear in ϕ arises because the free energy of the melt state depends on p_* and $F_{mix} = F-(1-\phi)F(\phi = 0) - \phi F(\phi = 1, p_*)$. Upon discarding terms linear in ϕ, $F_{int} = F_{mix} - F_{trans}$ is

$$\begin{aligned}\frac{F_{int}}{kT} &= \phi p\Delta\epsilon + \phi(1-\phi)[p\chi_{AS} + (1-p)\chi_{BS}] + \phi^2\chi_{AB}p(1-p) + \\ &\quad \phi[p\ln p + (1-p)\ln(1-p)] \end{aligned} \tag{2.25}$$

The equilibrium value of p for a given ϕ and T, $p_e = p_e(\phi)$, is specified by the condition $\partial F_{int}/\partial p = 0$ leading to

$$\begin{aligned}\frac{p_e}{1-p_e} &= K_K(\phi, p_e, T) = \\ &\quad \exp\left[-\Delta\epsilon - (1-\phi)(\chi_{AS} - \chi_{BS}) - \phi\chi_{AB}(1-2p_e)\right] \end{aligned} \tag{2.26}$$

where K_K is the equilibrium constant for the unimolecular intrachain $A \rightleftarrows B$ reaction. When $\chi_{AS} = \chi_{BS} = \chi$ and $\chi_{AB} = 0$, the parameters chosen by Bekiranov *et al* in their model, K_K is independent of ϕ. Consequently, for this case p_e is independent of ϕ, $\partial p_e/\partial\phi = 0$, thus leading, as we shall see, to $\partial\overline{\chi}_K/\partial\phi = 0$. To assure the stability of the $A \rightleftarrows B$ equilibrium we further invoke the condition $\partial^2 F/\partial p^2 > 0$

$$\frac{\partial^2 F}{\partial p^2} = \phi\left[\frac{1}{p(1-p)} - 2\phi\chi_{AB}\right] > 0. \tag{2.27}$$

This ensures that the free energy curve is concave and that fluctuation relax back to the equilibrium state according to the Le Châtelier principle.

2.5.2 Phase Diagram of PEO in Water

The equilibrium free energy specify the phase diagram of PEO in water (Figure 2.4). The K model is able to semiquantitatively fit the phase diagram. The experimental data are from [75].

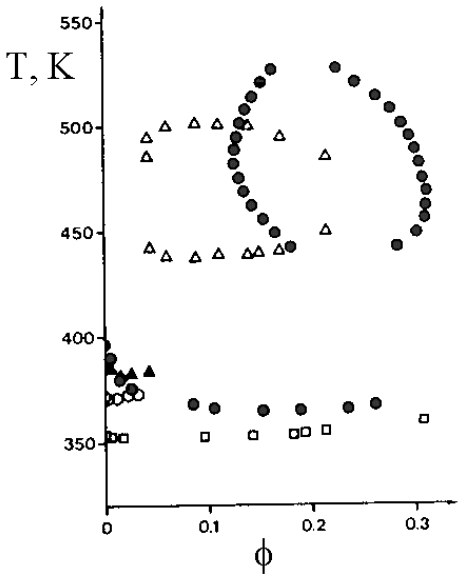

Figure 2.4: *Phase diagram of PEO in water for two molecular weights:* $M_w = 51.2$ *(open triangles – experimental data, filled circles – theoretical fit),* $M_w = 330$ *(filled triangles – experimental data, filled circles – theoretical fit) and* $M_w = 23200$ *(open diamonds – experimental data, open squares – theoretical fit). Theoretical fit is the result of a trial-and-error search. Redrawn from [21].*

2.5.3 Concentration Dependent $\overline{\chi}$

The concentration dependent $\overline{\chi}(\phi)$, eq. (2.2), can be obtained from the interaction free energy (2.25) as $\overline{\chi} = -\frac{d}{d\phi}\frac{F_{int}}{kT\phi}$. Using the equilibrium condition (2.26) we find

$$\overline{\chi}_K = p_e\chi_{AS} + (1-p_e)\chi_{BS} - \chi_{AB}p_e(1-p_e) \tag{2.28}$$

Thus, within the K model the ϕ dependence of $\overline{\chi}_K$ is due to $p_e(\phi)$. In order to specify $\partial\overline{\chi}_K/\partial\phi$ it is first necessary to obtain $\partial p_e(\phi)/\partial\phi$ by differentiating the equilibrium condition (2.26) with respect to ϕ leading to

$$\frac{\partial p_e(\phi)}{\partial\phi} = \frac{\partial\overline{\chi}_K}{\partial p_e}\frac{\phi}{\partial^2 F_{int}/\partial p^2}. \tag{2.29}$$

Here, and later in (2.30), $\partial^2 F_{int}/\partial p^2$ signifies the value of (2.27) in equilibrium i.e., $p = p_e(\phi)$. Equation (2.29) indicates that the sign of $\partial p_e(\phi)/\partial\phi$ is determined by $\partial\overline{\chi}_K/\partial p_e$. This reflects the concentration dependence of $K_K = const' \times \exp(\phi\partial\overline{\chi}_K/\partial p_e)$. Altogether

$$\frac{d\overline{\chi}_K}{d\phi} = \frac{\partial\overline{\chi}_K}{\partial p_e}\frac{\partial p_e}{\partial\phi} = \left(\frac{\partial\overline{\chi}_K}{\partial p_e}\right)^2\frac{\phi}{\partial^2 F_{int}/\partial p^2} \geq 0 \tag{2.30}$$

and $\overline{\chi}_K$ is an increasing function ϕ for any choice of the parameters χ_{AS}, χ_{BS}, χ_{AB} and $\Delta\epsilon$ except for the case $\chi_{AS} = \chi_{BS}$ and $\chi_{AB} = 0$ when $d\overline{\chi}_K/d\phi = 0$.

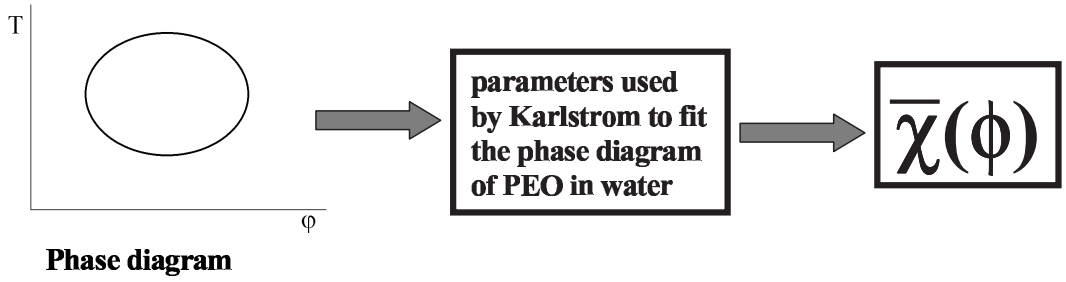

Figure 2.5: *Calculation of the $\overline{\chi}_K(\phi)$ for the K model.*

To calculate $\overline{\chi}_K(\phi)$ we utilize the parameters used to fit the phase diagram of PEO in water [21] as shown in the Figure 2.5. The calculated $\overline{\chi}_K(\phi)$ is in semiquantitative agreement with the experimental results for $\overline{\chi}(\phi)$ (Figure 2.6). The resulting curve is representative of the behavior of $\overline{\chi}_K(\phi)$ in general.

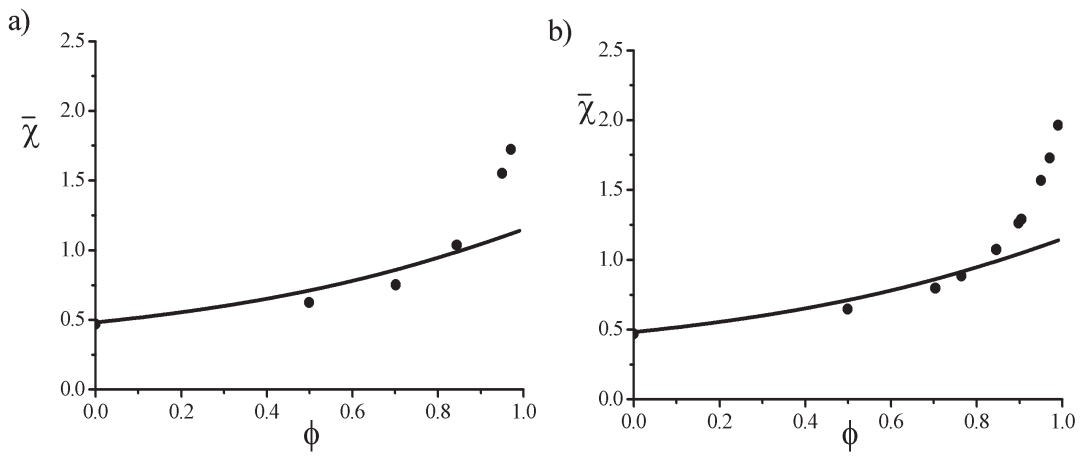

Figure 2.6: $\overline{\chi}_K$ vs. ϕ *(continuous line) calculated using* $\chi_{AS} = 80.0/T$, $\chi_{BS} = 684.5/T$, $\chi_{AB} = 155.6/T$ *and* $\Delta\epsilon = -625.2/T + \ln 8$, *the parameters used to fit the phase diagram of PEO, agree semiquantitatively with the experimental values of* $\overline{\chi}$ *(full circles) as measured with* $M_w = 3000$ *at (a)* $T = 55^o$ *C and (b)* $T = 65^o$ *C. While the numerical values and the curvature of* $\overline{\chi}_K$ *change with the choice of* χ_{AS}, χ_{BS}, χ_{AB} *and* $\Delta\epsilon$, *it is a monotonically increasing function of* ϕ.

2.6 Matsuyama-Bekiranov Model

The interconversion in the MB model is due to binding and unbinding of water to the backbone rather than the change in the state of a monomer as in the K model. It distinguishes between water bound to the chain and free water (Figure 2.7), though it ignores the hydrogen bonding in water.

2.6.1 Free Energy

The mixing energy per site in the MB model is identical in form to that of the K model

$$\frac{E_{mix}}{kT} = \phi p \Delta\epsilon + (1-\phi)\phi\left[p\chi_{AS} + (1-p)\chi_{BS}\right] + \phi^2 \chi_{AB} p(1-p) \tag{2.31}$$

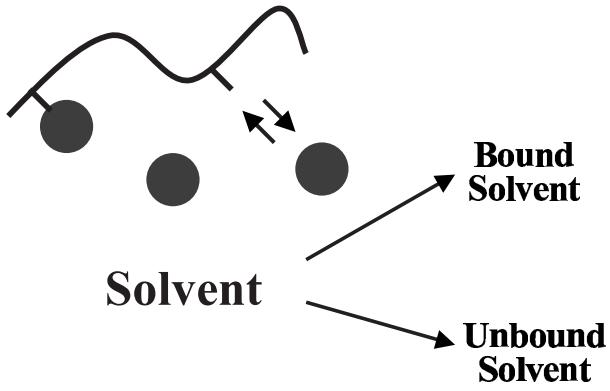

Figure 2.7: *Bound and unbound solvent in the MB model.*

while the mixing entropy per site is

$$\begin{aligned}\frac{S_{mix}}{k} &= -\phi[p\ln p+(1-p)\ln(1-p)]- \\ &\quad \left[\frac{\phi}{N}\ln\phi+(1-\phi-p\phi)\ln(1-\phi-p\phi)\right] \end{aligned} \tag{2.32}$$

These differ from the corresponding expressions within the K model in two respects: (i) Terms linear in ϕ are no longer present because the dependence on p_* disappears since $p(\phi=1)=0$ (ii) The translational entropy contribution to S_{mix} now depends on p because $\phi_0 = 1-\phi-p\phi$. $F_{int} = F_{mix} - F_{trans}$ is

$$\begin{aligned}\frac{F_{int}}{kT} &= \phi p\Delta\epsilon+\phi(1-\phi)[p\chi_{AS}+(1-p)\chi_{BS}]+\phi^2\chi_{AB}p(1-p) \\ &\quad +\phi[p\ln p+(1-p)\ln(1-p)]-p\phi\ln(1-\phi)+ \\ &\quad (1-p\phi-\phi)\ln\left(1-\frac{p\phi}{1-\phi}\right). \end{aligned} \tag{2.33}$$

The equilibrium value of p, for a given ϕ and T is specified by the condition $\partial F_{int}/\partial p = 0$

$$\begin{aligned}K_{MB}(\phi,p_e,T) &= \frac{p_e}{(1-p_e)(1-p_e\phi-\phi)} = \\ &\quad \exp\left[1-\Delta\epsilon-(1-\phi)(\chi_{AS}-\chi_{BS})-\phi\chi_{AB}(1-2p_e)\right] \end{aligned} \tag{2.34}$$

where $K_{MB} = eK_K$ is the equilibrium constant for the $B + S \rightleftarrows A$ reaction. As in the K model, K_{MB} is independent of ϕ when $\chi_{AS} = \chi_{BS}$ and $\chi_{AB} = 0$. However, in the MB model p_e depends on ϕ even when K_{MB} does not because of the loss of translational entropy of the bound water. The stability condition for the $B+S \rightleftarrows A$ reaction, $\partial^2 F/\partial p^2 > 0$, leads to

$$\frac{\partial^2 F}{\partial p^2} = \phi \left[\frac{1}{p(1-p)} - 2\phi\chi_{AB} + \frac{\phi}{1-\phi-p\phi} \right] > 0. \tag{2.35}$$

2.6.2 Phase Diagram of PEO in Water

In comparison to the K model, the MB model produces better phase diagram of the PEO in water (Figure 2.8). However, the fit remains semiquantitative.

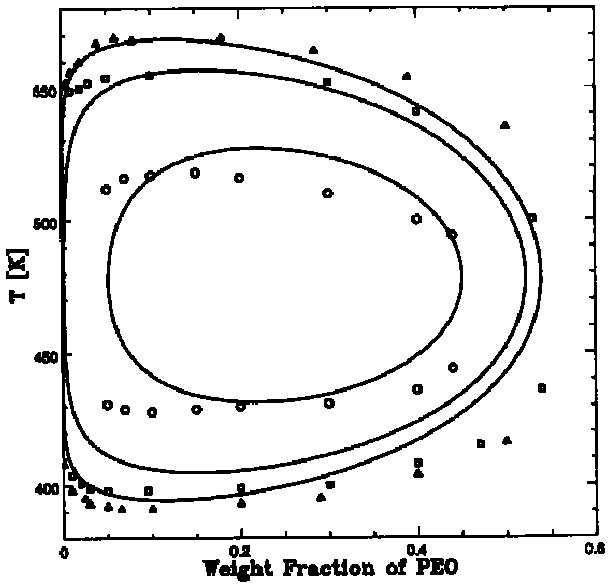

Figure 2.8: *Phase diagram of PEO in water in the MB model for different molecular weights. Experimental data are presented by scatter points, solid lines are theoretical fits. Redrawn from ref. [23].*

2.6.3 Concentration Dependent $\overline{\chi}$

Using $\overline{\chi} = -\frac{d}{d\phi}\frac{F_{int}}{kT\phi}$ and the equilibrium condition (2.34) we find

$$\overline{\chi}_{MB} = p_e\chi_{AS} + (1-p_e)\chi_{BS} - \chi_{AB}p_e(1-p_e) + \frac{p_e}{\phi} + \frac{1}{\phi^2}\ln\left(1 - \frac{p_e\phi}{1-\phi}\right). \quad (2.36)$$

While the first three terms are identical in form to $\overline{\chi}_K$ these are now supplemented

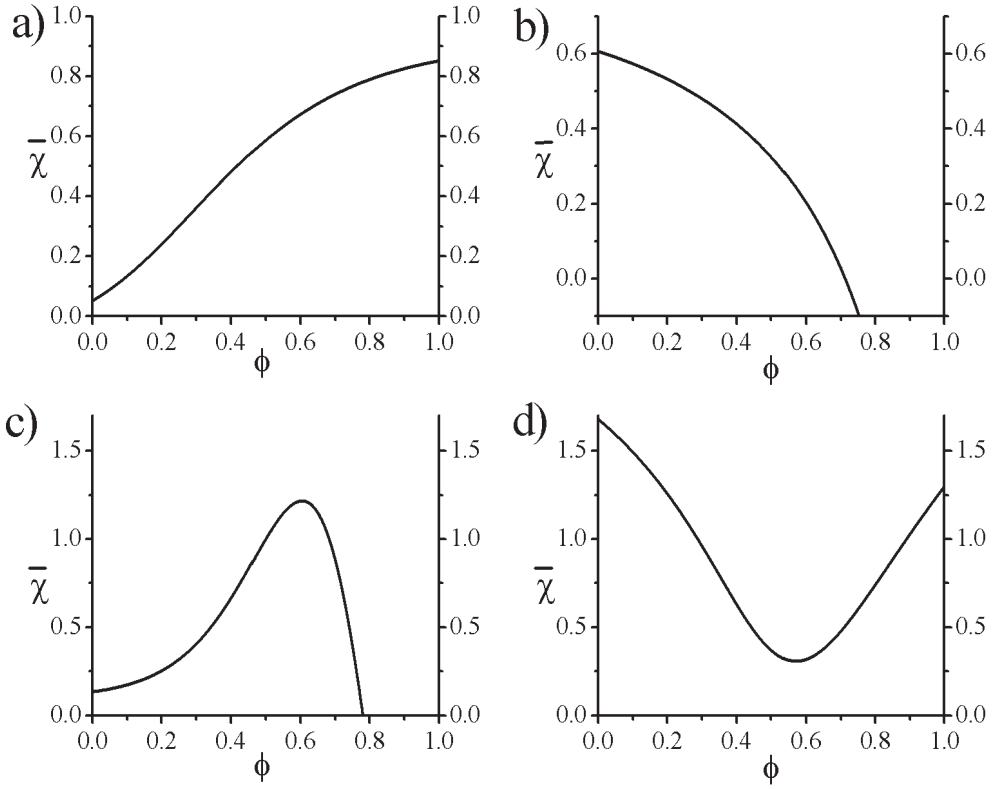

Figure 2.9: $\overline{\chi}_{MB}$ vs. ϕ *plots exhibit qualitatively different forms, depending on the choice of parameters (a) monotonically increasing* $\chi_{AS} = 0.7$, $\chi_{BS} = 0.9$, $\chi_{AB} = 2$ *and* $\Delta\epsilon = 4$, *(b) monotonically decreasing* $\chi_{AS} = 0.1$, $\chi_{BS} = 0.4$, $\chi_{AB} = -3$ *and* $\Delta\epsilon = 5$, *(c) maximum* $\chi_{AS} = 9$, $\chi_{BS} = 0.1$, $\chi_{AB} = 0.1$ *and* $\Delta\epsilon = -5$, *(d) minimum* $\chi_{AS} = 3$, $\chi_{BS} = 3$, $\chi_{AB} = 0.5$ *and* $\Delta\epsilon = -2$.

by two additional terms arising from the translational entropy of the water. When

$\chi_{AS} = \chi_{BS} = \chi$ and $\chi_{AB} = 0$ the interaction terms are constant, $\overline{\chi}_K = \chi$, and the ϕ dependence of $\overline{\chi}_{MB}$ reflects solely the entropic contribution. Again we obtain $\partial p_e(\phi)/\partial\phi$ by differentiating the equilibrium condition, (2.34), with respect to ϕ finding

$$\frac{\partial p_e(\phi)}{\partial \phi} = \frac{\partial \overline{\chi}_{MB}}{\partial p_e} \frac{\phi}{\partial^2 F_{int}/\partial p^2}. \tag{2.37}$$

In equation (2.37), and later in (2.38), $\partial^2 F_{int}/\partial p^2$ denotes the value of (2.35) in

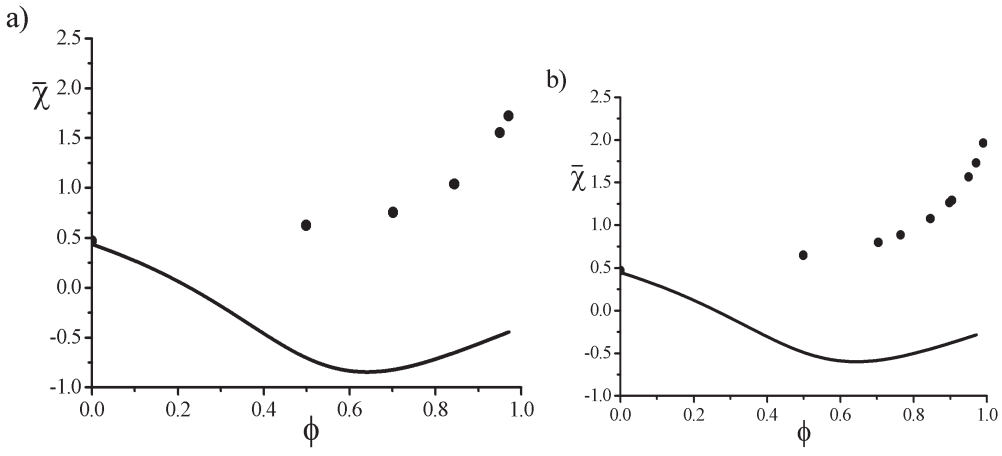

Figure 2.10: $\overline{\chi}_{MB}$ vs. ϕ *(continuous line) calculated using* $\chi_{AS} = \chi_{BS} = \chi = 2.885 - 0.0036T$, $\chi_{AB} = 0$ *and* $\Delta\epsilon = -625.2/T + \ln 8$, *the parameters used to fit the phase diagram of PEO, qualitatively differ from the experimental values of* $\overline{\chi}$ *(full circles) as measured with* $M_w = 3000$ *at (a)* $T = 55^o$ *C and (b)* $T = 65^o$ *C [31].*

equilibrium. While equation (2.37) is similar in form to (2.29) the two are not identical because the two models yield different p_e and because $\partial\overline{\chi}_{MB}/\partial p_e \neq \partial\overline{\chi}_K/\partial p_e$. As before the sign of $\partial p_e(\phi)/\partial\phi$ is determined by $\partial\overline{\chi}_{MB}/\partial p_e$. This reflects the concentration dependence of $K'_{MB} = (1 - \phi - p\phi)K_{MB}$ in particular, $\partial\overline{\chi}_{MB}/\partial p_e = \partial \ln K'_{MB}/\partial\phi$. Upon substituting $\partial p_e(\phi)/\partial\phi$ into $\partial\overline{\chi}_{MB}/\partial\phi$ as found from (2.36) we obtain

$$\frac{d\overline{\chi}_{MB}}{d\phi} = \left(\frac{\partial\overline{\chi}_{MB}}{\partial p_e}\right)^2 \frac{\phi}{\partial^2 F_{int}/\partial p^2} - \frac{2}{\phi^3}\ln\left(1-\frac{p_e\phi}{1-\phi}\right) - \frac{p_e}{\phi^2}\left[1+\frac{1}{(1-\phi)(1-p_e\phi-\phi)}\right] \tag{2.38}$$

The first two terms are positive. Of these, the first is analogous to the corresponding result within the K model. The third term is negative. As a result, $d\overline{\chi}_{MB}/d\phi$ is no longer positive definite. Depending on the choice of χ_{AS}, χ_{BS}, χ_{AB} and $\Delta\epsilon$ the calculated $\overline{\chi}_{MB}$ can be monotonically increasing or decreasing as well as exhibit a minimum or a maximum (Figure 2.9). In the case of PEO the calculated $\overline{\chi}_{MB}(\phi)$, utilizing the parameters used to fit the phase diagram of PEO, *differs qualitatively* from the experimentally measured $\overline{\chi}(\phi)$ (Figure 2.10).

2.7 Dormidontova Model

2.7.1 Free Energy

The D model allows for hydrogen bonds of two types: between polymer and water and among water molecules themselves. The energy gain due to hydrogen bonding is thus the sum

$$\frac{E_{hb}}{kT} = n_p\Delta\epsilon_p + n_q\Delta\epsilon_q \tag{2.39}$$

where $\Delta\epsilon_p$ is the energy difference between bare monomers and monomers forming a hydrogen bond, $\Delta\epsilon_q$ is the corresponding energy difference of association in water. n_p is the total number of hydrogen bonds between polymer and water and n_q is the number of water–water hydrogen bonds.

Assume, that the volume of a monomer is not equal to the volume of a water molecule. Then the volume fraction of polymer can be written as $\phi_p = \omega\phi$, where ω is the ration between volumes of a monomer and a water molecule, while the volume fraction of water is $\phi_q = 1-\phi$. In the D model $\omega = 1/3$ is a constant which

does not depend ni on temperature nor on volume fraction. Each oxygen atom on polymer and on water can form two hydrogen bonds. Thus, the total number of proton acceptors on polymer is $2NN_p$, where N is the polymerization degree and N_p is the number of polymer chains. The number of proton acceptors on water is $2N_q$, where N_q is the number of water molecules.

We can write the numbers of hydrogen bonds of two types per lattice site as

$$n_p \frac{a^3}{V} = 2p\phi_p = 2p\omega\phi \tag{2.40}$$

and

$$n_q \frac{a^3}{V} = 2q\phi_q = 2q(1-\phi) \tag{2.41}$$

where $p = n_p/(2NN_p)$ is the fraction of hydrogen bonds on polymer and $q = n_q/(2N_q)$ is the fraction of water – water hydrogen bonds.

With this, the mixing energy per lattice site, E_{mix}, is written in a similar in form to that in the K and MB models,

$$\begin{aligned} \frac{E_{mix}}{kT} &= 2\omega\phi p\Delta\epsilon_p + 2(1-\phi)q\Delta\epsilon_q + \phi(1-\phi)[p\chi_{AS} + (1-p)\chi_{BS}] \\ &\quad +\phi^2\chi_{AB}p(1-p) + \text{terms linear in } \phi \end{aligned} \tag{2.42}$$

where the last two terms accounts for the interaction of bare and hydrogen bonded monomers with water and between each other. Strictly speaking, these two terms should also contain ω, but it can be absorbed in χ_{AS}, χ_{BS} and χ_{AB} parameters.

The entropy of hydrogen bonds is calculated as follows. The hydrogen bonds can be formed between adjacent sites only. However, we first forget about this restriction and we calculate the number of ways to distribute donors and acceptors on the lattice, which are not necessary adjacent. The number of ways to select n_p acceptors on polymer among $2NN_p$ possible, n_q acceptors on water among $2N_w$ and $n_p + n_q$ proton donors out of $2N_w$ possible is [72]

$$Q = \frac{(2N_pN)!}{(2N_pN - n_p)!}\frac{(2N_w)!}{(2N_w - n_q)!}\frac{(2N_w)!}{(2N_w - n_p - n_q)!}\frac{1}{n_p!n_q!} \tag{2.43}$$

To take into account only donors and acceptors, which are adjacent, Q should be multiplied by the probability for a configuration of hydrogen bonds to contain only adjacent bonds [72]

$$P = (p_{w-w})^{n_q}(p_{p-w})^{n_p} \tag{2.44}$$

where p_{w-w} is the probability that a given donor–acceptor pair on water lie in adjacent cells and p_{p-w} is the probability that a given pair of a donor on water and an acceptor on polymer lie in adjacent cells [72].

The total entropy is a sum of the entropy of hydrogen bonds and the Flory mixing entropy

$$\frac{S}{k} = -\left[\frac{\phi}{N}\ln\phi + (1-\phi)\ln(1-\phi)\right] - \ln(QP) \tag{2.45}$$

Applying the Stirling approximation we get the total mixing entropy per lattice site in the form

$$\begin{aligned}\frac{S_{mix}}{k} \;=\; & -\left[\frac{\phi}{N}\ln\phi + (1-\phi)\ln(1-\phi)\right] - 2(1-\phi)q\ln p_{w-w} - 2\omega\phi p\ln p_{p-w} \\ & -2\omega\phi[p\ln p + (1-p)\ln(1-p)] - 2(1-\phi)q\left[\ln q + (1-q)\ln(1-q)\right] \\ & -\left[2(1-\phi)(1-q) - 2p\phi\omega\right]\ln\left[2(1-\phi)(1-q) - 2p\phi\omega\right] \\ & +2(1-\phi)\ln 2(1-\phi)\end{aligned} \tag{2.46}$$

The corresponding fraction of hydrogen bonds in pure water, $q_0 \neq 0$, and $F_{mix} = F - (1-\phi)F(\phi = 0, q = q_0) - \phi F(\phi = 1)$. As before, the interaction energy is $F_{int} = F_{mix} - F_{trans}$, where F_{trans} is determined by eq. (2.20).

$$\begin{aligned}\frac{F_{mix}}{kT} &= 2\omega\phi p\Delta f_p + 2(1-\phi)q\Delta f_q + \phi(1-\phi)[p\chi_{AS} + (1-p)\chi_{BS}] \\ &+\phi^2\chi_{AB}p(1-p) + \\ &-2\omega\phi[p\ln p + (1-p)\ln(1-p)] - 2(1-\phi)q\left[\ln q + (1-q)\ln(1-q)\right] \\ &-\left[2(1-\phi)(1-q) - 2p\phi\omega\right]\ln\left[2(1-\phi)(1-q) - 2p\phi\omega\right] \\ &+2(1-\phi)\ln 2(1-\phi) - \left[\frac{\phi}{N}\ln\phi + (1-\phi)\ln(1-\phi)\right] \\ &-2(1-\phi)\left[q_0\Delta f_q + (q_0\ln q_0 + (1-q_0)\ln(1-q_0)\right) \\ &+(1-q_0)\ln 2(1-q_0) - \ln 2] \end{aligned} \tag{2.47}$$

where $\Delta f_p = \Delta\epsilon_p + \ln p_{p-w}$ is the free energy per kT of polymer–water hydrogen bonds and $\Delta f_q = \Delta\epsilon_q + \ln p_{w-w}$ is the free energy per kT of self-association in water. The last term in (2.47) arises because of the association in water. Water molecules form hydrogen bonds among themselves and the free energy of pure water is nonzero.

The equilibrium value of p for a given ϕ and T, $p_e = p_e(\phi)$, is specified by the condition $\partial F/\partial p = 0$ leading to

$$\begin{aligned}&\frac{p_e}{(1-p_e)\left(2(1-q)(1-\phi) - 2\omega\phi p\right)} = K_D^{(p)}(\phi, p_e, q_e, T) = \\ &\exp\left[1 - \Delta f_p - (1-\phi)(\chi_{AS} - \chi_{BS}) - \phi\chi_{AB}(1-2p_e)\right]\end{aligned} \tag{2.48}$$

where $K_D^{(p)}$ is the equilibrium constant for the bimolecular intrachain $B + s \rightleftarrows A$ reaction. The equilibrium value of q is specified by the condition $\partial F/\partial q = 0$ leading to

$$\begin{aligned}&\frac{q_e}{(1-q_e)\left(2(1-q)(1-\phi) - 2\omega\phi p\right)} = K_D^{(q)}(\phi, p_e, q_e, T) = \\ &\exp\left[1 - \Delta f_q - (1-\phi)(\chi_{AS} - \chi_{BS}) - \phi\chi_{AB}(1-2p_e)\right]\end{aligned} \tag{2.49}$$

The stability conditions for bimolecular reactions, $\partial^2 F/\partial p^2 > 0$ and $\partial^2 F/\partial q^2 > 0$, are

$$\frac{\partial^2 F}{\partial p^2} = 2\omega\phi\left[\frac{1}{p(1-p)} + \frac{2\omega\phi}{2(1-q)(1-\phi) - 2\omega\phi p}\right] > 0 \tag{2.50}$$

$$\frac{\partial^2 F}{\partial q^2} = 2(1-\phi)\left[\frac{1}{q(1-q)} + \frac{2(1-\phi)}{2(1-q)(1-\phi) - 2\omega\phi p}\right] > 0 \qquad (2.51)$$

2.7.2 Phase Diagram of PEO in Water

Among the three models, the D model represent the best fit (Figure 2.11). The parameters are obtained by fitting one of high molecular weight polymers, while other curves was plotted using these parameters.

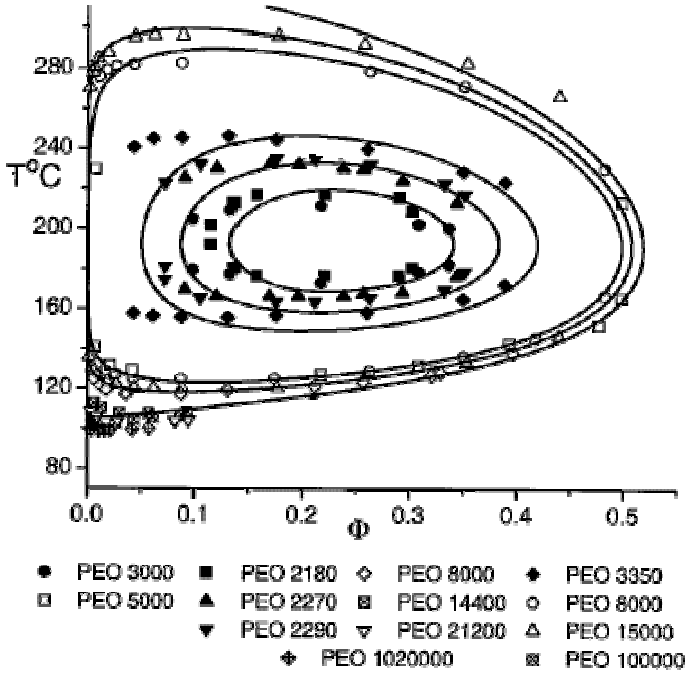

Figure 2.11: *Phase diagram of PEO in water. Inner loops correspond to small molecular weights of polymer, while outer loops correspond to high molecular wights. (Redrawn from [24])*

2.7.3 Concentration Dependent $\overline{\chi}$

As before, the concentration dependent $\overline{\chi}(\phi)$, eq. (2.2), can be obtained from the interaction free energy (2.25) as $\overline{\chi} = -\frac{d}{d\phi}\frac{F_{int}}{kT\phi}$. Assuming that $\chi_{AB} = 0$, $\chi_{AS} = \chi_{BS} = \chi$ after series of simplifications[2] we find

$$\overline{\chi}_D = \chi + \frac{2}{\phi}(p_e\omega - q_e) + \frac{2}{\phi^2}\left(q - q_0 + \ln\frac{q}{q_0(1-\phi)}\right) \tag{2.52}$$

where q, q_0 and p are determined from the equilibrium conditions (2.48-2.49).

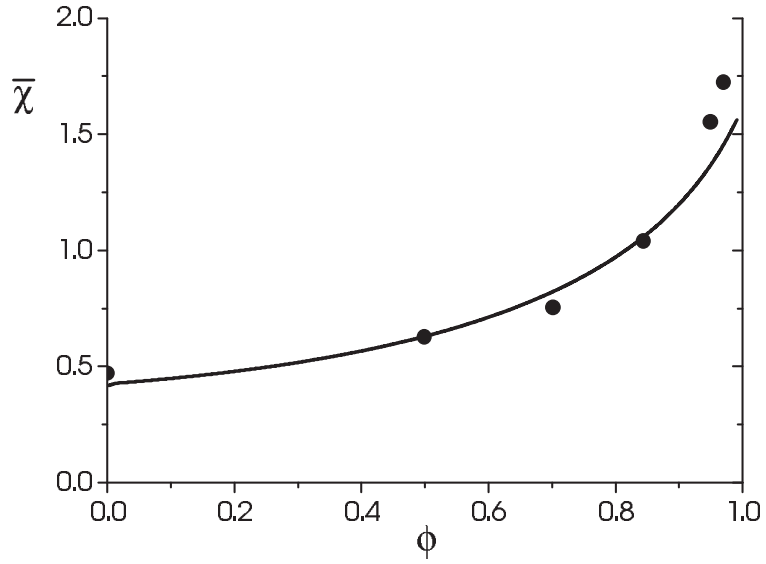

Figure 2.12: *$\overline{\chi}_D$ as a function of ϕ (continuous line) calculated using $\omega = 1/3$, $\chi_{AS} = \chi_{BS} = \chi = -0.211 + 93.5/T$, $\chi_{AB} = 0$ and $\Delta f_p = 4.35 - 2000/T$ and $\Delta f_p = 4.35 - 2000/T$, the parameters used to fit the phase diagram of PEO in the D model, qualitatively agrees with the experimental values of $\overline{\chi}$ (full circles) as measured with $M_w = 3000$ at $T = 65^o$ C [74].*

The morphology of the ϕ-dependence of $\overline{\chi}_D$ is similar to the MB model. It can exhibit increasing and decreasing dependencies. It can also have minimums and

[2] $\overline{\chi}$ can be calculated using two equilibrium conditions (2.48-2.49) as $\overline{\chi} = -\frac{\partial}{\partial\phi}\frac{F_{int}}{kT\phi} - \frac{\partial p}{\partial\phi}\frac{\partial}{\partial p}\frac{F_{int}}{kT\phi} - \frac{\partial q}{\partial\phi}\frac{\partial}{\partial q}\frac{F_{int}}{kT\phi}$, where $\partial/\partial\phi$ designates the partial derivative.

maximums. Utilizing the parameters used to fit the phase diagram of PEO in water [24] we can compare the experimental curve with the calculated one (Figure 2.12). This plot shows rather good agreement in a wide range of concentrations, except for the region of high concentrations.

2.8 Conclusion

As we have seen, three versions of the "hydrophobic-hydrophilic" two-state model for neutral water-soluble polymers in aqueous solutions lead to a ϕ dependent χ_{eff}. The K version, where the two-states undergo unimolecular intrachain conversion, results in $\partial\overline{\chi}/\partial\phi > 0$. Using χ_{AS}, χ_{BS}, χ_{AB} and $\Delta\epsilon$ as obtained by fitting the phase diagram of PEO this model yields $\overline{\chi}$ that agrees semiquantitatively with the experimentally observed values [1, 31] (Figure 2.6). Within the MB model the hydrophilic monomeric state binds a water molecule. As a result, the interconversion reaction is bimolecular and the translational entropy of the water plays a role in determining the equilibrium state. In this model $\overline{\chi}$ can display a number of scenarios (Figure 2.9): $\overline{\chi}(\phi)$ can be monotonically increasing, monotonically decreasing or exhibit an extremum (maximum or minimum). The $\overline{\chi}$ vs. ϕ as calculated with the parameters used to fit the phase diagram of PEO, differs qualitatively from the experimentally obtained curve (Figure 2.10). However, the $\partial\overline{\chi}/\partial\phi < 0$ behavior allowed by this model is of interest since it has been observed in aqueous solutions of the neutral water-soluble polymer PVP [32] (Figure 2.2). The D model allows for polymer–water and water–water hydrogen bonds. This leads to two bimolecular interconversion reactions. The D model also exhibits $\overline{\chi}(\phi)$ which can be increasing, decreasing function as well as to show extremum. The parameters used to fit phase diagram of PEO in water provide the best agreement among all three models for $\overline{\chi}(\phi)$.

These results stress the importance of using the experimental values of $\overline{\chi}$ in fitting χ_{AS}, χ_{BS}, χ_{AB} and $\Delta\epsilon$ and in evaluating the performance of the model. From the perspective of the general theory of polymers it is of interest that the "two-state"

models can account for the dependence of χ_{eff} on ϕ, T and the pressure while retaining the principal approximations of the Flory-Huggins theory, *i.e.* incompressibility, monomer and solvent of identical size and shape that equals the global one.

Chapter 3

Single-State Polymers: $\chi_{eff}(\phi)$-Parameter

3.1 Résumé

Le dépendance en concentration de $\overline{\chi}$ peut arriver avec les polymères habituels à un seul état dans les solutions non aqueuses. Les mesures expérimentales confirment que $\overline{\chi}$ peut être une fonction croissante de même que décroissante avec ϕ. Nous y discutons les modèles alternatifs applicable aux solutions aqueuses et non aqueuses qui mènent à $\chi_{eff}(\phi)$: le modèle n-cluster [76, 77], le modèle des Agrégats sur Réseau [78, 79, 80, 81] et le modèle de Painter *et al* [82].

3.2 Introduction

The concentration dependence of $\chi_{eff}(\phi)$ is not inherently related to the two-state models. This dependence can occur for usual single-state polymers. Experiments confirm that $\overline{\chi}$ can be increasing as well as decreasing function of ϕ not only for water-soluble polymers, but also for polymers in nonaqueous solutions [12, 25, 73, 83] (Figure 3.1).

In this section we discuss alternative mechanisms leading to $\chi_{eff}(\phi)$. They can be

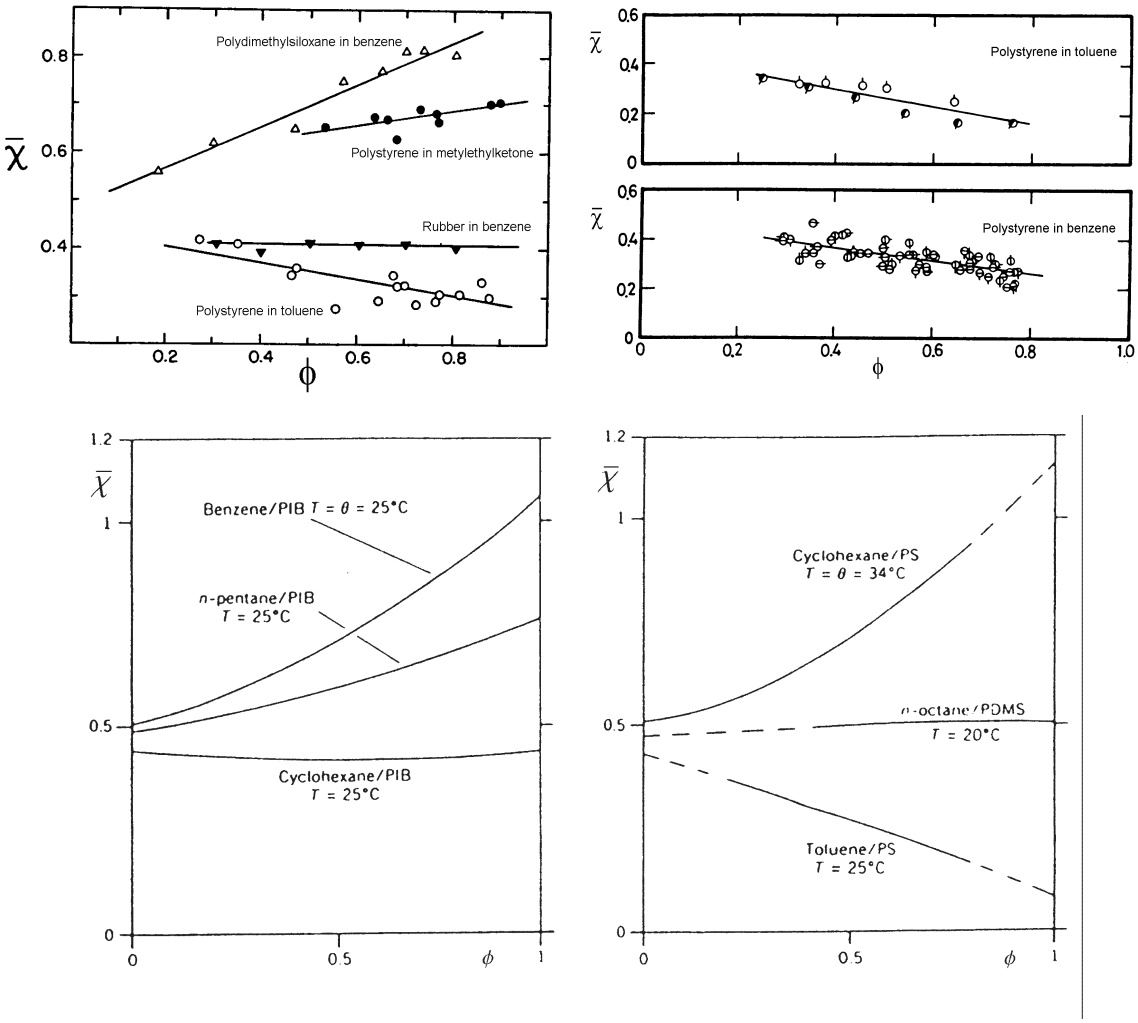

Figure 3.1: *Experimentally measured $\overline{\chi}$ vs. ϕ dependencies for different polymers in nonaqueous solvents [12, 25, 83].*

applied to aqueous and nonaqueous solutions of polymers. Considerable effort was devoted to clarifying the statistical mechanical origins of the $\chi_{eff}(\phi)$ dependence and other deviations from the Flory-Huggins theory. Various extensions of the Flory-Huggins theory allow for compressibility [84, 85], local composition [86, 87] and the role of intrachain contacts [82]. Recently, the lattice cluster theory utilized a more accurate solution of the lattice model while allowing for the structure of the monomers [78, 79]. For brevity we limit this discussion to three physically

transparent models.

3.3 Molecular Models Leading to $\chi_{eff}(\phi)$

3.3.1 n-Cluster Model

The n-cluster model was proposed by de Gennes for aqueous solutions of PEO [76, 77]. This model was motivated by two experimental observations concerning the behavior of such solutions: (i) the interpretation of calorimetric measurements in terms of the Flory mixing free energy yields a $\overline{\chi}$ that increases strongly with ϕ [1, 31] and (ii) reports of formation of aggregates in concentrated solutions of PEO [88]. Within this model the concentration dependence of χ_{eff} is attributed to attractive interactions leading to stable clusters of $n > 2$ monomers while binary monomer-monomer interactions remain repulsive (Figure 3.2).

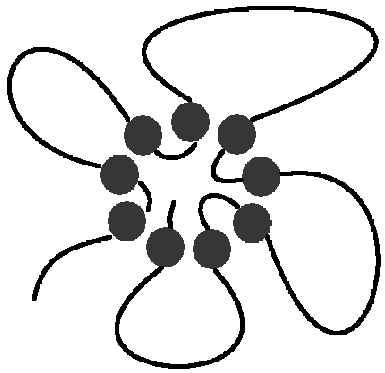

Figure 3.2: *Formation of a cluster of n monomers in the n-cluster model.*

This is another variation of a two-state model involving a dynamic equilibrium between "clustered" and "unclustered" monomers. In molecular terms, a n-cluster may correspond to a micelle or a mixed helix. The formation of the n-clusters gives rise to an additional term, $-\rho(T)\phi^n$ (with $\rho > 0$), in the interaction free energy.

Thus, the mixing free energy per site is

$$\frac{F_{mix}}{kT} = \chi\phi(1-\phi) + \rho(T)(\phi - \phi^n) + \frac{\phi}{N}\ln\phi + (1-\phi)\ln(1-\phi) \tag{3.1}$$

leading to

$$\chi_{eff} = \chi + \rho\frac{1-\phi^{n-1}}{1-\phi}. \tag{3.2}$$

The corresponding $\overline{\chi}$ is

$$\overline{\chi} = \chi + \rho(n-1)\phi^{n-2} \tag{3.3}$$

which is an increasing function of ϕ.

The n-cluster model is indeed capable of rationalizing the two experimental observations noted above. However of these, the second observation is now a subject of debate [89, 90]. Furthermore the molecular structure of the ethylenoxide monomers does not reveal amphiphilic motifs. It is thus difficult to justify the assumption of cluster formation in solutions of PEO. Accordingly, the validity of this model in the case of aqueous solutions of neutral water-soluble polymers such as PEO is not obvious. On the other hand, the model is indeed applicable to solutions of polysoaps where formation of inter and intrachain micelles does occur [91].

3.3.2 Lattice Cluster Model

Another molecular model that gives the concentration dependence of $\overline{\chi}$ is the Lattice Cluster model [78, 79, 80, 81]. It assumes that a monomer can occupy more than one lattice site (Figure 3.3). This assumption allows to take into account the monomer structure within the lattice Flory-type model. Such approach allows to predict miscibility pattern for different polymer blends.

In this model the ϕ-dependence of χ_{eff} arises from the packing constraints imposed by the monomer structures leading to different counting of nearest neighbor heterocontacts.

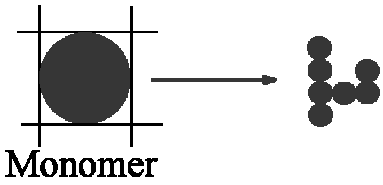

Figure 3.3: *Assumption that a monomer occupies more than one lattice site allows for the structure and the shape of the monomer.*

3.3.3 Model of Painter *et.al.*

This model, advanced by Painter *et al*, is applicable to all polymer solutions [82]. Within this model, the ϕ dependence of χ_{eff} is attributed to the interplay of intra-chain and interchain contacts (Figure 3.4).

The authors argue that there is a probability γ for intrachain monomer-monomer contacts. As a rough approximation, γ can be identified with the monomeric volume fraction, ϕ_G, within a Gaussian coil of radius $R_G \approx N^{1/2}a$ where N is the polymerization degree and a is the monomer size, $\phi_G \approx Na^3/R_0^3 \approx N^{-1/2}$. In a lattice comprising of N_T sites of coordination number z there are $N_T\phi$ sites occupied by monomers with a total of $N_T z\phi$ adjacent sites. Of the $N_T z\phi$ adjacent sites $N_T z\phi\gamma$ are occupied by monomers because of intrachain contacts. The total number of free,

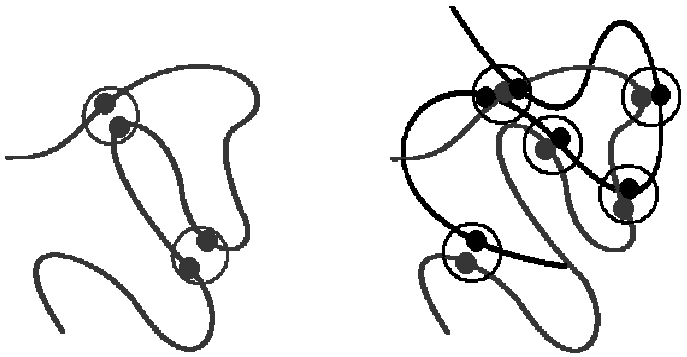

Figure 3.4: *The interplay between intra-chain and inter-chain contacts. Increasing concentration increases the number of intra-chain contacts.*

unblocked adjacent sites is thus $N_T z(1-\phi\gamma)$ while the number of free sites adjacent to monomers is $N_T z\phi(1-\gamma)$. The probability of a free site adjacent to a monomer is thus $\phi(1-\gamma)/(1-\phi\gamma)$. Accordingly, the number of monomer-solvent contacts is $N_T(1-\phi)\phi(1-\gamma)/(1-\phi\gamma)$. This expression allows for the requirement that a solvent molecule occupies an unblocked site adjacent to a monomer. Accordingly, the mixing energy term per site is $E_{mix}/kT = \chi(1-\phi)\phi(1-\gamma)/(1-\phi\gamma)$ yielding an enthalpic contribution to χ_{eff}

$$\chi_{eff} = \chi\frac{1-\gamma}{1-\phi\gamma} \tag{3.4}$$

and to a corresponding enthalpic $\overline{\chi}$

$$\overline{\chi} = \chi\left(\frac{1-\gamma}{1-\phi\gamma}\right)^2 \tag{3.5}$$

where, again, $\partial\overline{\chi}/\partial\phi > 0$. In their original paper, Painter *et al* supplemented this enthalpic $\overline{\chi}$ by an entropic one, allowing for the effect of the chain bending back on itself following the analysis of Huggins [26].

3.4 Conclusion

Aside from physical insight regarding the molecular origins of $\chi_{eff}(\phi)$, the above discussion identifies certain difficulties. Overall, it seems unlikely that one of the four models described above will emerge fully victorious. By construction, the n-cluster model is applicable only to solutions of associating polymers. The two "two-state" models are suitable candidates for the description of aqueous solutions of neutral water-soluble polymers exhibiting insolubility gap. While the model of Painter *et al* applies, in principle, to all polymeric systems it can not account for systems exhibiting $\partial\overline{\chi}/\partial\phi < 0$. Such behavior was actually observed in both aqueous and nonaqueous solutions, among the models considered above only the MB model and D model yield a scenario involving $\partial\overline{\chi}/\partial\phi < 0$. Altogether one can thus envision situations where *all the different mechanisms described may contribute simultaneously.* Another discouraging observation concerns the number of parameters involved. All

four models introduce additional parameters that do not appear in the familiar Flory-Huggins theory: γ in the model of Painter *et al*, ρ and n in the n-cluster model, $\Delta\epsilon$, χ_{AB}, χ_{AS} and χ_{BS} for the two "two-state" models. The necessity to unambiguously determine the additional parameters limits the predictive power of the models. Clearly, this problem is even more serious when a number of mechanisms contribute simultaneously to the ϕ dependence of χ_{eff}. Note however that this last difficulty can be partially resolved in certain cases. Thus the contribution of the mechanism of Painter *et al* can be separated from the one due to the "two-state" mechanism. This is because the mechanism of Painter *et al* is inherently a polymeric effect that disappears in the monomeric limit, $N = 1$. On the other hand, *the two-state models also apply to solution of the unpolymerized monomers, i.e.* χ_{eff} and $\overline{\chi}$ are independent of N.

Chapter 4

Signatures of $\chi_{eff}(\phi)$: Uniform Concentration

4.1 Résumé

Les conséquences macroscopique de $\chi_{eff}(\phi)$ sur le gonflement de chaînes isolées et de brosses planes sont étudié dans le cadre d'une théorie de champ moyen. La dépendance de $\chi_{eff}(\phi)$ engendre deux conséquences principales: un déplacement dans le crossover entre les régimes Gaussien et auto-évitant, et la possibilité d'une transition de phase du premier ordre pour les chaînes flexibles isolées. La discussion relate directement ces effets aux mesures thermodynamiques et n'implique pas un modèle microscopique spécifique.

4.2 Introduction

In this chapter we focus on the macroscopic consequences of $\chi_{eff}(\phi)$. In studying the signatures of $\chi_{eff}(\phi)$ one may adopt two strategies. One is to consider the problem within a specific microscopic model described in the previous chapter 3. While this approach allows to trace the physical origins of the effects, it suffers from two disadvantages. First, such analysis is limited to the $\chi_{eff}(\phi)$ predicted by

the particular model and is only relevant to systems where this model is physically reasonable. For example, some mechanisms are applicable to all polymeric solutions [78, 79, 82] while others operate only for solutions of associating polymers [91] or of neutral water-soluble polymers [34]. Second, each of the microscopic models proposed thus far introduces extra parameters that are presently unknown thus making confrontation with experiments difficult.

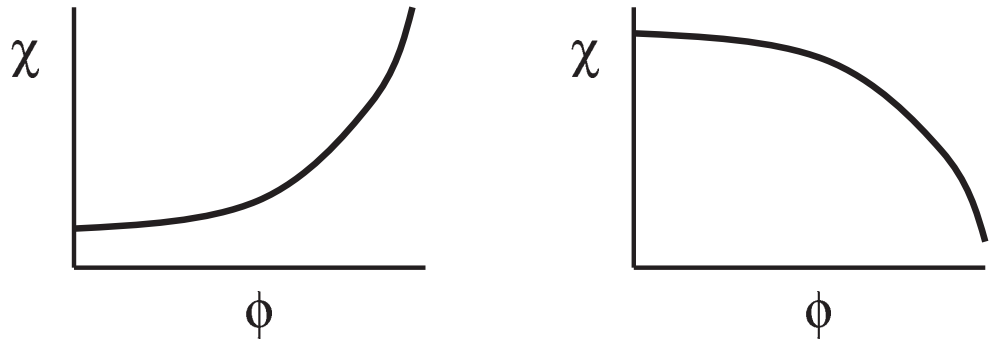

Figure 4.1: *In this section we forget about the origin of $\chi_{eff}(\phi)$ trying to understand the consequences of increasing and decreasing $\chi_{eff}(\phi)$.*

The second approach involves a phenomenological description utilizing $\chi_{eff}(\phi)$ as obtained from the colligative properties of polymer solutions (chapter 2.3). This strategy limits the physical understanding of the swelling behavior but allows to relate it to the solutions' colligative properties as observed experimentally. In the following we pursue the second, phenomenological approach (Figure 4.1). At present, the number of polymer-solvent system for which $\chi_{eff}(\phi)$ data are available is rather small. With this in mind we explore three routes: (i) investigate the consequences of certain experimentally measured $\chi_{eff}(\phi)$ curves (ii) utilize $\chi_{eff}(T, \phi)$ obtained from empirical equations whose parameters are determined by fitting the calculated phase diagram with the observed one (iii) study the signatures of hypothetical $\chi_{eff}(\phi)$ curves leading to qualitatively novel behavior.

This chapter concerns the signatures of $\chi_{eff}(\phi)$ in systems with *uniform* concentration. We start with the description of the solvent quality in systems with

$\chi_{eff}(\phi)$ in section 4.3. Background material on the thermodynamics of polymer solutions with $\chi_{eff}(\phi)$ and a brief unified description of the Flory and the Alexander approximations is provided in section 4.4. The next section 4.5 describes the effects of $\chi_{eff}(\phi)$ on the swelling behavior of isolated coils and planar brushes utilizing respectively the Flory and the Alexander approximations.

4.3 $\chi_{eff}(\phi)$ and Solvent Quality

In the Flory theory χ and the related second virial coefficient, $v = 1 - 2\chi$, measure the solvent quality. Thus $v > 0$ corresponds to a good solvent, $v = 0$ to a θ solvent while $v < 0$ indicates a poor one. An important characteristic of these three regimes is the associated swelling behavior: the span of an isolated chain in the three regimes scales respectively as $N^{3/5}$, $N^{1/2}$ and $N^{1/3}$. Typically, it is assumed that χ depends only on the temperature, $\chi = \chi(T)$ [12, 13, 14, 16]. However, the introduction of $\chi_{eff}(T, \phi)$ [1, 2, 12, 25, 26, 27, 28] requires, in turn, modification of the discussion of solvent quality. In the following we aim to clarify this issue by exploring some of the microscopic consequences of $\chi_{eff}(T, \phi)$[1].

The solvent quality of polymer solutions as characterized by $\chi_{eff}(T, \phi)$ concerns two issues: First is the stability of the solution with respect to phase separation due to diffusion of chains. The second is the degree of swelling of polymer coils. While the first issue was analyzed in considerable details [76, 77, 92, 93, 94, 95], less attention was given to the second topic [95, 96, 97]. Our purpose is to explore the signatures of $\chi_{eff} = \chi_{eff}(T, \phi)$ on the swelling behavior of isolated coils and of brushes of terminally anchored chains. In turn, these signatures of the solvent quality involve two aspects. One is a *"global"* solvent quality as revealed in systems of *uniform* density. To study this facet we consider the effect of $\chi_{eff}(\phi)$ on the swelling behavior in two cases: (i) an isolated coil within the Flory approximation [12, 13, 98, 99] in section 4.5.2 and (ii) a brush as described by the Alexander

[1] In the literature [25, 28, 29, 73], χ_{eff} is sometimes denoted by g while χ denotes $\overline{\chi} = \chi_{eff} - (1-\phi)\partial\chi_{ef}/\partial\phi$. Our notation aims to avoid confusion with the customary usage of χ.

model [100, 101] (section 4.5.3). As we shall discuss, the global solvent quality is characterized by $\overline{\chi}(\phi) = \chi_{eff} - (1-\phi)\partial\chi_{eff}/\partial\phi$ rather than by $\chi_{eff}(\phi)$. For systems involving *gradients* in ϕ, it is necessary to consider a *"local"* solvent quality. In such systems $\overline{\chi}(\phi)$ is no longer the sole measure of the solvent quality. The local solvent quality of brushes with concentration gradient is explored in chapter 5 using the SCF theory and Pincus approximation.

4.4 Thermodynamics of Polymer Solutions with $\chi_{eff}(\phi)$

To summarize the thermodynamics of polymer solutions characterized by $\chi_{eff}(T,\phi)$ we focus on the balance of osmotic pressure and elastic restoring force in determining the swelling behavior. This presentation makes for a direct relationship between the macroscopic thermodynamic properties and the microscopic swelling behavior. The replacement of $\chi = \chi(T)$ by $\chi_{eff} = \chi_{eff}(T,\phi)$[2] requires certain modifications in the thermodynamics of polymer solutions [25, 28].

The mixing free energy per lattice site in the units of kT, f, consists of two terms $f = f_{int} + f_{trans}$. One is an interaction free energy $f_{int} = \chi_{eff}(\phi)\phi(1-\phi)$ that is the counterpart of the mixing energy $\chi\phi(1-\phi)$. The second is the familiar translational free energy $f_{trans} = \phi/N \ln\phi + (1-\phi)\ln(1-\phi)$. As usual, the chemical potential of the solvent is $\mu_s = \mu_s^o(P,T) - \pi a^3$, where $\pi = a^{-3}\phi^2\partial(f/\phi)/\partial\phi$ is the osmotic pressure in units of kT

$$\pi a^3 = \frac{\phi}{N} - \phi - \ln(1-\phi) - \overline{\chi}\phi^2 \tag{4.1}$$

and a^3 is the volume of a unit cell in of the lattice. However, π now depends on $\overline{\chi}$

$$\overline{\chi} = \chi_{eff} - (1-\phi)\frac{\partial\chi_{eff}}{\partial\phi} \tag{4.2}$$

instead of χ. Since μ_s determines the colligative properties of the solution, measurements of such properties yield $\overline{\chi}$ rather than χ_{eff}. It is the $\overline{\chi}$ values that are usually

[2] For brevity we will often replace $\chi_{eff}(T,\phi)$ and $\overline{\chi}(T,\phi)$ by $\chi_{eff}(\phi)$ and $\overline{\chi}(\phi)$.

reported in the literature. Power series in ϕ provide a useful representation of the experimentally tabulated $\overline{\chi}$ values [25, 28]

$$\overline{\chi}(T,\phi) = \sum_{i=0}^{n} \overline{\chi}_i(T)\phi^i \tag{4.3}$$

Typically, it is sufficient to utilize the first three terms in this expansion, that is, $\overline{\chi}$ can be well fitted by $\overline{\chi}(T,\phi) = \overline{\chi}_0 + \overline{\chi}_1\phi + \overline{\chi}_2\phi^2$ where χ_0 is often close to 1/2 and all coefficients are, in principle, T dependent. From the measured $\overline{\chi}(\phi)$ it is possible to obtain $\chi_{eff}(\phi)$ up to an additive constant

$$\chi_{eff}(\phi) = \frac{\chi_{eff}(0) - \int_0^\phi \overline{\chi}(\phi)d\phi}{1-\phi}, \tag{4.4}$$

where the integration constant, $\chi_{eff}(0)$, is the value χ_{eff} at $\phi = 0$[3].

The replacement of $\chi(T)$ by $\chi_{eff}(T,\phi)$ can result in qualitative change in the phase behavior of the polymer solutions [27, 76, 77, 92, 93, 94]. In the following we focus, following de Gennes [76, 77], on the limit of $N \to \infty$ when the novel features of the phase behavior are simple to discern. Importantly, this is the limit relevant to brushes of grafted chains of finite N because the anchoring freezes out the translational degrees of freedom of the chains. In the familiar case, of $\chi(T)$ and $N \to \infty$, the resulting phase separation involves a coexistence of a concentrated polymer solution with a *pure* solvent. In marked contrast, solutions characterized by $\chi_{eff}(T,\phi)$ can exhibit a second type of phase separation in the $N \to \infty$ limit. This involves a coexistence of two phases of *nonzero* polymer concentration. This last feature is a necessary ingredient for the occurrence of a vertical phase separation within a brush. The features noted above can be discerned from the critical points of the solution, as specified by $\partial^2 f(\phi)/\partial\phi^2 = \partial^3 f(\phi)/\partial\phi^3 = 0$ or

$$\begin{cases} \frac{1}{N\phi_c} + \frac{1}{1-\phi_c} - 2\overline{\chi}(\phi_c) - \phi_c \left.\frac{\partial\overline{\chi}(\phi)}{\partial\phi}\right|_{\phi_c} = 0 \\ -\frac{1}{N\phi_c^2} + \frac{1}{(1-\phi_c)^2} - 3\left.\frac{\partial\overline{\chi}(\phi)}{\partial\phi}\right|_{\phi_c} - \phi_c \left.\frac{\partial^2\overline{\chi}(\phi)}{\partial\phi^2}\right|_{\phi_c} = 0 \end{cases} \tag{4.5}$$

[3] χ_{eff} is obtained by integrating $\overline{\chi}(\phi) = -\frac{\partial}{\partial\phi}[\chi_{eff}(\phi)(1-\phi)]$.

In the case of $\chi(T)$ these lead to the familiar critical point specified by $\phi_c = 1/(1+\sqrt{N})$ and $\chi_c = \frac{1}{2}(1+\frac{1}{\sqrt{N}})^2$. Accordingly, in the limit of $N \to \infty$ we have $\phi_c \to 0$ and $\chi_c \to 1/2$. When $\chi(T)$ is replaced by $\chi_{eff}(T,\phi)$ an additional critical point, associated with the second type of phase separation, emerges. For illustration purpose we will consider the $N \to \infty$ limit for the case of $\overline{\chi}(\phi) = 1/2 + \overline{\chi}_2(T)\phi^2$ when equation (4.5) yields an extra critical point at $\phi_c = 1/2$ and $\overline{\chi}_{2c} = 1$ *i.e.*, for $\overline{\chi}_2 > 1$ the system undergoes phase separation involving the coexistence of a dilute phase of concentration $\phi_- > 0$, and a dense phase of concentration $\phi_+ > \phi_-$[4]. At the vicinity of the critical point the binodal is well approximated by the spinodal curve $\partial^2 f(\phi)/\partial\phi^2 = 0$. In the limit $N \to \infty$ the spinodal is specified by

$$\frac{1}{1-\phi} - 1 - 4\overline{\chi}_2\phi^2 = 0. \tag{4.6}$$

The plot of this equation is presented in Figure 4.2.

The approximate values of ϕ_+ and ϕ_- are

$$\phi_\pm = \frac{1}{2} \pm \frac{1}{2}\sqrt{1 - \frac{1}{\overline{\chi}_2(T)}}. \tag{4.7}$$

Our discussion thus far concerned the thermodynamics of solutions of free polymers, when the translational degrees of freedom of the chains play a role. In the following, we mostly focus on the swelling behavior of free isolated chains and of brushes immersed in a pure solvent. In these situations f as discussed above is replaced by f_∞ corresponding to the limit of $N \to \infty$

$$f_\infty = (1-\phi)\ln(1-\phi) + \chi_{eff}(\phi)\phi(1-\phi). \tag{4.8}$$

[4]The choice of $\overline{\chi}(\phi)$ is motivated by two considerations: (i) the experimentally reported χ_0 is often close to 1/2 (ii) this is the simplest form yielding a second type of phase separation with $\chi_0 = 1/2$. It is useful to compare this form of $\overline{\chi}(\phi)$ to that obtained in the n-cluster model considered by de Gennes, where $f/kT = (1-\phi)\ln(1-\phi) + \rho(T)\phi(1-\phi^{n-1})$, $\chi_{eff}(\phi) = \rho(T)(1-\phi^{n-1})/(1-\phi)$ and $\overline{\chi}(\phi) = (n-1)\rho(T)\phi^{n-2}$ thus leading to $\phi_c = (n-2)/(n-1)$ and to $\rho_c = n^{-1}\left[(n-2)/(n-1)\right]^{2-n}$. Within the n-cluster model our choice of $\overline{\chi}(\phi)$ is closest to $n = 4$ and $\rho = \chi_2/(n-1)$ thus leading to $\phi_c = 2/3$ and to $\chi_{2c} = 27/16$. The differences between the two $\overline{\chi}(\phi)$ are due to the choice of χ_0, $\chi_0 = 1/2$ in our case *vs.* $\chi_0 = 0$ as chosen by de Gennes[76, 77].

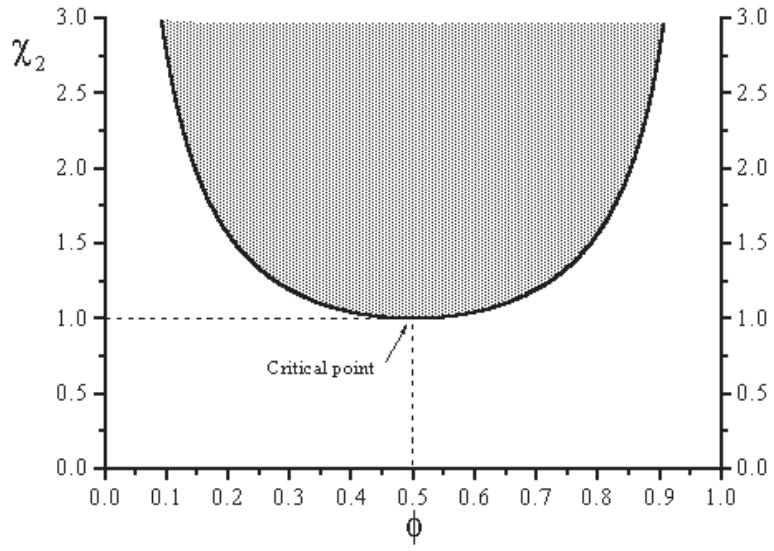

Figure 4.2: *Spinodal specified by (4.6) for* $\overline{\chi}(\phi) = 1/2 + \overline{\chi}_2(T)\phi^2$.

f_∞ determines the swelling behavior of brushes because the terminally anchored chains lose their translational entropy. Similarly, the swelling of isolated free coils is controlled by f_∞ because the motion of the chain center of mass is irrelevant to this process. In this last case it is important to note that ϕ refers to the monomer concentration within the coil rather than to the average concentration of the solution. The osmotic pressure corresponding to f_∞ in units of kT is

$$\pi_\infty a^3 = -\phi - \ln(1-\phi) - \overline{\chi}(\phi)\phi^2 \tag{4.9}$$

To gain insight concerning the significance of $\chi_{eff}(\phi)$ it is helpful to consider the expansions of f_∞ and π_∞. Two routes are of interest. In the first we follow the procedure adopted in the standard discussions involving $\chi(T)$ and replace the logarithmic term in (4.8) by its series expansion leading to

$$f_\infty = (\chi_{eff} - 1)\phi + \frac{1}{2}\widehat{v}\phi^2 + \frac{1}{6}\phi^3 + ... \tag{4.10}$$

Here the "excluded volume parameter" $\widehat{v}(T,\phi) = 1 - 2\chi_{eff}(T,\phi)$ is dependent on both T and ϕ. Note, that in this case it is important to retain the "linear" term

because of the ϕ dependence of χ_{eff}. The corresponding expression for π_∞ is

$$\pi_\infty a^3 \approx \frac{1}{2}\overline{v}\phi^2 + \frac{1}{3}\phi^3 + \frac{1}{4}\phi^4 + ..., \tag{4.11}$$

where $\overline{v}(T,\phi) = 1 - 2\overline{\chi}(T,\phi) \neq \widehat{v}$ is, again dependent on both T and ϕ. Thus when following this route the effect of replacing $\chi(T)$ by $\chi_{eff}(T,\phi)$ is two fold: (i) the coefficients of ϕ^2 in the expansions of f_∞ and of π_∞ become ϕ dependent (ii) The coefficients of ϕ^2 in the expansions of f_∞ and of π_∞ are different. All coefficients of higher order terms are positive constants. Clearly, this is also the case for f and for π. The second route is to replace $\chi_{eff}(T,\phi)$ and $\overline{\chi}(T,\phi)$ by their power series in ϕ. As was noted earlier, the power series of $\chi_{eff}(T,\phi)$ is specified by the one for $\overline{\chi}(T,\phi)$. Yet, for the purpose of our discussion it is sufficient to use $\chi_{eff}(T,\phi) = \sum_{i=0}^{n} \widehat{\chi}_i(T)\phi^i$ without specifying the relationship between $\widehat{\chi}_i(T)$ and $\overline{\chi}_i(T)$. Following this second route we obtain

$$f_\infty = (\widehat{\chi}_0 - 1)\phi + (\frac{1}{2} - \widehat{\chi}_0 + \widehat{\chi}_1)\phi^2 + (\frac{1}{6} - \widehat{\chi}_1 + \widehat{\chi}_2)\phi^3 + ... \tag{4.12}$$

$$\pi_\infty a^3 \approx (\frac{1}{2} - \overline{\chi}_0)\phi^2 + (\frac{1}{6} - \overline{\chi}_1)\phi^3 + (\frac{1}{4} - \overline{\chi}_2)\phi^4 + ..., \tag{4.13}$$

In this form none of the coefficients depend on ϕ but all are T dependent and capable of changing sign. In marked distinction, when $\chi(T)$ only the first coefficient is T dependent and capable of change of sign. The role of $v = 1 - 2\chi(T)$ as a measure of solvent quality is traceable to this last trait. The expansions (4.10) and (4.11) retain this characteristic at the price of introducing a ϕ dependence of $\overline{v}$ and $\widehat{v}$. As we shall discuss $\overline{\chi}(T,\phi)$ is the counterpart of $\chi(T)$ as an indicator of the solvent quality. Accordingly, $\overline{v}$ affords some of the usefulness of $v = 1 - 2\chi(T)$.

4.5 Uniform Concentration: Global Solvent Quality

The microscopic swelling behavior of coils and brushes, when modelled as systems of *uniform concentration*, is described respectively by the Flory and Alexander approximations. Within these approximations the swelling behavior reflects a balance

between the osmotic pressure π_∞ and the elastic restoring force. In the Flory approximation an isolated coil is viewed as a sphere of radius R with a uniform monomer density $\phi \approx Na^3/R^3$ where a is the monomer size. Within the Alexander model one considers a planar brush of terminally anchored chains such that the grafting density is uniform and the area per chain, σ, is constant. The grafting density is high so as to enforce chain crowding, $\sigma \leq R_F^2$ where $R_F \approx N^{3/5}a$ is the Flory radius of the isolated coil. The brush is considered as a planar layer of thickness R and uniform density $\phi \approx Na^3/\sigma R$.

The free energy per chain, in both cases, is

$$\frac{F_{chain}}{kT} = f_\infty \frac{V_{chain}}{a^3} + \frac{F_{el}}{kT} \tag{4.14}$$

where f_∞ is the mixing free energy per lattice site, V_{chain} is the volume per chain and F_{el} is its elastic free energy. In both cases the elastic free energy is approximated by

$$\frac{F_{el}}{kT} \approx \frac{R^2}{R_0^2} + \frac{R_0^2}{R^2}, \tag{4.15}$$

where $R_0 \approx N^{1/2}a$ is the radius of an ideal, Gaussian coil[5] [98, 99]. The free energies of the coil and the brush differ because of V_{chain}

$$V_{chain} \approx \begin{cases} R^3 & \text{coil} \\ R\sigma & \text{brush} \end{cases}. \tag{4.16}$$

In turn, this reflects the different geometries of the two systems. The coil is spherical while the brush is planar. The swelling behavior is specified by the equilibrium condition $\partial F_{chain}/\partial R = 0$. Since $\partial R \approx -(R/\phi)\partial\phi$ this leads to

$$\frac{\partial F_{el}/kT}{\partial R} \approx \pi_\infty \frac{dV_{chain}}{dR} \approx \begin{cases} \pi_\infty R^2 & \text{coil} \\ \pi_\infty \sigma & \text{brush} \end{cases}. \tag{4.17}$$

[5] While this interpolation form is not accurate around $R/R_0 \approx 1$, it is qualitatively correct and is sufficient for the semiqualitative discussion undertaken in the following. The performance of the various interpolation forms is discussed by Grosberg and Khokhlov [16]. A more rigorous form of the elastic penalty is presented in [102].

In the next two sections we will analyze the consequences of this equation for polymeric systems with $\chi_{eff}(\phi)$.

Before we proceed, a note of caution. The program outlined above calls for utilizing $\overline{\chi}(\phi)$, as obtained from thermodynamic measurements, to determine the swelling behavior of coils and brushes. It is based on the assumption that the measured $\overline{\chi}(\phi)$ is identical to the one experienced by the coils. This is non trivial assumption since in certain models (for example, the model of Painter *et al* described in chapter 3.3.3) the ϕ dependence of $\overline{\chi}(\phi)$ arises because of an interplay of intra and interchain contacts. Within such models the $\overline{\chi}(\phi)$ experienced by a coil may differ from the measured $\overline{\chi}(\phi)$.

4.5.1 Crossover between Self-Avoidance and Ideal Chain Statistics

The swelling behavior of an isolated coil is an important signature of the solvent quality. When $\chi_{eff}(T,\phi)$ replaces $\chi(T)$ the swelling behavior is modified. Two features are of special interest. One concerns the locus of the crossover, g_B, between the $N^{1/2}$ and $N^{3/5}$ scaling in the "nearly good solvent" regime. Chains with $N < g_B$ exhibit ideal coil behavior while longer chains exhibit good solvent statistics [13] and their span scales as $N^{3/5}$ (Figure 4.3). The ϕ dependence of $\overline{\chi}(\phi)$ can result in a significant shift in g_B. A second, qualitative, effect concerns the collapse transition within the Flory approximation. When $\overline{\chi}(\phi)$ increases with ϕ the collapse of flexible chains can assume the character of a first-order phase transition [95].

In good solvent conditions, when $\phi \ll 1$ and $R > N^{1/2}a$, only the first term in the elastic free energy (4.15) plays a role. The equilibrium condition for a coil, $\partial(F_{el}/kT)/\partial R \approx \pi_\infty R^2$, reduces to $R/Na^2 \approx \pi_\infty R^2$. Since $\phi \ll 1$ we retain only the first two terms in $\overline{\chi}(\phi) \approx \overline{\chi}_0 + \overline{\chi}_1\phi$, and obtain $\pi_\infty a^3 \approx \frac{1}{2}(1-2\overline{\chi}_0)\phi^2 + (\frac{1}{3}-\overline{\chi}_1)\phi^3$. $R \sim N^{3/5}$ scaling is obtained when the first term in the expansion for π_∞ is dominant while $R \sim N^{1/2}$ is found when the second term dominates. The crossover between the two regimes occurs when $\phi_B \approx (1-2\overline{\chi}_0)/(\frac{1}{3}-\overline{\chi}_1)$. Identifying $\phi_B \approx g_B a^3/r_B^3$,

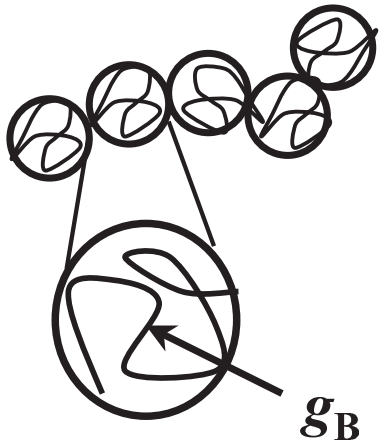

Figure 4.3: *Thermal blob comprising of g_B monomers. If the number of monomers is $\ll g_B$, a chain is ideal, $R \sim N^{1/2}$. For the number of monomers $\gg g_B$ a chain exhibits a self-avoidance, $R \sim N^{3/5}$.*

where $r_B \approx (\frac{1}{3} - \overline{\chi}_1)^{1/8} g_B^{1/2} a$ is the span of the corresponding ideal chain, leads to [103]

$$g_B \approx \frac{\left(\frac{1}{3} - \overline{\chi}_1\right)^{5/4}}{\left(1 - 2\overline{\chi}_0\right)^2} \tag{4.18}$$

where both χ_1 and χ_0 are T dependent. This expression for g_B reduces to the familiar one, as obtained for solutions characterized by $\chi(T)$, when $\chi_1 = 0$. The two asymptotic regimes for the radius of the chain are [103]

$$\frac{R}{a} \approx \begin{cases} \left(\frac{1}{3} - \overline{\chi}_1\right)^{1/8} N^{1/2} & N \ll g_B \\ \left(\frac{1}{2} - \overline{\chi}_0\right)^{1/5} N^{3/5} & N \gg g_B \end{cases} \tag{4.19}$$

As noted earlier, the effect on g_B can be significant. Thus for polystyrene in toluene at 25^o C $\overline{\chi}_0 = 0.431$ and $\overline{\chi}_1 = -0.311$ [25] and $g_B \approx 120$ as compared to $g_B \approx 50$ obtained when the ϕ dependence is neglected *i.e.*, $\chi_1 = 0$.

When the ϕ dependence of χ is overlooked it is convenient to obtain g_B in terms of a perturbative parameter ζ measuring the relative importance of the repulsive binary interactions as compared to an elastic energy of order kT. Within this

approach g_B corresponds to $\zeta = 1$ [13]. This approach can not however account for the contribution of T dependent higher order terms.

4.5.2 Single Polymer Chain in the Flory Approximation

An analytical solution of $\partial(F_{el}/kT)/\partial R = \pi_\infty R^2$ for arbitrary $\overline{\chi}(\phi)$ is not feasible. Yet, one may gain insight concerning the swelling and collapse behavior from the general features of the graphical solution of the equilibrium condition. Neglecting numerical factors $\partial(F_{el}/kT)/\partial R = \pi_\infty R^2$ can be written as

$$\overline{\chi}(\phi) \approx -\frac{\ln(1-\phi)+\phi}{\phi^2} + \frac{1}{N^{2/3}\phi^{1/3}} - \frac{1}{N^{4/3}\phi^{5/3}} \equiv \eta_c(\phi, N) \tag{4.20}$$

The equilibrium states correspond to the intersections of $\overline{\chi}(\phi)$ and $\eta_c(\phi, N)$ (Figure

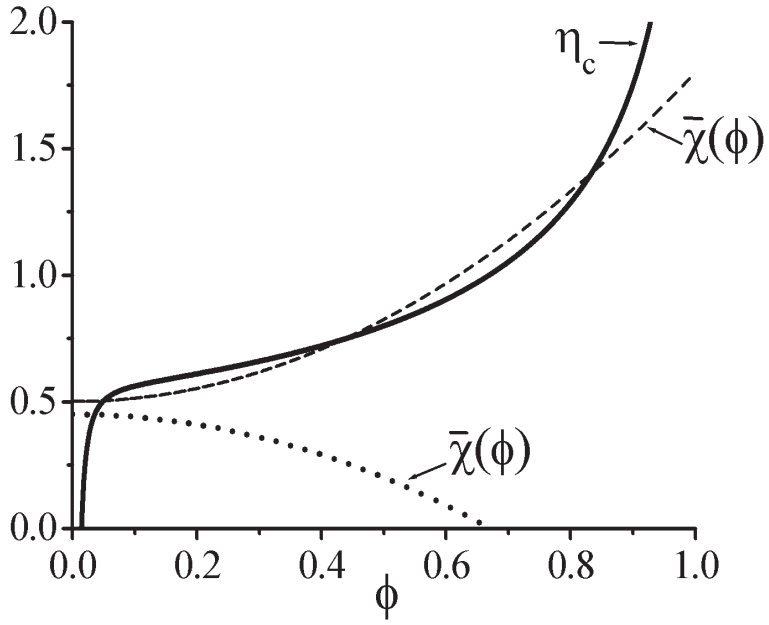

Figure 4.4: *Graphical solution of the equilibrium condition of an isolated coil ($N = 300$) depicting the crossing of $\eta_c(N, \phi)$, as given by (4.20) with $\overline{\chi}(\phi)$. The two curves cross once when $\overline{\chi}(\phi)$ decreases with ϕ (dots) but three intersections, indicating a first order phase transition, may occur when $\overline{\chi}(\phi)$ increases with ϕ (dashes).*

4.4). When $\chi_{eff}(\phi) = \overline{\chi}(\phi) = \chi$ the two curves intersect at one point only. This is also the case when $\overline{\chi}(\phi)$ is a decreasing function of ϕ. However, in this situation the intersection occurs at lower ϕ in comparison to the intersection between $\eta_c(\phi, N)$ and $\overline{\chi}(\phi) = \chi_0$ thus indicating stronger swelling.

When $\overline{\chi}(\phi)$ is an increasing function of ϕ it is possible to distinguish between two important scenarios: (i) $\overline{\chi}(\phi)$ and $\eta_c(\phi)$ intersect at a single point. In comparison to the intersection of $\eta_c(\phi, N)$ and $\overline{\chi}(\phi) = \chi_0$, this occurs at higher ϕ thus indicating weaker swelling. (ii) $\overline{\chi}(\phi)$ and $\eta_c(\phi)$ intersect at three points. This case corresponds to a F_{chain} (4.14) exhibiting two minima separated by a maximum thus indicating a collapse taking place as a first order phase transition. Note that this last scenario occurs only for $\overline{\chi}(\phi)$ that increases with ϕ. Arguing that higher $\overline{\chi}(\phi)$ values indicate a poorer solvent allows for a simple interpretation of this result. When R shrinks, ϕ increases leading to a higher $\overline{\chi}(\phi)$. Accordingly, the effective solvent quality diminishes with R thus giving rise to cooperativity leading to a first-order collapse transition[6].

The coil-globule transition curves are schematically depicted in Figure 4.5 for three distinctive cases. In the case of decreasing $\overline{\chi}(\phi)$ and constant χ the coil-globule transition is smooth, while for the increasing $\overline{\chi}(\phi)$ it is possible to reach the situation when the transition would be of the first order (three intersections on in Figure 4.4).

At this point it is important to stress the limitations of the Flory approach as described above. Since the monomer volume fraction, ϕ, is assumed to be uniform, this model does not allow for the possibility of radial phase separation within a

[6] The possibility of a first order collapse transition due to the ϕ dependence of $\overline{\chi}$ was already noted by Erman and Flory (EF) [95]. Their results differ from our in following respects: (i) The elastic free energy used by EF incorporates a $\ln(R/R_0)$ term. Following de Gennes [98, 99] we replaced this term by $(R/R_0)^2$.(ii) The EF analysis focuses on the condition for a critical point in a system described by $\overline{\chi}(T, \phi) = \overline{\chi}_0 + \overline{\chi}_1\phi + \overline{\chi}_2\phi^2$. This is expressed in terms of a $\overline{\chi}_1$ *vs.* $\overline{\chi}_0$ plot. Our discussion is based on a graphical solution of the equilibrium condition for the chain. It highlights the overall ϕ dependence $\overline{\chi}(T, \phi)$ that is required to induce a first order collapse transition.

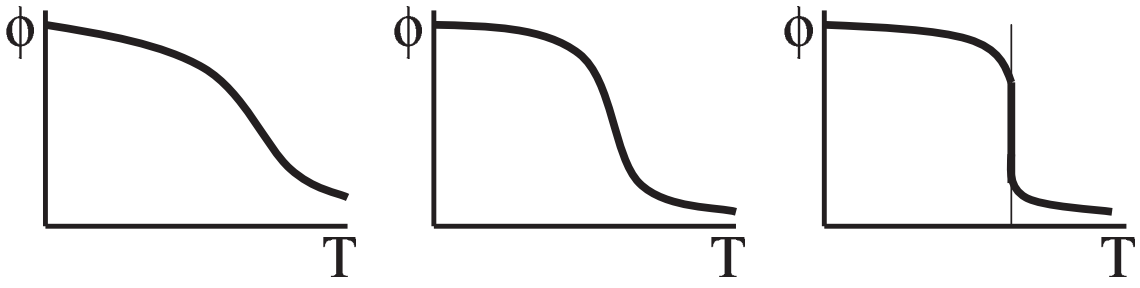

Figure 4.5: *Coil-globule transition plots for $\overline{\chi}$ which is decreasing (left), constant (center), and increasing (right) function of ϕ.*

single globule. To investigate such scenarios it is necessary to utilize the Lifshitz theory of collapse [104, 105]. This however is beyond the scope of this work.

While the character of the collapse transition within the Flory approximation is affected by the ϕ dependence of χ_{eff}, there is essentially no change in span of the collapsed chain as specified by the condition $\pi_\infty = 0$. When $\chi(T)$ is independent of ϕ and $\phi \ll 1$ this condition leads to $v\phi^2 \sim \phi^3$ and to $R/a \sim |v|^{-1/3}N^{1/3}$. For concentration dependent $\chi_{eff}(T,\phi)$, $\pi_\infty a^3 \approx \frac{1}{2}(1-2\overline{\chi}_0)\phi^2 + (\frac{1}{3} - \overline{\chi}_1\phi^3) = 0$, leads to

$$\frac{R}{a} \approx \left(\frac{\frac{1}{3} - \overline{\chi}_1}{\overline{\chi}_0 - \frac{1}{2}}\right)^{1/3} N^{1/3} \tag{4.21}$$

Thus $R \sim N^{1/3}$ is retained but with a modified numerical prefactor and an additional T dependence introduced by $\overline{\chi}_1$.

4.5.3 Polymer Brush within the Alexander Approximation

The Alexander model of a planar brush (Figure 4.6) invokes two assumptions: (i) uniform density that is, ϕ behaves as a step function thus endowing the brush with a sharp boundary. (ii) The chains are uniformly stretched with their ends straddling the sharp boundary of the brush. While this approximation allows to recover the correct scaling behavior of the brush, the two underlying assumption are in fact wrong. Both ϕ and the local extension of the chains vary with the distance from

the grafting surface, z, and the chain ends are distributed throughout the layer. The Self-Consistent Field (SCF) theory of brushes furnishes a rigorous description of these features [106, 107, 108] as we shall discuss in chapter 5.

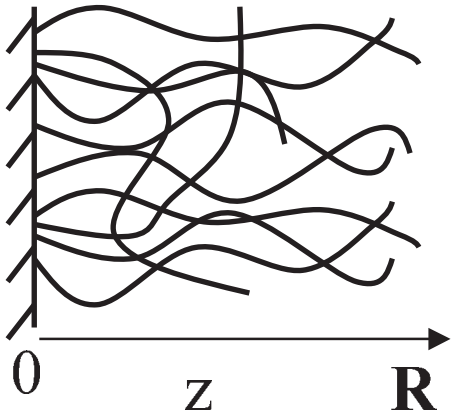

Figure 4.6: *Within the Alexander model the concentration in a polymer brush does not change with the height and the chains are uniformly stretched.*

The swelling behavior of a brush within the Alexander model exhibits similar trends to those found in the case of the isolated coil. In a good solvent, when $\phi \ll 1$ and $R > N^{1/2}a$, the equilibrium condition for the brush, $\partial(F_{el}/kT)/\partial R \approx \pi_\infty \sigma$, leads to $R/Na^2 \approx \pi_\infty \sigma$ or $R/a \approx N(\pi_\infty a^3)(\sigma/a^2)$. As in the case of the coil, the "nearly good solvent" case involves two regimes. The crossover occurs at

$$\sigma_B \approx r_B^2 \approx \left(\frac{1}{3} - \overline{\chi}_1\right)^{1/4} g_B a^2 \tag{4.22}$$

When $\sigma > \sigma_B$ the chains in the brush exhibit self-avoidance and $R/a \approx N\left(a^2/\sigma\right)^{1/3}$ while for $\sigma < \sigma_B$ one obtains $R/a \approx N\left(a^2/\sigma\right)^{1/2}$ corresponding to a brush of ideal chains.

As in the case of a collapsed globule, the thickness of the fully collapsed brush is essentially unaffected by the ϕ dependence of χ_{eff}. The thickness is determined by $\pi_\infty = 0$ but with $\phi \approx Na^3/\sigma R$ rather than $\phi \approx Na^3/R^3$ leading to

$$\frac{R}{a} \approx \left(\frac{\frac{1}{3} - \overline{\chi}_1}{\overline{\chi}_0 - \frac{1}{2}}\right) N\frac{a^2}{\sigma}. \tag{4.23}$$

that is, the $R \sim N(a^2/\sigma)$ scaling is retained with a modified prefactor and an additional T dependence due to χ_1.

Again, an analytical solution of $\partial(F_{el}/kT)/\partial R = \pi_\infty \sigma$ for arbitrary $\overline{\chi}(\phi)$ is not practical but it is of interest to consider the graphical solution of the equilibrium condition $\partial(F_{el}/kT)/\partial R = \pi_\infty \sigma$ expressed as

$$\overline{\chi}(\phi) \approx -\frac{\ln(1-\phi)+\phi}{\phi^2} - \frac{1}{\phi^3}\left(\frac{a^2}{\sigma}\right)^2 + \frac{\phi}{N^2}\left(\frac{\sigma}{a^2}\right)^2 \equiv \eta_b(\phi, N, \sigma) \tag{4.24}$$

The equilibrium state is specified by the intersections of $\overline{\chi}(\phi)$ and $\eta_b(\phi, N, \sigma)$ (Figure 4.7).

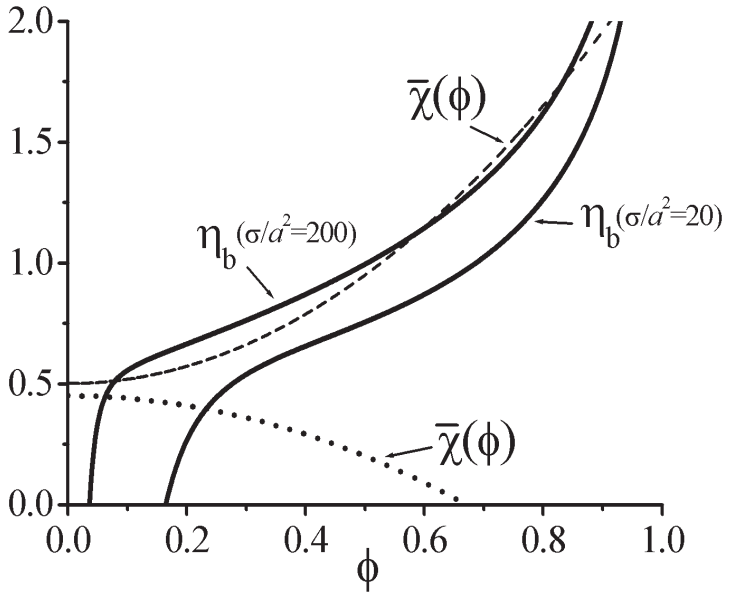

Figure 4.7: *Graphical solution of the equilibrium condition of a brush ($N = 300$) depicting the crossing of $\eta_b(N, \phi, \sigma)$, as given by (4.24) with $\overline{\chi}(\phi)$. The two curves cross once when $\overline{\chi}(\phi)$ decreases with ϕ (dots) but three intersections, indicating a first order phase transition, may occur when $\overline{\chi}(\phi)$ increases with ϕ (dashes).*

When $\chi_{eff}(\phi) = \overline{\chi}(\phi) = \chi$ the two curves intersect at one point. Similar behavior is found when $\overline{\chi}(\phi)$ is a decreasing function of ϕ. In comparison to the intersection

between $\eta_b(\phi, \sigma)$ and $\overline{\chi}(\phi) = \overline{\chi}_0$ the intersection occurs at lower ϕ thus signaling stronger swelling. As in the case of the coil, it is possible to distinguish between two important scenarios when $\overline{\chi}(\phi)$ increases with ϕ: (i) $\overline{\chi}(\phi)$ and $\eta_b(\phi, N, \sigma)$ intersect at a single point. This occurs at higher ϕ in comparison to the intersection of $\eta_b(\phi, N)$ and $\overline{\chi}(\phi) = \overline{\chi}_0$ and corresponds to weaker swelling. (ii) $\overline{\chi}(\phi)$ and $\eta_b(\phi, N, \sigma)$ intersect at three points. In this case F_{chain} exhibits two minima separated by a maximum and the collapse takes place as a first-order phase transition. As we shall discuss shortly, a first order "collapse transition" is indeed possible when $\overline{\chi}(\phi)$ increases with ϕ. However, this transition involves a vertical phase separation within the brush. To properly analyze this case it is necessary to allow for the spatial variation of ϕ thus requiring a more refined description of the brush. This topic is addressed in the next chapter.

4.6 Conclusion

As we have seen, the $\chi_{eff}(\phi)$ in systems with uniform concentration gives rise to two effects. First is a qualitative modification of the collapse transition that can assume, within these models, the character of a first-order phase transition. Second is a significant shift in the crossover between the behavior of an ideal chain to that of a self-avoiding one. The signatures of $\chi_{eff}(\phi)$ in systems with spatially varying concentration and the corresponding "local" solvent quality will be discussed in the next chapter for planar brushes within the SCF theory.

Chapter 5

Signatures of $\chi_{eff}(\phi)$: Self-Consistent Field Theory of a Planar Polymer Brush

5.1 Résumé

La théorie de champ auto-cohérent de brosses de polymères neutres solubles dans l'eau est formulée dans les termes de $\chi_{eff}(T, \phi)$. Nous y discutons les profils de concentration, les distributions des bouts libres et les profils de force de compression en présence et en l'absence d'une séparation de phase verticale. Une séparation de phase verticale dans la brosse résulte en un profil distinctif de force de compression aussi bien qu'en dépendance non monotone de l'épaisseur moyenne de la brosse en fonction de la densité de greffage. L'analyse est explicitement appliquée au modèle K [21].

5.2 Introduction

The discussion of the previous chapter concerned the "global" solvent quality in systems of assumed uniform density. To explore the coupling of the "local" solvent

quality with a spatially varying ϕ we reanalyze the swelling behavior of a planar brush using the SCF theory instead of the Alexander model. A significant part of our discussion is devoted to brushes of polymers capable of undergoing a second type of phase separation[1] [76, 77, 93, 94]. Within a brush, this type of phase separation can lead to a vertical phase separation associated with a discontinuous concentration profile [103, 109]. Our analysis focuses on the signatures of such phase separation. These include a non-monotonous variation of the brush thickness with the grafting density and the appearance of distinct regimes in the compression force profiles.

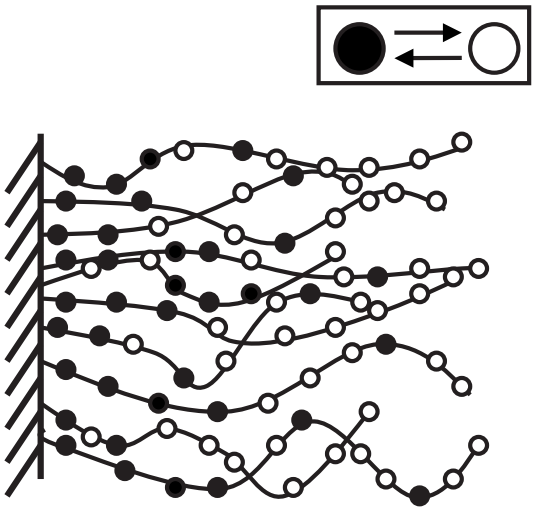

Figure 5.1: *Schematic picture of a brush of a "two-state polymer". Open and filled circles depict monomers in the different, interconverting, monomeric states.*

In this chapter we investigate the signatures of $\chi_{eff}(\phi)$ in the brush of neutral water-soluble polymers by taking advantage of physically realistic two-state models [21, 22, 23, 70, 72] described in chapter 2 (Figure 5.1). This approach is of interest because of a number of reasons: (i) $\chi_{eff}(T, \phi)$ determines a number of important characteristics of the brush among them the concentration profile, the distribution of free ends and the force profile associated with the compression of the brush. Thus,

[1] In the $N \to \infty$ limit, this involves coexistence of two solutions with a finite polymer concentration instead of a polymer rich phase in contact with a neat solvent.

a description of the brush behavior in terms of $\chi_{eff}(T,\phi)$ accounts for the leading brush properties and facilitates the comparison of the predictions of the different models. The specific features of the individual models and their parameters come into play when the distribution of the monomer states is of interest. However, as we shall discuss, even in this case it is convenient to first specify the brush characteristics in terms of $\chi_{eff}(T,\phi)$. (ii) The formulation of the theory in terms of $\chi_{eff}(T,\phi)$ underlines the relationship to the measurable

$$\overline{\chi}(T,\phi) = \chi_{eff} - (1-\phi)\partial\chi_{eff}/\partial\phi \tag{5.1}$$

as obtained from the study of the colligative properties of the polymer solutions (chapter 2.3). $\overline{\chi}(T,\phi)$ is helpful in determining the parameters of the models. In the context of brushes, the behavior of $\overline{\chi}(T,\phi)$ provides a useful diagnostic for systems expected to exhibit a vertical phase separation within the brush. (iii) While our discussion focuses on the two-state models discussed in chapter 2, the analysis can be extended to other models (chapter 3) that yield a ϕ dependent χ_{eff}. (iv) The SCF theory of brushes characterized by $\chi_{eff}(T,\phi)$ suggests useful tests for the occurrence of vertical phase separation. This is of interest, as we shall discuss in chapter 6, because of experimental indications that such behavior occurs in brushes of PNIPAM. (v) The concentration profiles obtained from the SCF theory are essentially identical to those derived [103] from the Pincus approximation where the distribution of free-ends is assumed rather than derived (Appendix A). In marked contrast, the compression force profiles are sensitive to the distribution of free-ends and the two methods yield different results.

The brush structure within the K model was studied using the numerical SCF theory of the Scheutjens-Fleer type [110, 111] and allowed to rationalize the aggregation behavior of copolymers incorporating PEO blocks [112]. The brush structure within the n-cluster model was studied using SCF theory [109] and by simulations [113]. These reveal the possibility of a vertical phase separation within the brush giving rise to a discontinuity in the concentration profile. In turn, this was invoked in order to rationalize observations about the collapse of PNIPAM brushes

[114, 115]. The force profiles due to the compression of brushes described by the n-cluster model were also analyzed [116, 117]. The studies of brushes of "two-state polymers" focused on a particular model and were formulated in terms of the corresponding free energy. This obscured common features between the different models and hampered the comparison between them. For example, while a vertical phase separation is possible within all two-state models, this scenario was mainly studied for the n-cluster model thus creating a misleading impression about the physical origins of this phenomenon.

Our discussion concerns a brush of flexible "two-state" chains, terminally grafted to a planar surface. We assume that the chains are monodisperse and that each chain incorporates N monomers. The surface area per chain, σ, is constant and the surface is assumed to be non-adsorbing for the two monomeric states. As before, the free energy per lattice site (4.8) in units kT is

$$f_\infty(\phi, T) = (1-\phi)\ln(1-\phi) + \chi_{eff}(\phi, T)\phi(1-\phi) \tag{5.2}$$

In this form the specific features of a particular model are grouped into $\chi_{eff}(\phi, T)$. This form corresponds to the $N \to \infty$ limit. It is appropriate for brushes of any N because the grafted chains lose their mobility and thus have no translational entropy. The application of our analysis to a particular case is illustrated for the K model. However, most of our analysis is model independent in that $\chi_{eff}(T, \phi)$ is not specified explicitly. The only assumption made is that $\overline{\chi}(T, \phi)$ can be expanded in powers of ϕ

$$\overline{\chi}(T, \phi) = \sum_{i=0} \overline{\chi}_i(T)\phi^i \tag{5.3}$$

where the $\overline{\chi}_i(T)$ are specific to a given model. For simplicity we further limit the discussion to systems where the first three terms provide an accurate description of $\overline{\chi}(T, \phi)$. As we shall discuss, the presence of a third order term is the minimal condition for the possibility of a vertical phase separation within the brush. The power series expansion of $\overline{\chi}(T, \phi)$ is clearly related to the virial expansion of the osmotic pressure, π. The two differ in that the second incorporates terms originating in the translational entropy. In discussions of the SCF theory $f_\infty(\phi)$ was often

approximated by the second and third terms in the virial expansion of the Flory-Huggins free energy. From this point of view it is important to note two points: (i) in the power series of $\overline{\chi}(T,\phi)$ all the coefficients are T dependent and can change sign. (ii) Use of $\overline{\chi}(T,\phi)$ series expansion including a ϕ^3 term corresponds to a virial expansion incorporating a ϕ^4 term.

The next six sections are devoted to the model independent aspects of the SCF theory based on $f_\infty(\phi,T)$ with ϕ dependent χ_{eff}. In section 5.3 we develop the analytical SCF model which is the generalization of the SCF theory of brushes [106, 107, 118, 119, 120] with ϕ-dependent $\chi_{eff}(\phi)$. In section 5.4 we describe the resulting concentration profiles. For $\chi_{eff}(\phi)$ they can be either continuous or discontinuous. Discontinuous profiles correspond to the vertical phase separation in the brush. The experimentally accessible average thickness of a brush with $\chi_{eff}(\phi)$ is described in section 5.5. Section 5.6 is devoted to the distribution of free ends in the brush for continuous and discontinuous profiles. Approximate analytical expressions for the discontinuous profiles and the end distribution functions are presented in section 5.7. The compression of the brush with an athermal wall is described in section 5.8. The compression can induce the vertical phase separation in a brush, which results in the discontinuous concentration profile. The application of the model independent results to the particular case of the K model is described in section 5.9. The last section summarizes the obtained results.

5.3 The SCF theory for $\chi_{eff}(T,\phi)$

Consider a brush of neutral and flexible polymers comprising N monomers of size a. Each chain is grafted by one end onto an impermeable, non-adsorbing, planar surface. The area per chain is denoted by σ and H is the maximal height of the brush. Following refs. [107, 118, 120], the free energy per chain, F_{chain}, consists of two terms: an interaction free energy, F_{int}, and an elastic free energy, F_{el}, $F_{chain} = F_{int} + F_{el}$. The interaction free energy per chain is

$$\frac{F_{int}}{kT} = \frac{\sigma}{a^3}\int_0^H f_\infty(\phi)dz \tag{5.4}$$

where the interaction free energy density $f_\infty(\phi)$ is given by (5.2). In a strong stretching limit, when the chains are extended significantly with respect to Gaussian dimensions, the elastic free energy is [118]

$$\frac{F_{el}}{kT} = \frac{3}{2a^2}\int_0^H g(z')dz'\int_0^{z'} E(z,z')dz. \tag{5.5}$$

Here $E(z,z') = dz/dn$ characterizes the local chain stretching at height z when the free end is at height z'. $g(z')$ specifies the height distribution of the free ends and obeys the normalization condition $\int_0^H g(z')dz' = 1$.

The concentration of monomers, $\phi(z)$, at height z is specified by

$$\phi(z) = \frac{a^3}{\sigma}\int_z^H \frac{g(z')dz'}{E(z,z')} \tag{5.6}$$

Since each chain consists of N monomers we have

$$N = \frac{\sigma}{a^3}\int_0^H \phi(z)dz \tag{5.7}$$

At the same time

$$N = \int_0^{z'} \frac{dz}{E(z,z')} \tag{5.8}$$

which can be regarded as a normalization condition for the function $E(z,z')$.

The equilibrium $\phi(z)$ in the brush is determined by the variation of the functional F_{chain} with respect to $E(z,z')$ and $g(z')$ subject to the constraints (5.7) and (5.8) yielding

$$E(z,z') = \frac{\pi}{2N}\sqrt{z'^2 - z^2} \tag{5.9}$$

and

$$\mu(\phi) = \lambda - Bz^2 \tag{5.10}$$

where $B = 3\pi^2/8N^2a^2$, λ is the Lagrange multiplier associated with constraint (5.7) and $\mu(\phi) = \partial f_\infty(\phi)/\partial\phi$ is the exchange chemical potential. Up to this point the SCF theory is identical to the familiar versions, as obtained for $\chi = \chi(T)$.

For dilute brushes, $\sigma \gg 1$, immersed in a good solvent and when χ is independent of ϕ, $\chi_{eff}(\phi,T) = \chi(T) < 1/2$, the chemical potential is linear in ϕ, $\mu(\phi) \sim \phi$. In this case, when binary interactions are dominant, eq. (5.10) leads to a *parabolic* concentration profile [107, 119]. At higher grafting densities, $\sigma \geqslant 1$, higher order terms become significant. These were typically handled by incorporation of the third virial term [107, 119]. However, as discussed in the Introduction, deviations from these scenarios are expected when $\chi_{eff}(\phi)$ varies with ϕ and $\mu(\phi)$, as obtained from (5.2), assumes the form

$$\mu(\phi) = -\ln(1-\phi) - 1 + \chi_{eff}(\phi) - 2\chi_{eff}(\phi)\phi + \phi(1-\phi)\frac{\partial\chi_{eff}(\phi)}{\partial\phi} \tag{5.11}$$

Since colligative measurements yield $\overline{\chi}(\phi) = \chi_{eff}(\phi) - (1-\phi)\partial\chi_{eff}(\phi)/\partial\phi$[2] rather than $\chi_{eff}(\phi)$ it useful to express $\mu(\phi)$ as

$$\mu(\phi) = -\ln(1-\phi) - 1 + \chi_{eff}(0) - \int_0^\phi \overline{\chi}(\phi)d\phi - \phi\overline{\chi}(\phi) \tag{5.12}$$

Finally, the Lagrange multiplier λ is determined by the concentration at the outer edge of the brush, $\phi_H \equiv \phi(z=H)$

$$\begin{aligned}\lambda &= BH^2 + \mu(z=H)\\ &= BH^2 - \ln(1-\phi_H) - 1 + \chi_{eff}(0) - \int_0^{\phi_H} \overline{\chi}(\phi)d\phi - \phi_H\overline{\chi}(\phi_H),\end{aligned} \tag{5.13}$$

In turn, ϕ_H of a free brush is set by the osmotic pressure at H that is, $\pi_{osm}(\phi_H) = \phi^2\partial\left[f_\infty(\phi)/\phi\right]/\partial\phi|_{\phi=\phi_H} = 0$, leading to

$$-\ln(1-\phi_H) - \phi_H - \overline{\chi}(\phi_H)\phi_H^2 = 0 \tag{5.14}$$

In a good solvent $\phi_H = 0$.

[2] This expression can be inverted as $\chi_{eff}(\phi) = \frac{\chi_{eff}(0) - \int_0^\phi \overline{\chi}(\phi)d\phi}{1-\phi}$.

5.4 Concentration Profiles

In order to obtain $\phi(z)$ it helpful to express (5.10) as

$$\Delta\mu(\phi) = B(H^2 - z^2) \tag{5.15}$$

where

$$\Delta\mu(\phi) = -\ln\frac{1-\phi}{1-\phi_H} - \int_{\phi_H}^{\phi}\overline{\chi}(\phi)d\phi + \phi_H\overline{\chi}(\phi_H) - \phi\overline{\chi}(\phi) \tag{5.16}$$

Equation (5.15) does not specify $\phi(z)$ directly. Rather, it yields $z(\phi) = \sqrt{H^2 - \Delta\mu(\phi)/B}$. The brush height is determined in terms of the monomer volume fraction at the surface, $\phi_0 = \phi(z=0)$, leading to $H = \sqrt{\Delta\mu(\phi_0)/B}$ and

$$z(\phi) = \sqrt{\frac{\Delta\mu(\phi_0) - \Delta\mu(\phi)}{B}} \tag{5.17}$$

$\phi(z)$ is determined by equation (5.17) together with the normalization condition (5.7), which relates ϕ_0 to the grafting density, $1/\sigma$.

We now distinguish between two cases. In one the concentration profile is continuous while in the second a discontinuity occurs due to the vertical phase separation. In the first case (5.7) may be expressed as

$$N = \frac{\sigma}{a^3}\int_{\phi_0}^{\phi_H}\phi\frac{\partial z}{\partial\phi}d\phi \tag{5.18}$$

The concentration profile for a given σ is fully specified by (5.17) and (5.18). A vertical phase separation in the brush results in a discontinuity at height H_t. At this altitude two phases coexist: a dense inner phase with a monomer volume fraction $\phi_+(H_t)$ and a dilute outer phase with $\phi_-(H_t)$. In this case the normalization condition (5.7) assumes the form

$$N = \frac{\sigma}{a^3}\int_{\phi_0}^{\phi_+(H_t)}\phi\frac{\partial z}{\partial\phi}d\phi + \frac{\sigma}{a^3}\int_{\phi_-(H_t)}^{\phi_H}\phi\frac{\partial z}{\partial\phi}d\phi \tag{5.19}$$

where $\phi_+(H_t)$ and $\phi_-(H_t)$ are determined by $\mu(\phi_+) = \mu(\phi_-)$ and $\pi(\phi_+) = \pi(\phi_-)$. $\phi(z)$ is now determined by equation (5.17) together with the normalization condition (5.19),

It is of interest to consider the phase behavior when $\overline{\chi}(\phi)$ is described by $\overline{\chi}(\phi) = \chi_0 + \chi_1\phi + \chi_2\phi^2$. In the case of $\overline{\chi}(\phi) = \chi_0$ or $\overline{\chi}(\phi) = \chi_0 + \chi_1\phi$ the critical point, as specified by $\partial^2 f_\infty(\phi)/\partial\phi^2 = \partial^3 f_\infty(\phi)/\partial\phi^3 = 0$

$$\frac{1}{1-\phi} - 2\overline{\chi}(\phi) - \phi\frac{\partial\overline{\chi}(\phi)}{\partial\phi} = 0 \tag{5.20}$$

$$\frac{1}{(1-\phi)^2} - 3\frac{\partial\overline{\chi}(\phi)}{\partial\phi} - \phi\frac{\partial^2\overline{\chi}(\phi)}{\partial\phi^2} = 0 \tag{5.21}$$

occurs at $\phi_c = 0$. This corresponds to the familiar case of a polymer rich phase in

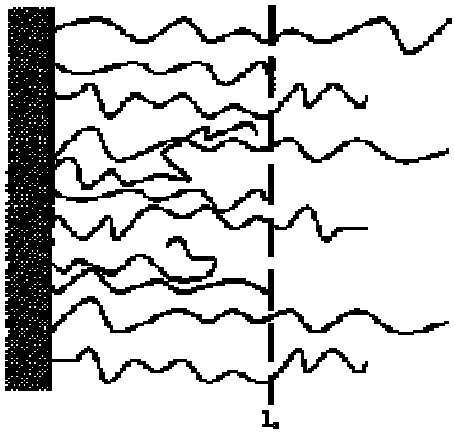

Figure 5.2: *Vertical phase separation in a brush. Dilute outer phase coexist with the dense phase.*

coexistence with a neat solvent. In this situation there is no vertical phase separation within the brush and the concentration profile is continuous. A second type of phase separation [76, 77, 93, 94], associated with a discontinuous $\phi(z)$ (Figure 5.2), is possible when higher order terms are involved. This case was first discussed by Wagner *et al* in the context of the n-cluster model [109, 116]. When $\overline{\chi}(\phi)$ increases

with ϕ to the extent that a bulk phase separation of the second type occurs, it is possible to distinguish between two regimes. For grafting densities lower than σ_c, to be specified below, $\phi_0 < \phi_-$. In this range $\phi(z) < \phi_-$ at all heights and there is no phase separation. On the other hand, when $\sigma > \sigma_c$ phase separation occurs within the brush leading to a discontinuous $\phi(z)$.

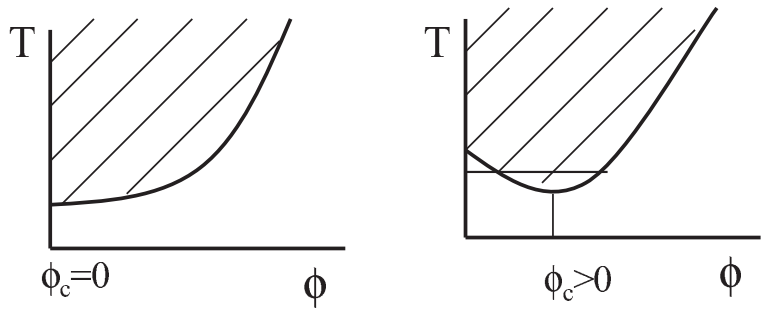

Figure 5.3: *Two possible phase diagrams of polymer brush with LCST. No vertical phase separation can occur, $\phi_c = 0$, (left) and the vertical phase separation is possible above $\phi_c > 0$.*

The onset of phase separation within the brush for $\sigma > \sigma_c$ is signalled by the appearance of multiple roots to equation (5.17). These are due to the van der Waals loop traced by $\mu(\phi)$ in the range $\phi_- < \phi < \phi_+$ (Figure 5.3). The coexistence within the brush is specified by two conditions: $\mu(\phi_+) = \mu(\phi_-)$ and $\pi(\phi_+) = \pi(\phi_-)$. Thus, the two coexisting phases are characterized by the monomer volume fractions, $\phi_+(H_t)$ and $\phi_-(H_t)$, of the bulk phases in the $N \to \infty$ limit. However, the coexistence occurs at a single height $z = H_i$ which can be found from eq. (5.15)

$$\Delta\mu(\phi_\pm) = B(H^2 - H_i^2) \tag{5.22}$$

thus leading to a discontinuity in $\phi(z)$.

Two approaches allow to explicitly calculate $\phi(z)$ when $\sigma > \sigma_c$. In one, the concentration profile is obtained from (5.17) for the intervals $\phi_0 \geq \phi \geq \phi_+$ and $\phi_- \geq \phi \geq 0$. In this case it is necessary first to obtain the bulk binodal by utilizing,

for example, the Maxwell equal area construction on the van der Waals loop traced by $\mu(\phi)$.[3] The second approach utilizes a Maxwell construction on the van der Waals loops occurring in the plots of $\phi(z)$ vs. z^2 [109]. It is equivalent to the first approach because z^2 is related to $\mu(\phi)$ via (5.15).

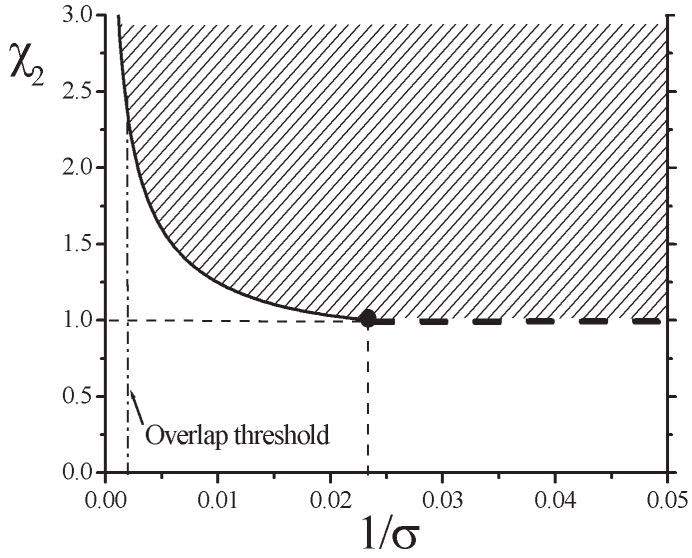

Figure 5.4: *The state diagram of a brush with* $\overline{\chi}(\phi) = 1/2 + \chi_2\phi^2$ *and* $N = 200$ *in the* χ_2, $1/\sigma$ *plane. Vertical phase separation occurs in the hatched region. At* • $\phi_0 = \phi_-(T)$. *The dashed line, at higher* $1/\sigma$, *corresponds to brushes exhibiting an inflection point at altitudes that increase with* $1/\sigma$. *The boundary for lower* $1/\sigma$ *corresponds to* ϕ_- ϕ_+ *coexistence at the grafting surface.*

A vertical phase separation as discussed above becomes possible once ϕ_0 exceeds ϕ_-. To estimate the threshold grafting density, σ_c we assume that for $\sigma < \sigma_c$ the brush thickness retains the scaling behavior of a single phase brush as obtained from the Alexander model. For a Gaussian brush $H/a \approx N\,(a^2/\sigma)^{1/2}$ while a brush exhibiting self-avoidance obeys $H/a \approx N\,(a^2/\sigma)^{1/3}$. Since $\Delta\mu(\phi_0) = BH^2$ this leads

[3] The equality $\pi = \phi\mu - f_\infty$ leads to $\partial\pi/\partial\phi = \phi\partial\mu/\partial\phi$ and thus to $\pi(\phi_+) - \pi(\phi_-) = \int_{\phi_-}^{\phi_+} (\phi\partial\mu/\partial\phi)\, d\phi$. Since the binodal is determined by $\pi(\phi_+) = \pi(\phi_-)$ and $\mu(\phi_+) = \mu(\phi_-)$ the equal area construction is specified by $\mu(\phi_\pm)(\phi_+ - \phi_-) = \int_{\phi_-}^{\phi_+} \mu(\phi) d\phi$.

to $\sigma_c \approx [\Delta\mu(\phi_-)]^{3/2}$ in the self-avoidance case and to $\sigma_c \approx \Delta\mu(\phi_-)$ for the Gaussian one. This estimate can serve as guidelines when $\Delta\mu_\infty(\phi_0)$ is known, that is when

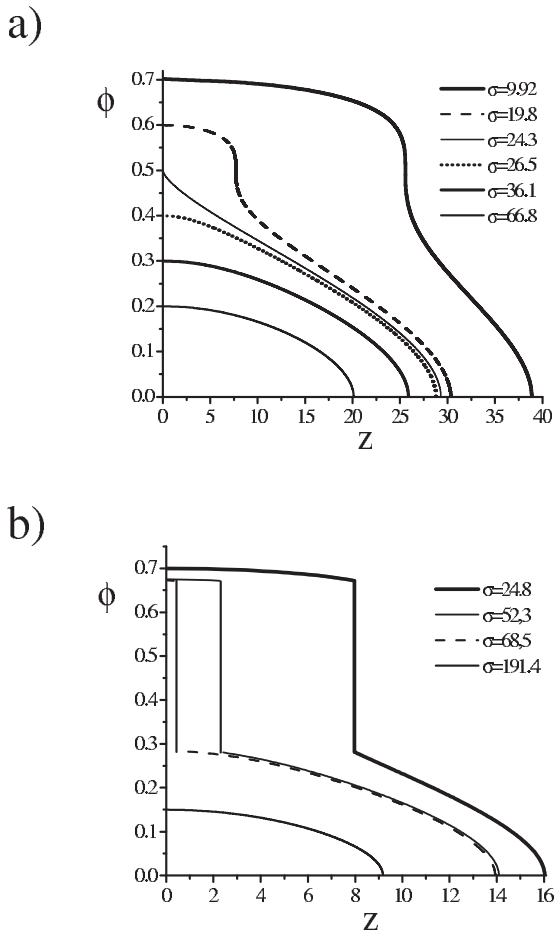

Figure 5.5: *$\phi(z)$ for different areas per chain σ when $\overline{\chi}(\phi) = 1/2 + \chi_2\phi^2$. (a) $\chi_2 = 1$ (b) $\chi_2 = 1.05$. In every case $N = 200$.*

$\overline{\chi}(\phi)$ is available. When this is not the case one may roughly estimate σ_c by further assuming that the brush is sufficiently dilute to ensure $\Delta\mu(\phi) \sim \phi$ thus leading to

$$\sigma_c \approx \begin{cases} \phi_-^{3/2} & \text{self-avoidance} \\ \phi_- & \text{Gaussian} \end{cases} \tag{5.23}$$

This last form is of interest because it permits a crude estimate of σ_c on the basis of the phase diagram even when $\overline{\chi}(\phi)$ is unknown.

For $\overline{\chi}(\phi) = 1/2 + \chi_2\phi^2$ a critical point occurs at $\phi_c = 1/2$ and $\chi_{2c} = 1$. In the vicinity of the critical point, for $\chi_2 \gtrsim 1$ and $\phi \gtrsim 1/2$ the coexistence curve is well approximated by the spinodal line $\partial^2 f_\infty(\phi)/\partial\phi^2 = 0$

$$\frac{1}{1-\phi} - 1 - 4\chi_2\phi^2 = 0 \tag{5.24}$$

leading to $\phi_\pm = \frac{1}{2} \pm \frac{1}{2}\sqrt{1 - 1/\chi_2}$.

The state diagram of a brush in the $\chi_2, 1/\sigma$ plane when eq. (5.24) applies is shown in Figure 5.4. Concentration profiles obtained from $\overline{\chi}(\phi)$ of this form are depicted in Figure 5.5. The above discussion is of the mean-field type and scaling refinements are ignored. Clearly, a more sophisticated analysis may lead to modifications of the results, especially in the vicinity of the critical point [121].

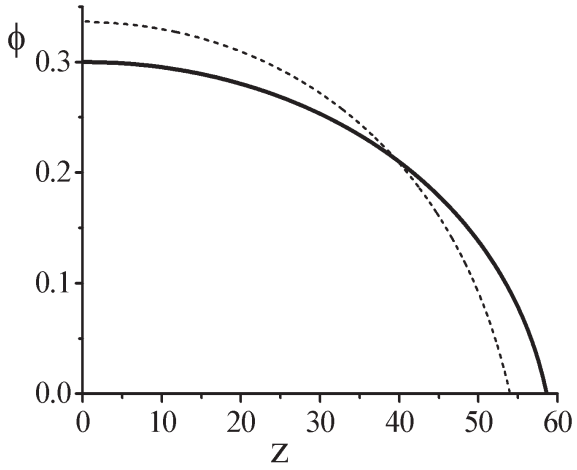

Figure 5.6: *The concentration profile, ϕ vs. z plots, for a brush of polystyrene in toluene with $N = 300$, $\sigma/a^2 = 22.5$ $(\sigma/R_F^2 = 0.024)$ $T = 25^0C$ calculated using $\overline{\chi}(\phi) = 0.431 - 0.311\phi - 0.036\phi^2$ [25]. The dashed line depicts the case $\overline{\chi}(\phi) = \overline{\chi}_0$ while the continuous line describes $\phi(z)$ for the full $\overline{\chi}(\phi)$.*

Equations (5.16-5.18) allows to examine the deviations from the parabolic profile for real systems with $\chi_{eff}(T, \phi)$. The concentration profile $\phi(z) \sim z^2$ in the case of

$\chi(T)$ which does not depend on concentration or, in general, when f_∞ is approximated by $f_\infty \approx v(T)\phi^2$. Upon replacing $\chi(T)$ by $\chi_{eff}(T,\phi)$ the concentration profile of the brush $\phi(z)$ is modified because the solvent quality varies, in effect, with the height z. As a result, $\phi(z)$ is no longer parabolic.

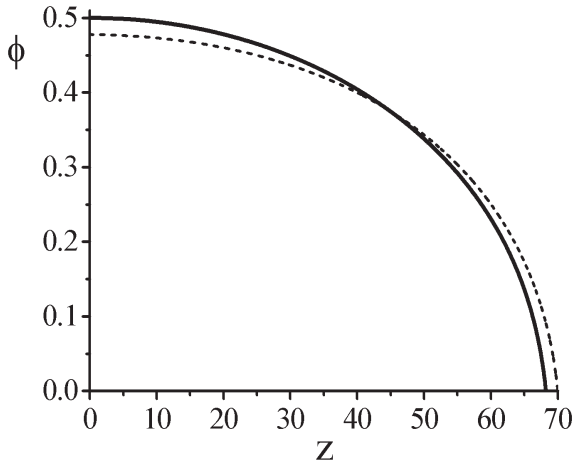

Figure 5.7: *The concentration profile, ϕ vs. z plots, for a brush of PEO in water with $N = 300$, $\sigma/a^2 = 11$ ($\sigma/H_F^2 = 0.012$), $T = 25^0C$ calculated using $\overline{\chi}(\phi) = 0.469 + 0.060\phi - 0.241\phi^2 + 0.370\phi^3$ obtained by polynomial fit of the $\overline{\chi}(\phi)$ data in [1]. The dashed line depicts the case $\overline{\chi}(\phi) = \chi_0$ while the continuous line describes $\phi(z)$ for the full $\overline{\chi}(\phi)$.*

In the absence of a phase separation of the second type, two principle scenarios are possible. When $\overline{\chi}(\phi)$ is a decreasing function of ϕ the brush height, H, increases while the concentration at the grafting surface, ϕ_0, decreases. Such behavior is expected, for example, for brushes of polystyrene in toluene (Figure 5.6). When $\overline{\chi}(\phi)$ is an increasing function of ϕ the brush height, H decreases while the concentration at the grafting surface, ϕ_0 increases. This is the case for PEO brushes in water (Figure 5.7).

The concentration profiles discussed above can be obtained from simpler arguments within the Pincus approximation [116, 122]. The level of this approximation is roughly midway between the Alexander model and the SCF theory. It retains the uniform stretching assumption but allows for spatial variation in ϕ and in the dis-

tribution of the free ends. As a result, it allows to get correct concentration profiles, but it fails in the description of the distribution of free ends near the grafting surface and the compression force profiles. The discussion of the Pincus approximation is given in Appendix A.

5.5 Average Thickness of the Brush

Experimentally, the brush thickness H is inaccessible. Certain experimental technique yield $\phi(z)$ allowing one to obtain moments of $\phi(z)$

$$\langle z \rangle = \frac{\int_0^H z\phi(z)dz}{\int_0^H \phi(z)dz} = \frac{\sigma}{Na^3}\int_0^H z\phi(z)dz \tag{5.25}$$

and

$$\langle z^2 \rangle = \frac{\int_0^H z^2\phi(z)dz}{\int_0^H \phi(z)dz} = \frac{\sigma}{Na^3}\int_0^H z^2\phi(z)dz. \tag{5.26}$$

Other techniques, such as ellipsometry, measure $\langle z \rangle$ [123]. As we shall discuss, the

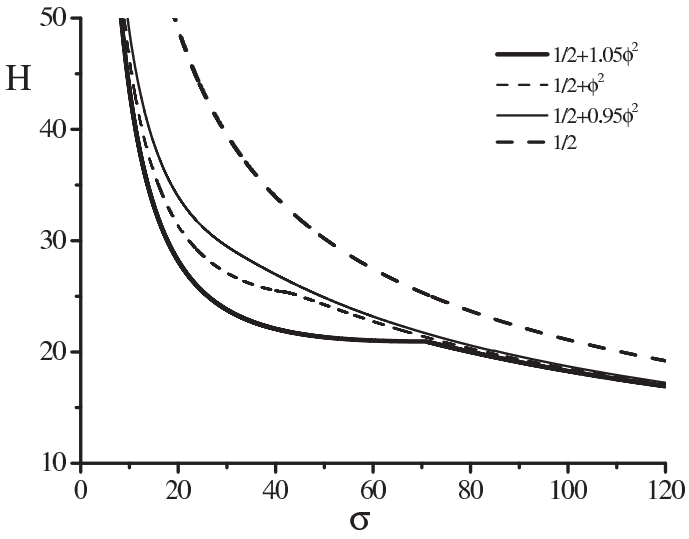

Figure 5.8: *H as a function of σ for different χ_2 values and $N = 300$.*

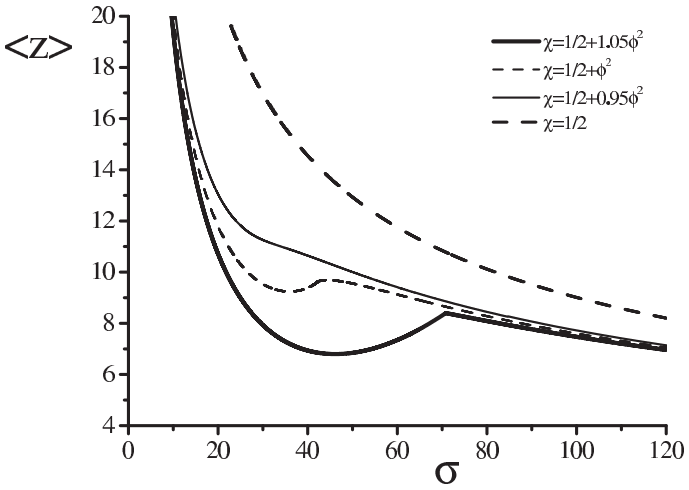

Figure 5.9: $\langle z \rangle$ *as a function of* σ *for different* χ_2 *values and* $N = 300$.

σ dependence of the moments provides useful information on the brush structure. The details of the calculation of these moments are described in Appendix B.1.

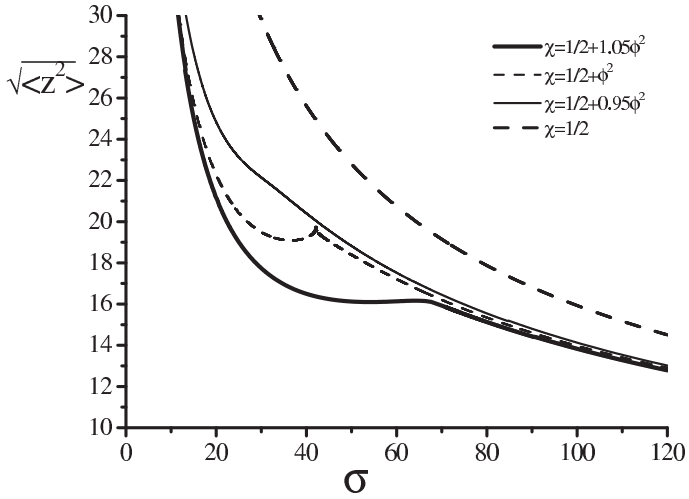

Figure 5.10: $\sqrt{\langle z^2 \rangle}$ *as a function of* σ *for different* χ_2 *values and* $N = 300$.

When $\phi(z)$ is continuous, both moments increase smoothly with the grafting density. In marked contrast, vertical phase separation within the brush gives rise to

a non-monotonic behavior. In particular, both $\langle z \rangle$ and $\sqrt{\langle z^2 \rangle}$ exhibit a minimum at intermediate σ. A vertical phase separation gives rise to a plateau in the H vs. σ plot (Figure 5.8) while in the plots of $\langle z \rangle$ and $\sqrt{\langle z^2 \rangle}$ vs. σ it is associated with a minimum (Figure 5.9 and Figure 5.10).

The physical origin of this behavior is the partitioning of the monomers between the inner dense phase and the outer dilute one. The process of swapping of monomers between coexisting phases is shown schematically in Figure 5.11. The minima are

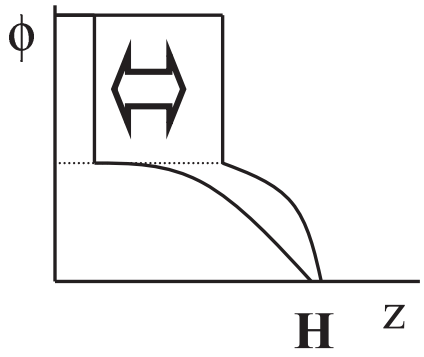

Figure 5.11: *The change in the concentration profile with changing grafting density.*

traceable to the higher weight give to the inner phase. Since the inner phase is denser, the onset of vertical phase separation is associated with a decrease $\langle z \rangle$ and $\sqrt{\langle z^2 \rangle}$. These features provide a useful diagnostic for the occurrence of a vertical phase separation in the brush. The SCF analysis in this section confirms earlier results [103] obtained by utilizing the Pincus approximation [122, 124]. As we shall discuss this is the case for properties that are insensitive to the precise form of $g(z)$. In marked contrast, the compression force profile (section 5.8) does depend on $g(z)$ and the SCF result differ from the one obtained from the Pincus approximation.

5.6 Distribution of Free Ends

The SCF formalism allows to obtain the distribution of free ends, $g(z)$ as a function of height z. Current experimental techniques do not allow to probe $g(z)$ directly.

However, $g(z)$ is of interest because it plays a role in the calculation of the com-

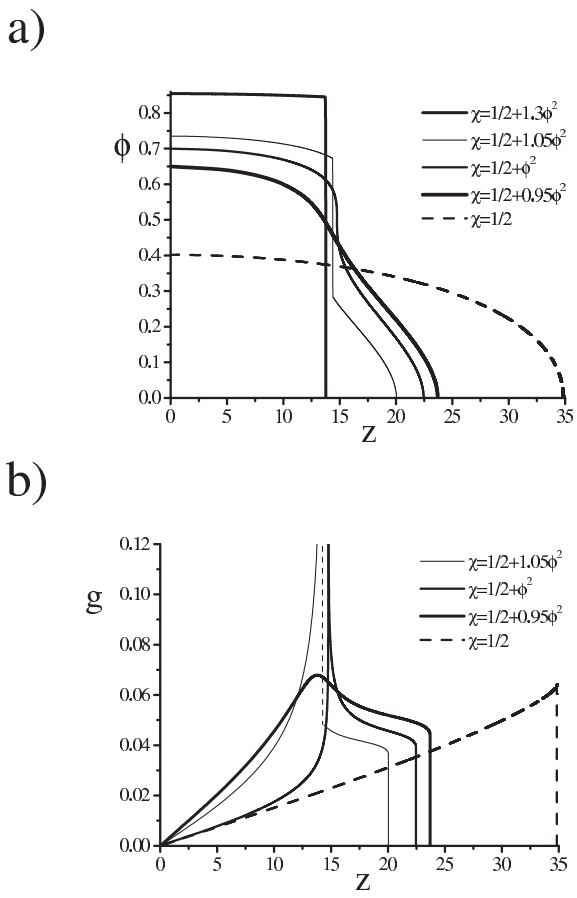

Figure 5.12: *Plots of $\phi(z)$ (a) and $g(z)$ (b) above and below the critical point for $\overline{\chi}(\phi) = 1/2 + \chi_2\phi^2$, $\sigma = 17$ and $N = 200$. In all cases, the outer phase is swollen.*

pression force profile. When $\chi = const$ the brush structure is dominated by the contributions of the second and third virial terms of F_{int}. Three scenarios emerge. In a good solvent the ends are distributed throughout the brush and $g(z)$ is a smooth function vanishing at $z = 0$ and $z = H$. When the brush is collapsed in a poor solvent the ends reside preferentially at the outer edge of the brush and $g(z)$ diverges at H. In a θ solvent $g(z)$ increases smoothly with z but does not diverge [107, 120]. As we shall see, a new scenario emerges when a vertical phase separation occurs.

In particular, $g(z)$ will then diverge at the phase boundary indicating localization of the ends at the boundary. We will obtain $g(z)$ from the integral equation (5.6). The details of the calculation are described in Appendix B.2.

$g(z)$ of a brush with a continuous profile (Figure 5.12) is specified by

$$g(z) = z\frac{\sigma}{Na^3}\left(\frac{\phi_H}{\sqrt{H^2-z^2}} + \sqrt{B}\int_{\phi_H}^{\phi}\frac{d\phi'}{\sqrt{\Delta\mu(\phi)-\Delta\mu(\phi')}}\right) \tag{5.27}$$

where ϕ and z are related by (5.15). When a vertical separation occurs within the brush, equation (5.6) yields two expressions, for $\phi(z)$. At the outer edge, $H_t < z < H$

$$\phi(z) = \frac{a^3}{\sigma}\int_z^H \frac{g(z')dz'}{E(z,z')} \tag{5.28}$$

while at the inner dense phase, $0 < z < H_t$

$$\phi(z) = \frac{a^3}{\sigma}\int_z^{H_t} \frac{g(z')dz'}{E(z,z')} + \frac{a^3}{\sigma}\int_{H_t}^H \frac{g(z')dz'}{E(z,z')} \tag{5.29}$$

In the outer region only free ends with $H_t < z$ contribute while for the inner phase all free ends are involved.

The expression for $g(z)$ in the two regions are given below while the details of the derivation are presented in Appendix B.2. At the outer phase, $H_t < z < H$

$$g(z) = z\frac{\sigma}{Na^3}\left(\frac{\phi_H}{\sqrt{H^2-z^2}} + \sqrt{B}\int_{\phi_H}^{\phi}\frac{d\phi'}{\sqrt{\Delta\mu(\phi)-\Delta\mu(\phi')}}\right). \tag{5.30}$$

while in the inner phase, $0 < z < H_t$

$$g(z) = \frac{z\sigma}{Na^3}\left[\frac{\phi_+(H_t)-\phi_-(H_t)}{\sqrt{H_t^2-z^2}} + \frac{\phi_H}{\sqrt{H^2-z^2}} + \sqrt{B}\int_{\phi_+(H_t)}^{\phi}\frac{d\phi'}{\sqrt{\Delta\mu(\phi)-\Delta\mu(\phi')}}\right.$$
$$+\frac{\sqrt{B}}{\pi}\sqrt{H_t^2-z^2}\int_{\phi_H}^{\phi_-(H_t)}\frac{\frac{d\Delta\mu(\phi')}{d\phi'}d\phi'}{\left(H^2-z^2-\frac{\Delta\mu(\phi')}{B}\right)\sqrt{H^2-H_t^2-\frac{\Delta\mu(\phi')}{B}}}\times$$
$$\left.\int_{\phi_H}^{\phi'}\frac{d\phi''}{\sqrt{\Delta\mu(\phi')-\Delta\mu(\phi'')}}\right]. \tag{5.31}$$

The first integral allows for the contribution of the inner phase and the second for

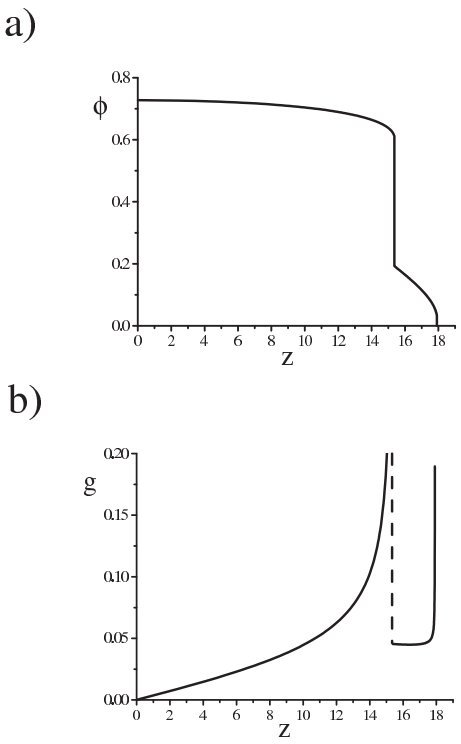

Figure 5.13: *Plots of $\phi(z)$ (a) and $g(z)$ (b) for the case of two coexisting dense phases with $\overline{\chi}(\phi) = 0.51 + \chi_2\phi^2$, $\sigma = 18$ and $N = 200$.*

the contribution of the outer phase. $g(z)$ (5.31) at the interval $0 < z < H_t$ diverges at the phase boundary $z = H_t$. $g(z)$ (5.30) at the interval $H_t < z < H$ diverges at H when the outer phase is collapsed and $\phi_H > 0$. In this case the two coexisting phases are dense (Figure 5.13). When $\phi_H = 0$ the outer phase is swollen and $g(z)$ does not diverge at H (Figure 5.12b). A rough approximation yielding closed form expressions for $g(z)$ for discontinuous brushes is described in the next section.

At this point it is of interest to compare the concentration profiles and the distribution of free ends as obtained for $\overline{\chi}(\phi)$ and for constant χ. The concentration profiles with $\overline{\chi}(\phi)$ exhibit richer behavior, Figure 5.14. The corresponding distribution functions of ends are presented in Figure 5.15.

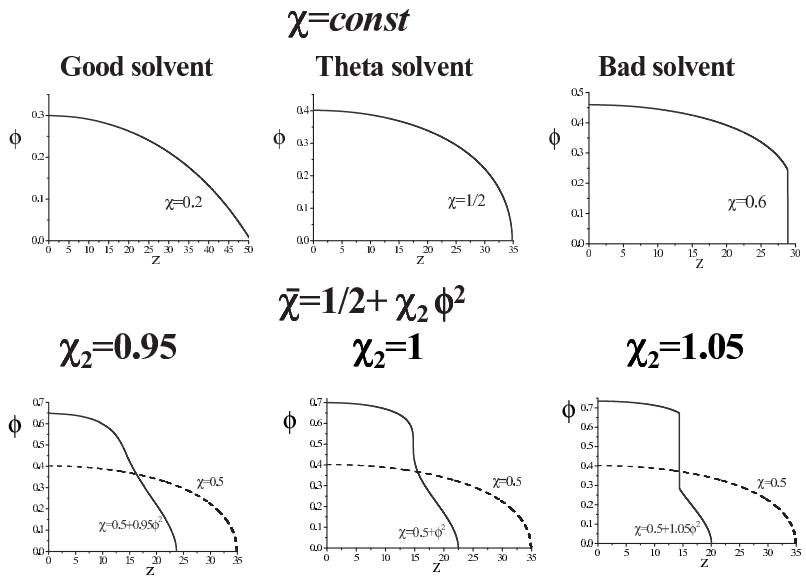

Figure 5.14: *Concentration profiles for three different regimes for the constant χ (top) and $\overline{\chi}(\phi)$ (bottom). The parameters used: $N = 200$ and $\sigma = 17$.*

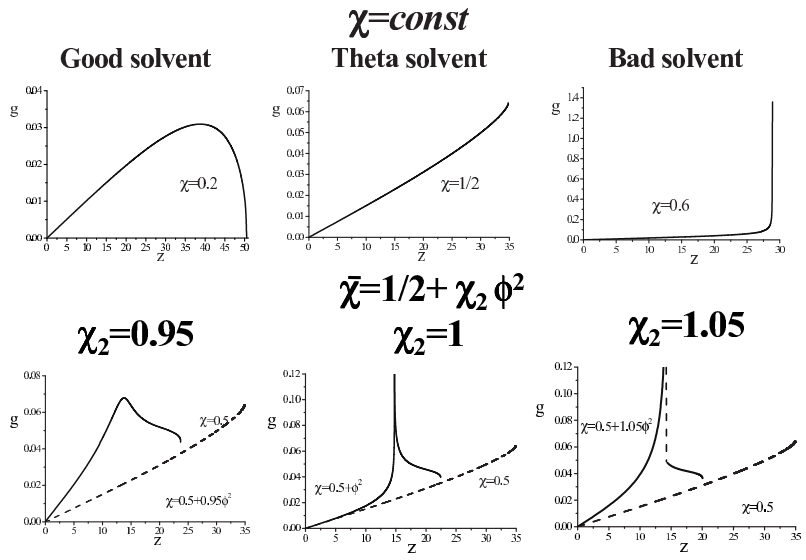

Figure 5.15: *Distribution of ends for three different regimes for the constant χ (top) and $\overline{\chi}(\phi)$ (bottom). The parameters used: $N = 200$ and $\sigma = 17$.*

5.7 Model Concentration Profiles

A rough approximation allows to obtain analytical expression for $g(z)$ of a brush in the presence of a vertical phase separation. In the dense phase the variation of ϕ is slow and we can approximate it as constant, $\phi_+ = \phi_0$. In the outer phase dilute phase ϕ is rather low and we can neglect nonconstant terms in $\overline{\chi}(\phi)$. Thus

$$\phi(z) = \begin{cases} \phi_0, 0 < z < H_t \\ \phi(z), H_t < z < H \end{cases} \tag{5.32}$$

where $\phi(z)$ is determined by (5.15) with $\chi = const$, while the value of ϕ_0 is set by (5.7). As before, $g(z)$ in the outer phase is determined by (5.30) while in the inner phase it is determined by (5.31).

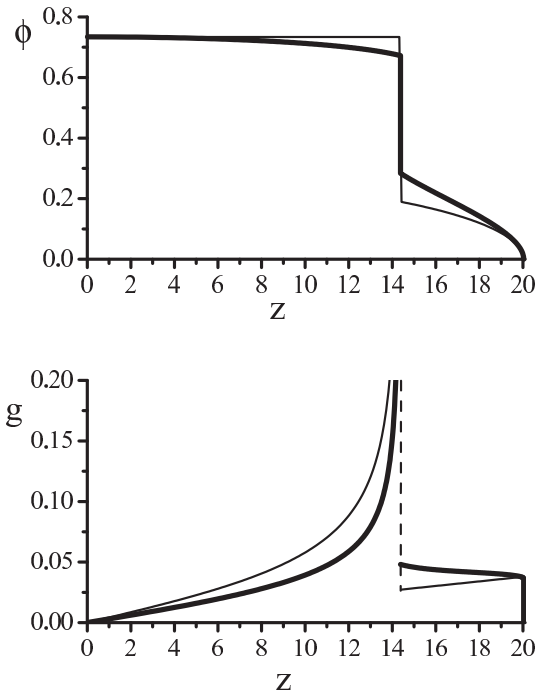

Figure 5.16: *Comparison between the exact $\phi(z)$ and $g(z)$ and their approximate values as calculated from for the case of $\overline{\chi}(\phi) = 1/2 + 1.05\phi^2$, $\sigma = 120$ and $N = 300$.*

First, consider the case of $\chi = 1/2$ leading to $\Delta\mu(\phi) = -\ln(1-\phi) - \phi \approx \phi^2/2$

and eq. (5.30) yields

$$g(z) = z\frac{\sigma\pi}{2Na^3}\sqrt{2B} \tag{5.33}$$

Substitution of (5.33) into (5.31) gives the expression for $g(z)$ in the inner phase

$$g(z) = \frac{z\sigma}{Na^3}\left[\frac{\phi_+(H_t) - \phi_-(H_t)}{\sqrt{H_t^2 - z^2}} + \sqrt{2B}\arctan\sqrt{\frac{H^2 - H_t^2}{H_t^2 - z^2}}\right] \tag{5.34}$$

where $\phi_-(H_t) = \sqrt{2B(H^2 - H_t^2)}$ and $\phi_+(H_t) = \phi_0$. This function is discontinuous and diverges at the phase boundary $z = H_t$. The value of ϕ_0 can be found from (5.7)

$$\phi_0 = \frac{Na^3}{\sigma H_t} - \sqrt{\frac{B}{2}}\left[\frac{H^2}{H_t}\left(\frac{\pi}{2} - \arcsin\frac{H_t}{H}\right) - \sqrt{H^2 - H_t^2}\right] \tag{5.35}$$

When $\chi = 0$ eq. (5.30) specifies $g(z)$ at the outer phase, $H_t < z < H$

$$g(z) = z\frac{\sigma}{Na^3}B\sqrt{H^2 - z^2}. \tag{5.36}$$

and eq. (5.31) for $g(z)$ in the inner phase, $0 < z < H_t$, yields

$$g(z) = \frac{z\sigma}{Na^3}\left[\frac{\phi_+(H_t) - \phi_-(H_t)}{\sqrt{H_t^2 - z^2}} + 2B\left(2\sqrt{H^2 - H_t^2} + \sqrt{H_t^2 - z^2} - \sqrt{H^2 - z^2}\right)\right]. \tag{5.37}$$

Again, $g(z)$ of the inner phase diverges at the phase boundary. The performance of this approximation is illustrated in Fig 5.16. It captures the main features of $\phi(z)$ and the behavior of $g(z)$ in the inner region. However $g(z)$ at the outer region increases rather than decrease.

5.8 Compression of a brush

The surface force apparatus allows to measure the restoring force arising upon compression of a brush. For brushes of polymers characterized by a constant χ the

force increases smoothly with the compression and the force profile is essentially featureless. When the brush consists of polymers characterized by $\overline{\chi}(\phi)$ the compression can induce a vertical phase separation even if the concentration profile of the brush is initially continuous. The existence of a vertical phase separation, be it compression induced or not, gives rise to distinctive regimes in the force profile. In particular, the slope of the force vs. distance curve in different compression regimes can be markedly different. In such experiments H is determined by the compressing surface rather than by σ. Accordingly, ϕ_H is set by the normalization condition (5.7) and not by $\pi(\phi_H) = 0$. The compression increases F_{chain} and the restoring force per area σ is

$$f(H) = -\frac{\partial F_{chain}}{\partial H} \tag{5.38}$$

In the following we obtain this force law for the case of compression by impenetrable, non-adsorbing surface.

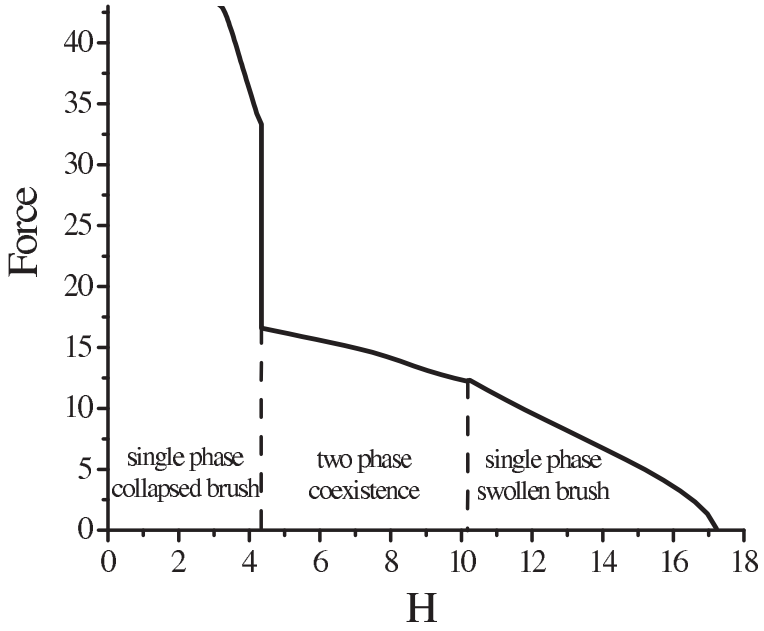

Figure 5.17: *The compression force profile for a brush with* $\overline{\chi}(\phi) = 1/2 + 1.05\phi^2$, $\sigma = 120$ *and* $N = 300$. *The uncompressed brush is in a single phase state* ($\phi_0 < \phi_-$).

For a brush with a continuous $\phi(z)$

$$\frac{F_{chain}}{kT} = \int_{\phi_0}^{\phi_H} \left[\frac{\sigma}{a^3} f_\infty(\phi) + \frac{3}{2a^2} \frac{\pi^2}{8N} z^2(\phi) g(\phi) \right] \frac{\partial z}{\partial \phi} d\phi \tag{5.39}$$

obtained by invoking $\int_0^{z'} E(z', z)dz = z'^2\pi^2/(8N)$. Here $g(z)$ is given by (5.27),

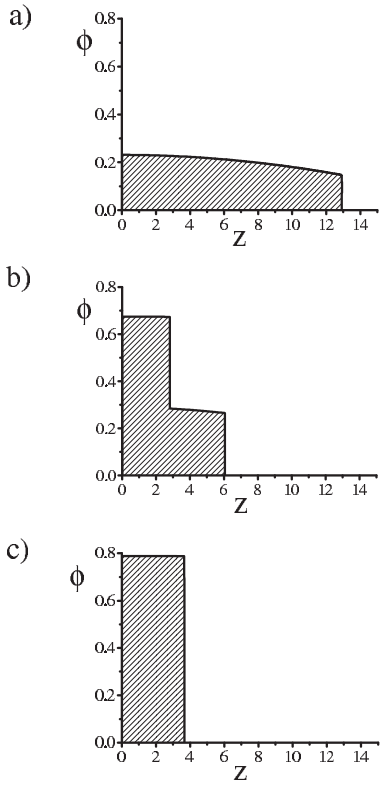

Figure 5.18: *$\phi(z)$ plots corresponding to the three regimes in Figure 5.17. (a) single phase swollen phase, $H = 12.9$, (b) a coexistence of a dense and a dilute phase, $H = 6.1$, (c) single dense phase, $H = 3.7$. In every case $\sigma = 120$ and $N = 300$.*

while $z(\phi)$ and $\partial z/\partial \phi$ are specified by (5.17). $f(H)$ is calculated numerically subject to the constraint (5.18). When the concentration at the wall, ϕ_0, exceeds ϕ_-, the brush undergoes a vertical phase separation and $\phi(z)$ is no longer continuous. In this case F_{chain} assumes the form

$$\frac{F_{chain}}{kT} = \frac{\sigma}{a^3}\int_{\phi_0}^{\phi_H} f_\infty(\phi)\frac{\partial z}{\partial \phi}d\phi + \frac{3}{2a^2}\frac{\pi^2}{8N}\left[\int_{\phi_0}^{\phi_+(H_t)} z^2(\phi)g(\phi)\frac{\partial z}{\partial \phi}d\phi + \int_{\phi_-(H_t)}^{\phi_H} z^2(\phi)g(\phi)\frac{\partial z}{\partial \phi}d\phi\right] \quad (5.40)$$

where $g(\phi)$ is specified by eqs. (5.31) for the inner phase and by (5.30) for the outer one. The conservation of monomers is enforced by the constraint (5.19).

When the conditions permit a vertical phase separation within the brush, it can take place in two ways. It can occur when the grafting density exceeds a certain critical value thus causing $\phi_0 > \phi_-$. Alternatively, it can also take place as a result of compression when the grafting density does not lead to phase separation in the unperturbed brush. The development of $\phi(z)$ and $f(H)$ for this second case is depicted in figures 5.17 and 5.18 respectively.

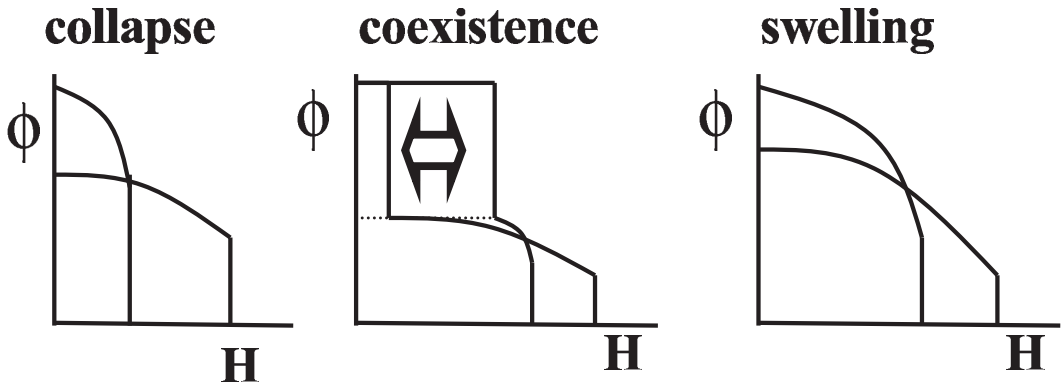

Figure 5.19: *Three regimes in the compression of a two-state brush.*

There are three main regions on the compression curve (Figure 5.19). Initially, the brush retains the single phase structure and the associated force law. When the compression enforces $\phi_0 > \phi_-$, a vertical phase separation occurs and is signalled by a weaker slope of the $f(H)$ vs. H curve. Stronger compression causes complete conversion to a dense phase thus causing an abrupt increase in $f(H)$.

5.9 Karlstrom Two-State Model: Distribution of States

Thus far, our discussion concerned brushes characterized by an arbitrary $\chi_{eff}(\phi)$. We now illustrate these considerations for the case of the K model [21] discussed in chapter 2.5. We focus on this model because of its simplicity and its semiquantitative agreement with the phase diagram of aqueous solutions of PEO at atmospheric pressure [21] and the measured $\overline{\chi}(T,\phi)$ [34].

The equilibrium value of the fraction of monomers in the hydrophilic A state, p, for a given ϕ is specified by (2.26)

$$\frac{p}{1-p} = \exp\left[-\Delta\epsilon - (1-\phi)(\chi_{AS}-\chi_{BS}) - \phi\chi_{AB}(1-2p)\right] \tag{5.41}$$

The equilibrium $\chi_{eff}(\phi)$ and $\overline{\chi}(\phi)$ are obtained from the expression for the interaction free energy (2.25) and eq. (5.41) as

$$\begin{aligned}\chi_{eff}(\phi) &= p\chi_{AS} + (1-p)\chi_{BS} + \\ &\quad \frac{\phi}{1-\phi}\left[\chi_{AB}p(1-p) + p\Delta\epsilon\right] + \frac{p\ln p + (1-p)\ln(1-p)}{1-\phi}\end{aligned} \tag{5.42}$$

and $\overline{\chi}(\phi)$ (2.28)

$$\overline{\chi}(\phi) = p\chi_{AS} + (1-p)\chi_{BS} - \chi_{AB}p(1-p) \tag{5.43}$$

Both $\chi_{eff}(\phi)$ and $\overline{\chi}(\phi)$ can be expanded in powers of ϕ. The coefficients in the expansion depend on the parameters, $\Delta\epsilon$, χ_{AS}, χ_{BS}, χ_{AB}. Using the parameters used to fit the phase diagram of PEO in water, $\chi_{As} = 80.0/T$, $\chi_{Bs} = 684.5/T$, $\chi_{AB} = 155.6/T$, $\Delta\varepsilon = -625.2/T + \ln 8$, $N = 300$, for $T = 60^o$ C the expansion yields: $\overline{\chi}(\phi) \approx 0.48 + 0.31\phi + 0.07\phi^2$. Since high order terms are of negligible importance this expansion provides a good approximation for $\overline{\chi}(\phi)$.

Equation (5.41) allows to relate the volume fraction ϕ to p, the fraction of hydrophilic A states, as

$$\phi(p) = \frac{\ln\frac{p}{1-p} + \Delta\epsilon + \chi_{AS} - \chi_{BS}}{\chi_{AS} - \chi_{BS} - \chi_{AB}(1-2p)} \tag{5.44}$$

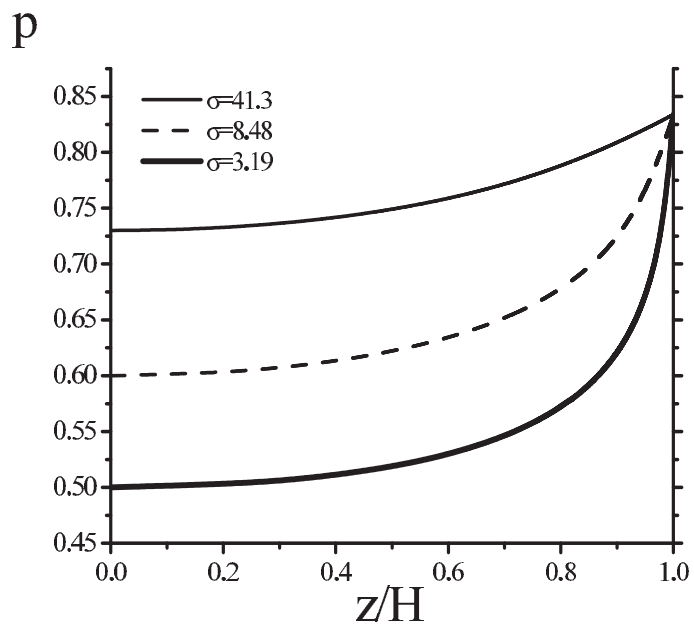

Figure 5.20: *A plot of the fraction of hydrophilic states, p vs. z, in the K model (chapter 2.5) for different grafting areas σ. In every case* $\chi_{As} = 80.0/T$, $\chi_{Bs} = 684.5/T$, $\chi_{AB} = 155.6/T$, $\Delta\varepsilon = -625.2/T + \ln 8$, $N = 300$, $T = 60^o$ *C.*

Accordingly, the exchange chemical potential can be specified in terms of p, *i.e.* $\Delta\mu(\phi(p))$. In turn, eq. (5.15) enables us to obtain $z = z(p)$. To this end we invoke two boundary conditions: (i) In this range of parameters the brush is swollen and ϕ vanishes at the outer edge, $\phi_H = \phi(p = p_H) = 0$ where p_H is the value of p at the height H. (ii) At the grafting surface we have $\Delta\mu(z = 0, p = p_0) = BH^2$, where p_0 is the value of p at $z = 0$. In addition we utilize the conservation of monomers as given by (5.18). The corresponding plots of $p = p(z)$ as well as the concentration profiles of the two states are depicted, for different σ, in Figure 5.20 and in Figure 5.21. Since all brushes considered are swollen, with $\phi_H = 0$, the p values at the outer edge of the brush, $z = H$ are identical, $p = p_H$. Increasing grafting density leads to higher concentration at the grafting surface. This favors the hydrophobic B state and lower p at the surface. For the chosen parameters, the minimal value of p, corresponding to a PEO melt ($\phi = 1$), is $p_* = 0.45$.

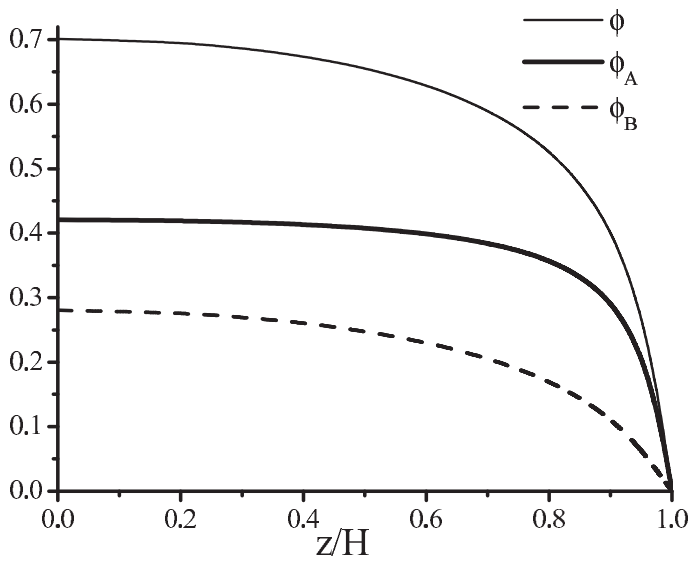

Figure 5.21: *The overall $\phi(z)$ and the corresponding concentration profiles of the monomeric states $\phi_A(z) = p(z)\phi(z)$ and $\phi_B(z) = [1-p(z)]\phi(z)$ within the K model for the conditions specified in Figure 5.20.*

5.10 Conclusion

We presented a common framework for the analysis of the structure of planar brushes of neutral water-soluble polymers that own their solubility to the formation of hydrogen bonds with water. Our analysis concerned a family of two-state models developed for PEO (chapter 2.4) but applicable, in principle, to other neutral water-soluble polymers. The particular aspects of the models were grouped into $\chi_{eff}(T, \phi)$ thus allowing for a unified discussion of the brush structure within these models [108].

The ϕ dependence of $\overline{\chi}(\phi)$ gives rise to deviations from the parabolic concentration profile as obtained when $\chi = \chi(T)$. In certain cases it leads to a first-order, vertical phase separation within the brush that can occur for polymers capable of a second type of phase separation. Significant part of the discussion concerned brushes exhibiting such behavior. In particular, we examined the distinctive behavior of plots of $\langle z \rangle$ and $\sqrt{\langle z^2 \rangle}$ vs. σ and the compression force profiles associated with

such brushes. $\phi(z)$ and its moments are insensitive to the precise form of $g(z)$ and the SCF analysis recovers the results obtained by the use of the Pincus approximation (Appendix A). In marked contrast, the compression force law does depend on $g(z)$ and a full SCF analysis is necessary in order to obtain the correct results. The compression induces the growth of the inner dense phase and the force increase with decreasing distance between the compression surfaces. These features are useful criteria for the occurrence of vertical phase separation. Such criteria are of interest because of indirect experimental indications that brushes of PNIPAM exhibit this effect. We shall discuss experiments supporting this idea in the next chapter.

Chapter 6

Illustrative example: PNIPAM

6.1 Résumé

Les modèles à deux états et $\overline{\chi}(\phi)$ pourront être utilisés comme preuve indirecte que le fait de la transition de phase verticale peut se produire dans les brosses de PNIPAM. Les données expérimentales correspondantes aux géométries différentes confirment aussi cette conclusion.

6.2 Introduction

The results of the previous chapters suggest, that a qualitatively novel scenarios for the collapse of isolated coils and for the structure of polymer brushes can occur when $\overline{\chi}(\phi)$ increase with ϕ. This behavior is apparently realized by Poly(N-isopropylacrylamide) (PNIPAM) in water, a system exhibiting a lower critical solution temperature (LCST) behavior at room temperatures (chapter 1.6.3). In this chapter we implement the results of chapter 5 for the case of PNIPAM brushes using an empirical expression for $\chi_{eff}(T, \phi)$ obtained from the phase diagram. Thus, $\chi_{eff}(T, \phi)$ allows us to relate thermodynamic data concerning a solution of polymers with numerous other experimental data on polymer brushes and isolated coils.

6.3 Experimental Observations Concerning PNIPAM

6.3.1 PNIPAM brushes

Five items concerning PNIPAM brushes are of interest for our discussion. First, is an early study by Zhu and Napper [114, 115] of the collapse of PNIPAM brushes grafted to latex particles immersed in water. This revealed a collapse involving two stages. An "early collapse", took place below 30^o C, at better than "θ-conditions", and did not result in flocculation of the neutral particles. Upon raising the temperature to worse than "θ-conditions" the collapse induced flocculation. This indicates that the colloidal stabilization imparted by the PNIPAM brushes survives the early collapse. It lead to the interpretation of the effect in terms of a vertical phase separation within the brush due to a second type of phase separation as predicted by the n-cluster model. However, a vertical phase separation is possible within all two-state models, while the discussion within the n-cluster model creates a misleading impression about the physical origins of this phenomenon.

Second item concerns the recent observations on PNIPAM brushes synthesized on the surface of self-assembled monolayer on gold [56]. Surface plasmon resonance (SPR) spectroscopy was used to study the temperature induced brush collapse. It was shown that the PNIPAM brush collapses gradually over a wide range of temperatures, $10 - 40^o$ C. In contrast, water contact angle measurements exhibit a discontinuous jump of the advancing contact angle at $T \sim 32^o$ C. These experiments suggests that PNIPAM brushes undergo a vertical phase separation associated with the second type of phase separation. This rationalize the two stages in the collapse behavior of PNIPAM brush in the experiment. The inner, hydrophobic phase is shielded from water by the outer hydrophilic phase. The gradual collapse is associated with the inner phase, while the abrupt jump of the advancing contact angle may be related to the disappearance of the outer phase and direct contact of hydrophobic phase with water as modelled in Figure 5.12.

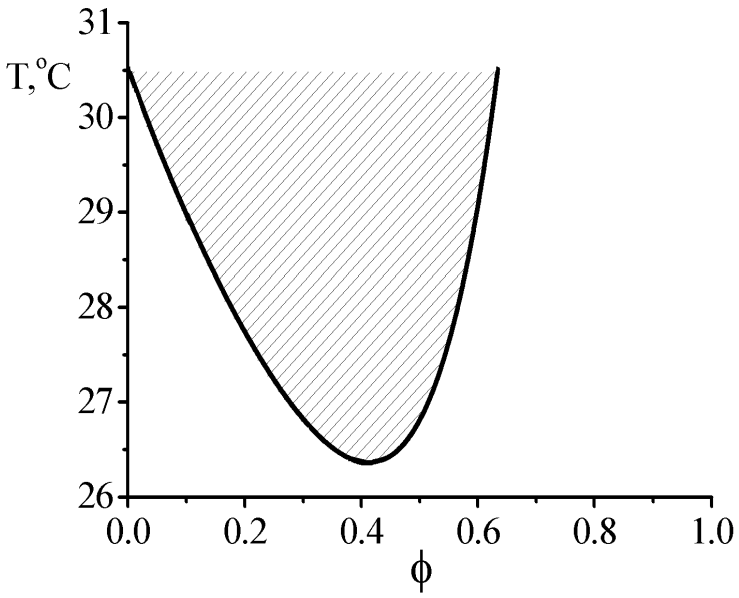

Figure 6.1: *The phase diagram of PNIPAM in the limit of $N \to \infty$ as obtained from the $\chi_{eff}(\phi)$ of Afroze et al [36].*

This picture is also supported by recent study of the phase behavior of PNIPAM by Afroze *et al* [36]. Early study of the phase behavior of PNIPAM in water, by Heskins and Guillet [52], identified a LCST at $\phi_c \simeq 0.16$ and $T_c \simeq 31.0^o$ C. In marked contrast, the work of Afroze *et al* [36] identified PNIPAM as a polymer undergoing a second type of phase separation. In particular: (i) While the LCST of PNIPAM depends on N, the LCST occurs around $T_c \simeq 27 - 28^o$ C and $\phi_c \simeq 0.43$ (ii) In the limit of $\phi \to 0$, the phase separation occurs, depending on N, between 30^o C and 34^o C as shown in Figure 6.1. Thus, the phase diagram of Afroze *et al* suggests that a vertical phase separation is indeed expected in brushes of PNIPAM [103].

Another item concerns the systematic Neutron Reflectometry (NR) studies of PNIPAM brushes will eventually provide clearer picture of the situation. Early studies were hampered by high polydispersity as well as difficulties in determining N and σ [125]. With this in mind, the NR results revealed that the structure of PNIPAM brushes in acetone is very different from their structure in water, both

at 20^o C and at 55^o C. In acetone the concentration profile is smoothly decaying while in water it consists of a narrow, inner, dense region and an outer, extended and dilute region. More recent work utilized NR [126], to study samples with lower polydispersity and higher grafting density between 20^o C and 40^o C. Importantly, the results indicate that most of the conformational change occurred between 28^o C and 34^o C though the corresponding concentration profiles are not reported. The results suggest a repartitioning of the monomers between a dilute outer tail and an inner dense region [127].

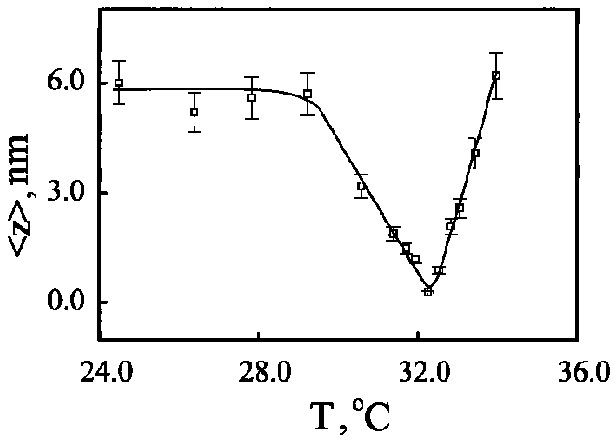

Figure 6.2: *The average thickness of the brush layer on microgel particle vs. temperature. Redrawn from [128].*

Finally, recent experimental results of Hu *at al* [128] are suggestive of the predictions obtained above concerning the variation of $\langle z \rangle$ upon decreasing σ (Figure 5.9). Hu *et al* studied the thickness of a PNIPAM brush grafted to spherical microgels of copolymers of PNIPAM and acrylic acid 2-hydroxyethyl ester (HEA). The microgels shrink as T increases from 24^o C to 36^o C thus inducing a decrease in σ. Remarkably, the thickness of the brush initially decreases in the range 27^o C to 32^o C but subsequently increases upon further heating in the range 27^o–32^o C (Figure 6.2). Unfortunately, in this experiment it is impossible to separate the effects due to change in T from those to the change in σ because the T is used to tune σ.

The items listed above suggest that PNIPAM indeed exhibits the collapse behavior expected when $\overline{\chi}(\phi)$ increases with ϕ, thus: (i) Zhu and Napper provided evidence for the occurrence of a vertical phase separation within a PNIPAM brush; (ii) the SPR spectroscopy measurements suggest that there are two stages in the collapse of PNIPAM brushes; (iii) the phase diagram measured by Afroze *et al* permits the interpretation of Zhu and Napper concerning PNIPAM brushes. Furthermore, as we shall see, their $\chi_{eff}(T,\phi)$ yields a $\overline{\chi}(\phi)$ increasing with ϕ, allowing to construct the concentration profiles of PNIPAM brushes. (iv) The NR studies show that PNIPAM brushes has significantly different structure in water than in acetone. (v) The study of PNIPAM brushes grafted to microgel particles gives an indirect evidence on the minimum in the variation of the brush thickness with σ.

6.3.2 Isolated PNIPAM Chains

In addition, the experimental study of the collapse behavior of isolated PNIPAM chains [129] supports indirectly our conclusions. This study concerned dilute aque-

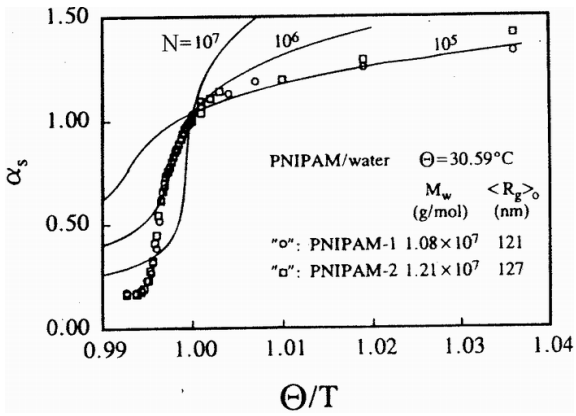

Figure 6.3: *Static expansion factor $\alpha_s = R_g(T)/R_g(\theta)$ as a function of the relative temperature θ/T, where R_g is the radius of gyration and $\theta = 30.59^o$ C. Experimental curve does not coincide with theoretical curves for different N, number of monomers in the chain. Redrawn from [129].*

ous solutions of high molecular weight PNIPAM heated to above the "θ-temperature". It provided detailed R vs. T plots characterizing the collapse of individual chains. This study was made possible by the apparent decoupling of the collapse and bulk phase separation in the case of PNIPAM. For the present discussion, the conclusion of interest is that the collapse was steeper than expected on the basis of a driving force due to simple binary attractions as modelled by $-v\phi^2$ with $v = 1 - 2\chi(T)$ (Figure 6.3). The experimental curve cannot be fitted with the Flory theory of coils assuming constant χ.

6.4 Concentration Profiles of a PNIPAM Brush

In the following we utilize the results of Afroze *et al* because they are consistent with the results of Zhu and Napper in that they enable a vertical phase separation within a PNIPAM brush below 30^o C.

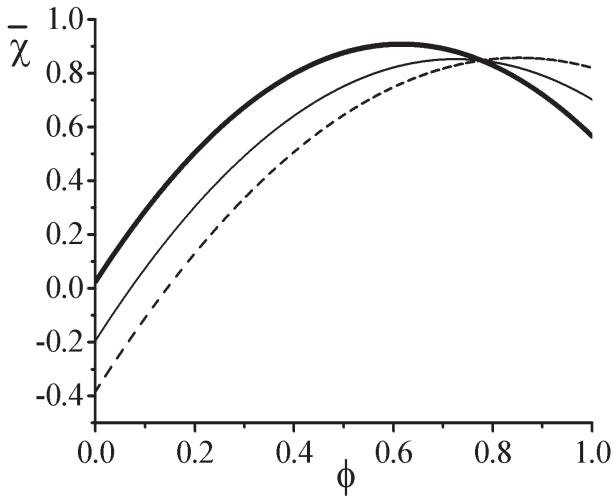

Figure 6.4: *A plot of $\overline{\chi}(\phi)$ vs. ϕ for PNIPAM as described by the $\chi_{eff}(\phi)$ of Afroze et al [36] for $T = 26^o$ C (dash), $T = 28^o$ C (thin line) and $T = 30^o$ C (thick line).*

Using the $\overline{\chi}(\phi)$ by Afroze *et al* (Figure 6.4) we can calculate the concentration profiles of PNIPAM brushes in water. The concentration profiles of a PNIPAM

brush, $\phi(z)$ *vs.* z, thus obtained confirm that a vertical phase separation is indeed expected within the brush (Figure 6.5).

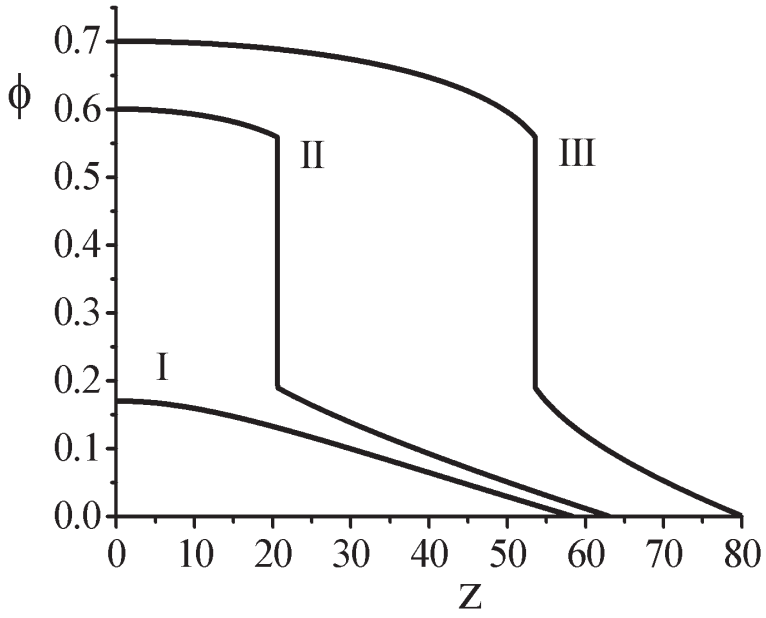

Figure 6.5: *ϕ vs. z plots for PNIPAM brushes for $N = 300$ and $T = 28^o$ C as obtained from the $\chi_{eff}(\phi)$ of Afroze et al [36] Curves I, II and III correspond respectively to $\sigma/a^2 = 53(\sigma/R_F^2 = 0.056)$, $\sigma/a^2 = 19(\sigma/R_F^2 = 0.020)$, $\sigma/a^2 = 8(\sigma/R_F^2 = 0.009)$.*

These plots suggest that PNIPAM in water is a promising system for the study of the novel signatures of $\overline{\chi}(\phi)$ that increases with ϕ thus leading to a second type of phase separation. At the same time, it is important to stress that the performance $\chi_{eff}(T, \phi)$ proposed by Afroze *et al* is not faultless. Using this $\chi_{eff}(T, \phi)$ enabled Afroze *et al* to reproduce satisfactorily only one of the four phase diagrams they studied. With this in mind, the plots in Figure 6.5 should be considered as preliminary. Hopefully, better results can be obtained when direct measurements of $\overline{\chi}(T, \phi)$ for PNIPAM in water will become available.

6.5 Discussion

In this chapter we focused on the relationship between $\overline{\chi}(T, \phi)$, a macroscopic property, and the microscopic swelling and collapse behavior of PNIPAM brushes. This approach allows to relate different experimental measurements. As we showed, on the basis of thermodynamic data concerning a solution of polymers we can construct the concentration profiles and indicate a system exhibiting the unusual properties. In addition, it allows to get an idea of the range of grafting densities, molecular weights and temperatures involved. It also helps to gain insight into the significance of $\overline{\chi}(T, \phi)$ and $\chi_{eff}(T, \phi)$ for a real system.

Clearly, this approach does not yield insights concerning the molecular origins of $\overline{\chi}(T, \phi)$ and $\chi_{eff}(T, \phi)$. Consequently, it does not identify molecular design parameters allowing to tune $\overline{\chi}(T, \phi)$ and $\chi_{eff}(T, \phi)$. The applicability of this method is also limited by the paucity of systematic tabulations of $\overline{\chi}(T, \phi)$.

Conclusion

Cette thèse est consacrée à l'étude d'origines et signatures de $\chi_{eff}(\phi)$ pour les polymères neutres solubles dans l'eau. Nous avons pu montrer que toutes les trois versions du modèle " hydrophile - hydrophobe " à deux états : le modèle K [21], le modèle MB [22, 23] et le modèle D [24, 72] mènent à $\chi_{eff}(\phi)$ (chapitre 2). La dépendance en concentration de χ_{eff} peut être utilisée comme une diagnostique permettant de distinguer entre les modèles différents et tester leurs paramètres impliqués. De cette façon, les modèles K et D donnent une dépendance de $\overline{\chi}(\phi)$ qualitativement exacte pour POE dans l'eau, alors que le modèle MB est en désaccord grave avec les données expérimentales. D'autre part, le modèle K ne peut produire que $\overline{\chi}(\phi)$ croissantes avec la concentration, pendant que les modèles MB et D montrent le comportement riche de $\overline{\chi}(\phi)$.

La dépendance en concentration de χ_{eff} n'apparaît pas seulement dans des modèles à deux états. $\chi_{eff}(\phi)$ signale un échec de l'énergie libre de Flory d'un polymère à un seul état. En particulier, nous avons discuté l'apparition de $\chi_{eff}(\phi)$ à partir des trois modèles à un seul état qui peuvent s'appliquer aux solutions de polymère aqueuses aussi bien que non aqueuses: (i) le modèle dit n-cluster [76] postulant l'agrégation de monomères en groupement de n-monomères ; (ii) le modèle des Agrégats sur Réseau [78, 79, 80, 81] qui tient au compte la structure d'un monomère et permet à un monomère occuper plus d'un site de réseau et (iii) le modèle de Painter *et al* [82] qui fait la distinction entre les contacts entre les monomères appartenants aux chaînes différentes et ceux appartenant à la même chaîne. Tous ces modèles mènent à $\chi_{eff}(\phi)$ (chapitre 3).

Conclusion

Dans le chapitre 4 nous avons discuté les conséquences macroscopiques de $\chi_{eff}(\phi)$ pour les systèmes de polymères à la concentration uniforme. Notamment, nous nous sommes concentrés sur la liaison entre $\overline{\chi}(T,\phi)$, une caractéristique macroscopique, et le comportement microscopique, à savoir gonflement et effondrement des brosses et de chaînes isolées dans le cadre d'approximation d'Alexander et Flory. Il y a deux résultats principaux : (i) $\chi_{eff}(\phi)$ entraîne le déplacement du crossover entre les régimes Gaussien et auto-évitant, g_B; et (ii) la transition de phase pelote – globule des chaînes flexibles isolées peut être du premier ordre quand $\overline{\chi}(\phi)$ est une fonction croissante.

Par ailleurs le paramètre $\overline{\chi}(\phi)$ croissant peut induire la séparation de phase verticale dans une brosse plane. Cet effet est attribué au deuxième type de séparation de phase dans la solution des chaînes linéaires qui implique la coexistence de deux phases de concentration finie. La séparation de phase verticale a été étudiée dans le chapitre 5 dans le cadre de théorie de champ auto-cohérent. Cette séparation de phase se manifeste dans le minimum de la courbe de l'épaisseur moyenne de la brosse en fonction de la densité de greffage. Ce minimum causé par le transfert de monomères entre les phases coexistant. De cette façon, l'existence de tel minimum est un critère utile pour l'événement de la séparation de phase verticale, car il est accessible expérimentalement. Ainsi, en étudiant ce phénomène nous avons examiné les profils de concentration, les fonctions de distribution de bouts libres et les profils de force de compression associés avec la séparation de phase verticale.

Cette approche a été invoquée par la suite dans l'interprétation des indications expérimentales indirectes qui suggère que les brosses de PNIPAM exposent cet effet (chapitre 6). Elle nous a permi d'indiquer la gamme des densités de greffage, des masses moléculaires et des températures où la séparation de phase verticale pourrait être observée.

Conclusion

In this thesis we described the origin and signatures of $\chi_{eff}(\phi)$ for neutral water-soluble polymers. It was shown, that all three versions of the "hydrophobic-hydrophilic" two-state model: K model [21], MB model [22, 23] and D model [24, 72] lead to a concentration dependent χ_{eff} (chapter 2). The concentration dependent χ_{eff} can be used as a useful diagnostic which allows to distinguish between different models and test involving parameters. Thus, K and D models give a qualitatively correct dependence $\overline{\chi}(\phi)$ of PEO in water, while MB model disagree qualitatively with experimental data. On the other hand, K model can reproduce only increasing $\overline{\chi}(\phi)$, while MB and D models exhibit rich behavior of $\overline{\chi}(\phi)$.

The concentration dependence of χ_{eff} emerges not only from the two-state models. $\chi_{eff}(\phi)$ signals a failure of the Flory free energy of a single-state polymers. In particular, we discussed the emergence of the concentration dependence of $\chi_{eff}(\phi)$ within three non two-state models applied both to aqueous and nonaqueous solutions of polymers: (i) The n-cluster model [76] postulating the aggregation of monomers into clusters. (ii) The Lattice Cluster model [78, 79, 80, 81] which accounts for the monomer structure and allows for a monomer to occupy more than one lattice site. (iii) The model of Painter *et al* [82] which distinguishes between monomer-monomer contacts due to intrachain contacts and those due to interchain ones. All of these models lead to $\chi_{eff}(\phi)$ (chapter 3).

In chapter 4 we discussed the macroscopic consequences of $\chi_{eff}(\phi)$ for polymer systems with *uniform* concentration. Namely, we focused on the relationship between $\overline{\chi}(T, \phi)$, a macroscopic property, and the microscopic swelling and collapse

behavior of coils and brushes in the Flory and the Alexander approximation. (i) The $\chi_{eff}(\phi)$ results in the shift in the crossover between ideal chain and self-avoidance statistics, g_B; and (ii) it allows for a first-order collapse transition for flexible isolated chains when $\overline{\chi}(\phi)$ increases with ϕ.

Increasing $\overline{\chi}(\phi)$ can induce a vertical phase separation in a brush, which attributes to the second type of phase separation in a polymer solution involving coexistence of two phases of finite concentration. The vertical phase separation was studied in chapter 5 within the SCF theory. We showed that the experimentally accessible average thickness vs. grafting area dependence exhibits a minimum due to partitioning of monomers between the coexisting phases. This feature is a useful criterion for the occurrence of the vertical phase separation. We investigated the concentration profiles, the distribution functions of free ends and the compression force profiles associated with the vertical phase separation.

This approach was subsequently invoked in the interpretation of the indirect experimental indications that brushes of PNIPAM exhibit this effect (chapter 6). It allowed to indicate the range of grafting densities, molecular weights and temperatures where the vertical phase separation can be observed.

Appendix A

Polymer Brush within the Pincus Approximation

The SCF theory allows for a basis for a rigorous analysis of the coupling of $\chi_{eff}(\phi)$ and $\phi(z)$. However, it is possible to obtain correct concentration profiles within a simpler scheme proposed by Pincus [116, 122]. Within the Pincus approximation the free energy per unit area of the brush is $\gamma = a^{-3}\int_0^H f_{brush}dz$, where f_{brush} is the corresponding free energy density per kT

$$f_{brush} = f_\infty + \frac{z^2}{Na^2}\Psi(z) - \lambda\phi(z) \tag{A.1}$$

The second term allows for the elastic free energy of the chains. A chain having an end at the height z is assumed to be uniformly stretched and is thus allocated an elastic penalty of $F_{el}/kT \approx z^2/Na^2$. The chains' ends are assumed to be distributed throughout the layer with a volume fraction $\Psi(z)$. The core of the Pincus approximation is the assumption that the local concentration of ends scales as the fraction of ends within the chain, $1/N$, that is

$$\Psi(z) = \frac{\phi(z)}{N} \tag{A.2}$$

As opposed to the SCF theory, $\Psi(z)$ is assumed and not derived. Finally, λ is a Lagrange parameter fixing the number of monomers per chain, N. While $\Psi(z)$ is

wrong for small heights the approximation yield the correct $\phi(z)$ because $F_{el} \approx z^2$ and the large z contribution, where the assumed $\Psi(z)$ is reasonable, dominates.

The equilibrium concentration profile $\phi(z)$ is specified by the condition $\delta\gamma/\delta\phi = 0$. Since f_{brush} does not depend on $d\phi/dz$ the equilibrium condition is $\delta\gamma/\delta\phi = \partial f_{brush}/\partial\phi = 0$ or

$$\mu(\phi) = \lambda - Bz^2 \tag{A.3}$$

Here $\mu = \partial f_\infty/\partial\phi$ is the exchange chemical potential as obtained from (5.2)[1]

$$\mu(\phi) = -\ln(1-\phi) - 1 + \chi_{eff}(\phi)\,(1-\phi) - \phi\overline{\chi}(\phi) \tag{A.4}$$

In the following we utilize $B = 3\pi^2/8N^2a^2$, as obtained from the SCF theory (chapter 5.3), rather than the value obtained from the Pincus model. Upon making this substitution, equation (A.3) is *identical* to the one obtained from the rigorous SCF theory, eq. (5.10). We impose the condition $\phi_H \equiv \phi(H) = 0$. This condition is sufficient for the discussion f the deviations from the parabolic profile and and a vertical phase separation within a brush due to a "second type" of phase separation involving coexistence of two phases of finite concentration. In the general case, the condition $\phi_H = 0$ is replaced by $\pi_\infty(\phi_H) = 0$, thus allowing for a fully collapsed brush where $\phi_H > 0$. Since in our case $\phi_H = 0$, equation (A.3) specifies λ

$$\lambda = BH^2 + \mu(0) \tag{A.5}$$

thus enabling us to rewrite (A.3) in the form identical to eq. (5.15)

$$\Delta\mu(\phi) = B(H^2 - z^2) \tag{A.6}$$

where $\Delta\mu(\phi) \equiv \mu(\phi) - \mu(0)$ or $\Delta\mu(\phi) = \mu(\phi) + 1 - \chi_{eff}(0)$. Equation (A.6) determines the height H of the brush for a given $\phi(z=0) \equiv \phi_0$

$$H = \sqrt{\Delta\mu(\phi_0)/B} \tag{A.7}$$

[1] This expression coincide with eq. (5.11) within the SCF theory.

and the concentration profile in the form (identical to (5.17))

$$z(\phi) = \sqrt{\frac{\Delta\mu(\phi_0) - \Delta\mu(\phi)}{B}} \tag{A.8}$$

The grafting density corresponding to ϕ_0 is then specified by the constraint

$$\frac{Na^3}{\sigma} = \int_0^H \phi(z)dz \tag{A.9}$$

This set of equations allows to examine the deviations from the parabolic profile due to $\chi_{eff}(\phi)$. It can also be used to study the vertical phase separation in a brush with $\chi_{eff}(\phi)$.

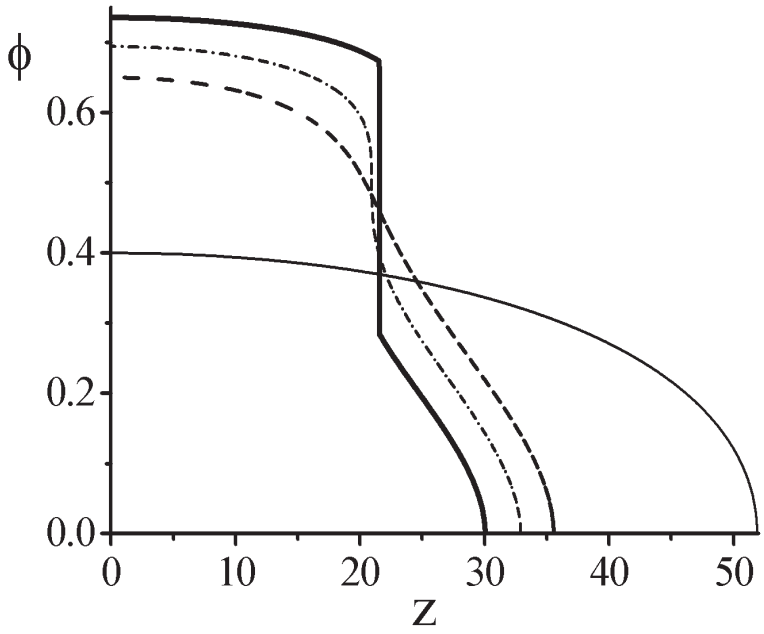

Figure A.1: *ϕ vs. z plots, for brushes with $N = 300$, $\sigma/a^2 = 18$ ($\sigma/R_F^2 = 0.019$) subject to interactions described by $\overline{\chi}(\phi) = 1/2$ (thin line), $\overline{\chi}(\phi) = 1/2 + 0.95\phi^2$ (dashes), $\overline{\chi}(\phi) = 1/2 + 1.00\phi^2$ (dash-dots), $\overline{\chi}(\phi) = 1/2 + 1.05\phi^2$ (thick line).*

For example, we can illustrate the vertical phase separation for the hypothetical case considered in chapters 4 and 5, that is of $\overline{\chi}(\phi) = 1/2 + \overline{\chi}_2\phi^2$. In this case the critical point is specified by $\overline{\chi}_{2c} = 1$ and $\phi_c = 1/2$ so that phase separation occurs

when $\overline{\chi}_2 \geqslant \overline{\chi}_{2c}$ and $\phi > \phi_c$. Representative $\phi(z)$ curves for $\overline{\chi}(\phi)$: $\overline{\chi}(\phi) = 1/2$, $\overline{\chi}(\phi) = 1/2 + 0.95\phi^2$, $\overline{\chi}(\phi) = 1/2 + \phi^2$ and $\overline{\chi}(\phi) = 1/2 + 1.05\phi^2$ are depicted in Figure A.1.

Appendix B

SCF Calculation of Equilibrium Properties of a Polymer Brush

B.1 Calculation of the Average Thickness, $\langle z \rangle$

For a $\phi(z)$ (5.25) is evaluated using integration by parts utilizing $d\Delta\mu = -2Bzdz$:

$$\langle z \rangle = \frac{\sigma}{Na^3}\frac{1}{2B}\int_0^{BH^2}\phi(z)d\Delta\mu = \frac{\sigma}{Na^3}\left(H^2\frac{\phi_0}{2} - \frac{1}{2B}\int_{\phi_H}^{\phi_0}\Delta\mu(\phi)d\phi\right), \tag{B.1}$$

For a discontinuous $\phi(z)$ (5.25) this procedure leads to

$$\begin{aligned}
\langle z \rangle &= \frac{\sigma}{Na^3}\int_0^{H_t} z\phi_+(z)dz + \frac{\sigma}{Na^3}\int_{H_t}^{H} z\phi_-(z)dz \\
&= \frac{\sigma}{Na^3}\left(\frac{1}{2B}\int_{B(H^2-H_t^2)}^{BH^2}\phi_+(z)d\Delta\mu + \frac{1}{2B}\int_0^{B(H^2-H_t^2)}\phi_-(z)d\Delta\mu\right) \\
&= \frac{\sigma}{Na^3}\left(H^2\frac{\phi_0}{2} - \left(H^2 - H_t^2\right)\frac{\phi_+(H_t)-\phi_-(H_t)}{2}\right. \\
&\quad \left. -\frac{1}{2B}\int_{\phi_+(H_t)}^{\phi_0}\Delta\mu(\phi)d\phi - \frac{1}{2B}\int_{\phi_H}^{\phi_-(H_t)}\Delta\mu(\phi)d\phi\right).
\end{aligned} \tag{B.2}$$

Appendix B

The evaluation of (5.26) in the case of a continuous $\phi(z)$ involves introducing the variable $\Delta\mu = B(H^2 - z^2)$,invoking $z = \sqrt{H^2 - \Delta\mu/B}$. Integration by parts leads to

$$\begin{aligned}\langle z^2\rangle &= \frac{\sigma}{Na^3}\frac{1}{2B}\int_0^{BH^2} z\phi(z)d\Delta\mu = -\frac{\sigma}{Na^3}\frac{1}{2B}\int_{\Delta\mu=0}^{\Delta\mu=BH^2}\Delta\mu d(z\phi(z)) \\ &= -\frac{\sigma}{Na^3}\frac{1}{2B}\int_{\phi_H}^{\phi_0}\left(\phi\frac{\partial z}{\partial\phi}+z\right)\Delta\mu d\phi, \end{aligned} \tag{B.3}$$

where the relationship $z = \sqrt{H^2 - \Delta\mu/B}$ was used.

Using

$$\frac{\partial z}{\partial\phi} = -\frac{1}{B\sqrt{H^2-\Delta\mu/B}}\frac{\partial\Delta\mu}{\partial\phi} \tag{B.4}$$

we obtain the final expression

$$\langle z^2\rangle = \frac{\sigma}{Na^3}\frac{1}{2B^2}\int_0^{\phi_0}\frac{\phi\Delta\mu\frac{\partial\Delta\mu}{\partial\phi}}{\sqrt{H^2-\Delta\mu/B}}d\phi - \frac{1}{2B}\int_0^{\phi_0}\Delta\mu\sqrt{H^2-\Delta\mu/B}d\phi, \tag{B.5}$$

where $\Delta\mu$ is specified by (5.16).

Following a similar procedure for a discontinuous $\phi(z)$ (5.26) yields

$$\begin{aligned}\langle z^2\rangle &= \frac{\sigma}{Na^3}\int_0^{H_t} z^2\phi_+(z)dz + \frac{\sigma}{Na^3}\int_{H_t}^{H} z^2\phi_-(z)dz \\ &= \frac{\sigma}{Na^3}\left(\frac{1}{2B}\int_{B(H^2-H_t^2)}^{BH^2} z\phi_+(z)d\Delta\mu + \frac{1}{2B}\int_0^{B(H^2-H_t^2)} z\phi_-(z)d\Delta\mu\right) \\ &= \frac{\sigma}{Na^3}\left[\frac{1}{2B^2}\int_{\phi_+(H_t)}^{\phi_0}\frac{\phi\Delta\mu\frac{\partial\Delta\mu}{\partial\phi}}{\sqrt{H^2-\Delta\mu/B}}d\phi - \frac{1}{2B}\int_{\phi_+(H_t)}^{\phi_0}\Delta\mu\sqrt{H^2-\Delta\mu/B}d\phi\right. \\ &\quad + \frac{1}{2B^2}\int_0^{\phi_-(H_t)}\frac{\phi\Delta\mu\frac{\partial\Delta\mu}{\partial\phi}}{\sqrt{H^2-\Delta\mu/B}}d\phi - \frac{1}{2B}\int_0^{\phi_-(H_t)}\Delta\mu\sqrt{H^2-\Delta\mu/B}d\phi \\ &\quad \left. -H_t\left(H^2-H_t^2\right)\frac{\phi_+(H_t)-\phi_-(H_t)}{2}\right] \end{aligned} \tag{B.6}$$

B.2 Calculation of the Distribution Function of Free Ends

Upon introducing the variables $\rho = H^2 - z^2$, $t = H^2 - z'^2$ and $g(z')dz' = -f(t)dt$ eq. (5.6) assumes the form of an Abel integral equation

$$v(\rho) = \int_0^\rho \frac{f(t)dt}{\sqrt{\rho - t}}, \tag{B.7}$$

where $v(\rho) = \frac{\pi\sigma}{2Na^3}\phi(z)$ whose solution (B.7) is

$$f(\rho) = \frac{1}{\pi}\left(\frac{v(0)}{\sqrt{\rho}} + \int_0^\rho \frac{1}{\sqrt{\rho - t}}\frac{dv(t)}{dt}dt\right). \tag{B.8}$$

It is convenient to rewrite the integral in (B.8) as

$$\int_0^\rho \frac{1}{\sqrt{\rho - t}}\frac{dv(t)}{dt}dt = \int_{v(H)}^{v(z)} \frac{dv}{\sqrt{\rho - t(v)}} = \frac{\pi\sigma}{2Na^3}\sqrt{B}\int_{\phi_H}^{\phi} \frac{d\phi'}{\sqrt{\Delta\mu(\phi) - \Delta\mu(\phi')}} \tag{B.9}$$

where $\Delta\mu(\phi)$ is given by (5.15).

Substituting this integral into (B.8) while noting that $v(0) = \frac{\pi\sigma}{2Na^3}\phi_H$ and $g(z) = 2zf(\rho)$, leads to $g(z)$ in the form (5.27). This equation yields a simple form $z(\phi)$ rather than for $\phi(z)$. Thus, it is naturally to consider $g(z)$ as a parametric function

The structure of this equation allows to express in a simple form $z(\phi)$ rather than $\phi(z)$. Thus, it is naturally to consider $g(z)$ as a parametric function

$$\begin{aligned} g(\phi) &= \frac{\sigma}{Na^3}\sqrt{H^2 - \Delta\mu(\phi)/B}\left(\frac{\phi_H}{\sqrt{\Delta\mu(\phi)/B}} + \right. \\ &\quad \left. \sqrt{B}\int_{\phi_H}^{\phi} \frac{d\phi'}{\sqrt{\Delta\mu(\phi) - \Delta\mu(\phi')}}\right) \end{aligned} \tag{B.10}$$

$$z(\phi) = \sqrt{\frac{\Delta\mu(\phi_0) - \Delta\mu(\phi)}{B}} \tag{B.11}$$

These two equations are augmented by (5.18) relating σ to ϕ_0.

Appendix B

In the case of discontinuous $\phi(z)$ it is necessary to obtain $g(z)$ in the outer and inner phases separately. For the outer phase the introduction of the variables $\rho = H^2 - z^2$, $t = H^2 - z'^2$ and $g_-(z')dz' = -f_-(t)dt$ transforms (5.28) into an Abel integral equation (B.7) whose solution is (5.30).

To obtain $g_+(z)$ at the inner phase we substitute (5.30) into (5.29) and transform the first term of (5.29) into an Abel integral (B.7) by introducing the variables $\rho' = H_t^2 - z^2$, $t' = H_t^2 - z'^2$ and $g_+(z')dz' = -f_+(t)dt$. This leads to

$$\frac{\pi\sigma}{2Na^3}\phi_+(z) - \int_0^{H^2-H_t^2} \frac{f_-(t)dt}{\sqrt{\rho - t}} = \int_0^{\rho'} \frac{f_+(t')dt'}{\sqrt{\rho' - t'}} \tag{B.12}$$

where $f_-(t') = g_-(z')/2z'$, and $\rho = \rho' + H^2 - H_t^2$. Thus, $v(\rho')$ in the solution of the Abel equation (B.7) is

Thus, the function $v(\rho')$ in the solution of the Abel equation (B.7) is written as

$$v(\rho') = \frac{\pi\sigma}{2Na^3}\phi_+(z) - \int_0^{H^2-H_t^2} \frac{f_-(t)dt}{\sqrt{\rho - t}} \tag{B.13}$$

and its value at $\rho' = 0$ is

$$v(0) = \frac{\pi\sigma}{2Na^3}\phi_+(H_t) - \int_0^{H^2-H_t^2} \frac{f_-(t)dt}{\sqrt{H^2 - H_t^2 - t}} = \frac{\pi\sigma}{2Na^3}\left[\phi_+(H_t) - \phi_-(H_t)\right], \tag{B.14}$$

where eq. (B.7) with $\rho = H^2 - H_t^2$ was used in order to calculate the second term in (B.14). In addition

$$\frac{dv(\rho')}{d\rho'} = \frac{\pi\sigma}{2Na^3}\frac{d\phi_+(z)}{d\rho'} + \frac{1}{2}\int_0^{H^2-H_t^2} \frac{f_-(t)dt}{\left(H^2 - H_t^2 + t' - t\right)^{3/2}} \tag{B.15}$$

All together, upon substituting (B.13), (B.14) and (B.15) into (B.8) we obtain

$$\begin{aligned} f_+(\rho') \;=\; & \frac{\sigma}{2Na^3}\left[\frac{\phi_+(H_t) - \phi_-(H_t)}{\sqrt{H_t^2 - z^2}} + \int_0^{\rho'} \frac{1}{\sqrt{\rho' - t'}}\frac{d\phi_+(z')}{dt'}dt'\right] + \\ & \frac{1}{2\pi}\int_0^{\rho'} \frac{dt'}{\sqrt{\rho' - t'}} \int_0^{H^2-H_t^2} \frac{f_-(t)dt}{\left(H^2 - H_t^2 + t' - t\right)^{3/2}} \end{aligned} \tag{B.16}$$

Changing the variables and expressing ρ' and t' via chemical potential (5.15) in the first integral and changing the order of integration in the second integral one obtains

$$\begin{aligned} f_+(\rho') &= \frac{\sigma}{2Na^3}\left[\frac{\phi_+(H_t)-\phi_-(H_t)}{\sqrt{H_t^2-z^2}}+\sqrt{B}\int_{\phi_+(H_t)}^{\phi_+}\frac{d\phi'_+}{\sqrt{\Delta\mu(\phi_+)-\Delta\mu(\phi'_+)}}\right]+ \\ &\frac{1}{2\pi}\int_0^{H^2-H_t^2} f_-(t)dt\int_0^{\rho'}\frac{dt'}{\sqrt{\rho'-t'}\left(H^2-H_t^2+t'-t\right)^{3/2}} \end{aligned} \tag{B.17}$$

The inner integral in (B.17) is

$$\int_0^{\rho'}\frac{dt'}{\sqrt{\rho'-t'}\left(H^2-H_t^2+t'-t\right)^{3/2}}=\frac{2\sqrt{\rho'}}{\left(\rho'+H^2-H_t^2-t\right)\sqrt{H^2-H_t^2-t}} \tag{B.18}$$

leading to

$$\begin{aligned} f_+(\rho') &= \frac{\sigma}{2Na^3}\left[\frac{\phi_+(H_t)-\phi_-(H_t)}{\sqrt{H_t^2-z^2}}+\sqrt{B}\int_{\phi_+(H_t)}^{\phi_+}\frac{d\phi'_+}{\sqrt{\Delta\mu(\phi_+)-\Delta\mu(\phi'_+)}}\right]+ \\ &\frac{\sqrt{\rho'}}{\pi}\int_0^{H^2-H_t^2}\frac{f_-(t)dt}{\left(\rho'+H^2-H_t^2-t\right)\sqrt{H^2-H_t^2-t}} \end{aligned} \tag{B.19}$$

Substitution of $f_-(t)=g_-(z)/2z$ from (5.30) yields the final expression for $g_+(z)$ in the form

$$\begin{aligned} g_+(z) &= \frac{z\sigma}{Na^3}\left[\frac{\phi_+(H_t)-\phi_-(H_t)}{\sqrt{H_t^2-z^2}}+\frac{\phi_H}{\sqrt{H^2-z^2}}+\right. \\ &\sqrt{B}\int_{\phi_+(H_t)}^{\phi_+}\frac{d\phi'_+}{\sqrt{\Delta\mu(\phi_+)-\Delta\mu(\phi'_+)}}+ \\ &\frac{\sqrt{B}}{\pi}\sqrt{H_t^2-z^2}\int_0^{H^2-H_t^2}\frac{dt}{\left(H^2-z^2-t\right)\sqrt{H^2-H_t^2-t}}\times \\ &\left.\int_{\phi_H}^{\phi'_-(t)}\frac{d\phi''_-}{\sqrt{\Delta\mu(\phi'_-)-\Delta\mu(\phi''_-)}}\right] \end{aligned} \tag{B.20}$$

It is convenient to express $g_+(z)$ in terms of the concentration of the dense phase, ϕ_+ utilizing $z(\phi_+) = \sqrt{H^2 - \Delta\mu(\phi_+)/B}$. Introducing the variables $t = \Delta\mu(\phi'_-)/B$ and $dt = 1/B(d\Delta\mu(\phi'_-)/d\phi'_-)d\phi'_-$ in the last integral leads to (5.31).

Index

Bibliography

[1] P. Molyneux, *Water. A comprehensive treatise, Editor F. Franks*, vol. 4 (Plenum Press, New York, 1975). 3, 5, 9, 10, 58, 63, 71, 100

[2] P. Molyneux, *Water Soluble Syntetic Polymers: Properties and Uses*, vol. 1 (CRC Press, Boca Raton, Florida, 1983). 3, 9, 26, 27, 28, 29, 29, 71

[3] M.-J. Chang, A. S. Myerson, and T. K. Kwei, J. Appl. Polym. Sci. **66**, 279 (1997). 3, 9

[4] Y. Maeda, T. Nakamura, and I. Ikeda, Macromolecules **34**, 1391 (2001). 3, 9

[5] Y. Maeda, T. Nakamura, and I. Ikeda, Macromolecules **35**, 217 (2002). 3, 9

[6] A. Mitsutake and Y. Okamoto, J. Chem. Phys. **112**, 10638 (2000). 3, 9

[7] G. D. Smith, D. Bedrov, and O. Borodin, J. Am. Chem. Soc. **122**, 9548 (2000). 3, 9

[8] D. Bedrov and G. D. Smith, J. Phys. Chem. B **103**, 3791 (1999). 3, 9

[9] G. D. Smith and D. Bedrov, J. Phys. Chem. A **105**, 1283 (2001). 3, 9

[10] D. Bedrov, M. Pekny, and G. D. Smith, J. Phys. Chem. B **102**, 996 (1998). 3, 9

[11] S. Saeki, N. Nakata, and M. Kaneko, Polymer **17**, 685 (1976). 3, 9

[12] P. Flory, *Principles of Polymer Chemistry* (Cornell Univercity, Itaca, NY, London, 1953). 3, 4, 5, 9, 10, 10, 61, 62, 71, 71, 71

[13] P.-G. de Gennes, *Scaling Concepts in Polymer Physics* (Cornell University Press, Ithaca and London, 1985), 2nd ed. 3, 4, 9, 10, 28, 71, 71, 78, 80

[14] M. Doi, *Introduction to Polymer Physics* (Clarendon Press, Oxford, 1996). 3, 4, 9, 10, 28, 71

[15] H. Yamakawa, *Modern Theory of Polymer Solutions* (Harper and Row, New York, 1971). 3, 9, 28

[16] A. Y. Grosberg and A. R. Khokhlov, *Statistical Physics of Macromolecules* (AIP Press, New York, 1994). 3, 4, 9, 10, 28, 71, 77

[17] J. Hirschfelder, D. Stevenson, and H. Eyring, J. Chem Phys. **5**, 896 (1937). 4, 10

[18] R. Goldstein, J. Chem. Phys. **80**, 5340 (1984). 4, 10, 34

[19] P. H. Poole, F. Sciortino, T. Grande, H. E. Stanley, and C. A. Angell, Phys. Rev. Lett. **73**, 1632 (1994). 4, 10, 41

[20] G. Andersen and J. Wheeler, J. Chem. Phys. **69**, 3403 (1978). 4, 10

[21] G. Karlstrom, J. Phys. Chem. **89**, 4962 (1985). 4, 10, 33, 33, 34, 34, 34, 37, 41, 45, 46, 87, 88, 113, 113, 125, 127

[22] A. Matsuyama and F. Tanaka, Phys. Rev. Lett. **65**, 341 (1990). 4, 10, 88, 125, 127

[23] S. Bekiranov, R. Bruinsma, and P. Pincus, Phys. Rev. E **55**, 577 (1997). 4, 10, 33, 33, 34, 34, 34, 38, 41, 41, 49, 88, 125, 127

[24] E. Dormidontova, Macromolecules **35**, 987 (2002). 4, 10, 34, 34, 34, 42, 56, 58, 125, 127

[25] N. Schuld and B. Wolf, *Polymer Handbook* (Wiley, New York, 1999), 4th ed. 5, 5, 10, 11, 35, 35, 43, 61, 62, 71, 71, 72, 73, 79, 99

[26] M. Huggins, *Physical Chemistry of High Polymers* (John Willey and Sons, London, 1958). 5, 10, 66, 71

[27] P. J. Flory, Disc. Faraday Soc. **49**, 7 (1970). 5, 10, 71, 73

[28] R. M. Masegosa, M. G. Prolongo, and A. Horta, Macromolecules **19**, 1478 (1986). 5, 10, 71, 71, 72, 73

[29] H.-M. Petri, N. Schuld, and B. Wolf, Macromoleules **28**, 4975 (1995). 5, 10, 35, 35, 71

[30] I. C. Sanchez, Polymer **30**, 471 (1989). 5, 10

[31] G. N. Malcolm and J. S. Rowlinson, Trans. Faraday Soc. **53**, 921 (1957). 5, 11, 51, 58, 63

[32] M. C. Stuart, Ph.D. thesis, Wageningen University (1980). 5, 11, 35, 36, 58

[33] T. Narayanan and A. Kumar, *Physics Reports* (1994), vol. 249, chap. Reentrant phase transitions in multicomponent liquid mixtures, pp. 135–218. 5, 9, 11

[34] V. A. Baulin and A. Halperin, Macromolecules **35**, 6432 (2002). 6, 11, 70, 113

[35] T. Baltes, F. Garret-Flaudy, and R. Freitag, J. Polym. Sci. A: Polym. Chem. **37**, 2977 (1999). 9, 30

[36] F. Afroze, E. Nies, and H. Berghmans, J. Molecular Structure **554**, 55 (2000). 9, 30, 31, 119, 119, 119, 122, 123

[37] R. Ludwig, Angew. Chem. Int. Ed. **40**, 1808 (2001). 13, 22, 22, 24, 25, 26

[38] F. H. Stillinger, Science **209**, 451 (1980). 13, 13, 17, 22, 22, 23, 23, 24

[39] D. Eisenberg and W. Kauzmann, *The Structure and Properties of Water* (Calerdon Press, Oxford, 1969). 14, 14, 17, 24, 25, 25, 25

[40] G. C. Pimentel and A. L. McClellan, *The Hydrogen Bond* (W. H. Freeman and Co., San Francisco and London, 1960). 14, 15, 18, 19, 19, 19, 20, 20, 21

[41] C. A. Coulson, *Valence* (Clarendon press, Oxford, 1961), 2nd ed. 14

[42] P. Schuster, G. Zundel, and C. Sandorfy, *The Hydrogen Bond. Recent developments in theory and experiments*, vol. I (North-Holand Pub. Co., Amsterdam and New York and Oxford, 1976). 17

[43] A. Rahman and F. H. Stillinger, J. Am. Chem. Soc. **95**, 7943 (1973). 22, 23, 23, 23, 23, 25

[44] A. Karpfen, *Advances in Chemical Physics* (Wiley, 2002), vol. 123, chap. Cooperative Effects in Hydrogen Bonding, pp. 469–511. 22

[45] F. H. Stillinger and A. Rahman, J. Chem. Phys. **60**, 1545 (1974). 23, 24

[46] A. Geiger, F. H. Stillinger, and A. Rahman, J. Chem. Phys. **70**, 4185 (1979). 23, 23, 25

[47] A. Rahman and F. H. Stillinger, J. Chem. Phys. **55**, 3336 (1971). 24, 25

[48] H. E. Stanley and J. Teixeira, J. Chem. Phys. **73**, 3404 (1980). 25

[49] R. Ludwig, Phys. Chem. Chem. Phys. **4**, 5481 (2002). 25

[50] H. Kabrede and R. Hentschke, J. Phys. Chem. B **107**, 3914 (2003). 25

[51] S. S. Borick, P. G. Debenedetti, and S. Sastry, J. Phys. Chem. **99**, 3781 (1995). 25

[52] M. Heskins and J. E. Gillet, J. Macromol. Sci. Chem. **A2**, 1441 (1968). 30, 30, 31, 119

[53] L.-T. Lee and C. Bernard, Macromolecules **30**, 6559 (1997). 30, 30, 30

[54] G. Bokias, D. Hourdet, I. Iliopoulos, G. Staikos, and R. Audebert, Macromolecules **30**, 8293 (1997). 30

[55] P. Bruscolini, C. Buzano, A. Pelizzola, and M. Pretti, Phys. Rev. E **64**, 050801R (2001). 30

[56] S. Balamurugan, S. Mendez, S. S. Balamurugan, M. J. OBrienII, and G. P. Lopez, Langmuir **19**, 2545 (2003). 30, 118

[57] E. Kato, J. Chem. Phys. **106**, 3792 (1997). 30

[58] A. Larsson, D. Kuckling, and M. Schonhoff, Colloids and Surfaces A: Physicochemical and Engineering Aspects **190**, 185 (2001). 30

[59] Y. Murase, T. Onda, K. Tsujii, and T. Tanaka, Macromolecules **32**, 8589 (1999). 30

[60] K. S. Oh, J. S. Oh, H. S. Choi, and Y. C. Bae, Macromolecules **31**, 7328 (1998). 30

[61] A. Percot, X. X. Zhu, and M. Lafleur, J. Polym. Sci. B: Polym. Phys. **38**, 907 (2000). 30

[62] Y. Suetoh and M. Shibayama, Polymer **41**, 505 (2000). 30

[63] Z. Tong, F. Zeng, X. Zheng, and T. Sato, Macromolecules **32**, 4488 (1999). 30

[64] C. Wu and S. Zhou, Macromolecules **28**, 8381 (1995). 30, 30

[65] X. Wang, X. Qiu, and C. Wu, Macromolecules **31**, 2972 (1998). 30, 30

[66] L. Yan, Q. Zhu, and P. U. Kenkare, J. Appl. Polym. Sci. **78**, 1971 (2000). 30

[67] C. Wu and S. Zhou, Phys. Rev. Lett. **80**, 4092 (1998). 30, 30

[68] X. Wang, X. Qiu, and C. Wu, Macromolecules **31**, 2972 (1998). 30, 30

[69] Y. Yang, F. Zeng, Z. Tong, X. Liu, and S. Wu, J. Polym. Sci. B: Polym. Phys. **39**, 901 (2001). 30

[70] E. Dormidontova, A. Grosberg, and A. Khokhlov, Vysok. Mol. Soed. Ser. A **34**, 126 (1992). 33, 33, 88

[71] A. Matsuyama and F. Tanaka, Phys. Rev. Lett. **65**, 341 (1990). 34, 34, 34, 41

[72] B. A. Veytsman, J. Phys. Chem. **94**, 8499 (1990). 34, 38, 53, 54, 54, 88, 125, 127

[73] N. Schuld and B. A. Wolf, J. Pol. Sci.: Part B: Polymer Physics **39**, 651 (2001). 35, 61, 71

[74] B. A. Wolf, private communication. 36, 57

[75] S. Saeki, N. Kuwahara, M. Nakata, and M. Kaneko, Polymer **17**, 685 (1976). 45

[76] P.-G. de Gennes, CR Acad. Sci, II (Paris) **1117**, 313 (1991). 61, 63, 71, 73, 73, 74, 88, 95, 125, 127

[77] P.-G. de Gennes, *Simple Views on Condensed Matter* (World Scientific, Singapore, 1992). 61, 63, 71, 73, 73, 74, 88, 95

[78] K. W. Foreman and K. F. Freed, Adv. Chem. Phys. **103**, 335 (1998). 61, 62, 64, 70, 125, 127

[79] W. Li, K. F. Freed, and A. M. Nemirovsky, J. Chem. Phys. **98**, 8469 (1993). 61, 62, 64, 70, 125, 127

[80] K. F. Freed and J. Dudowicz, Macromolecules **31**, 6681 (1998). 61, 64, 125, 127

[81] J. Dudowicz, K. F. Freed, and J. F. Douglas, Phys. Rev. Lett. **88**, 095503 (2002). 61, 64, 125, 127

[82] P. Painter, L. Berg, B. Veytsman, and M. Coleman, Macromolecules **30**, 7529 (1997). 61, 62, 65, 70, 125, 127

[83] I. Noda, Y. Higo, N. Ueno, and T. Fujimoto, Macromolecules **17**, 1055 (1984). 61, 62

[84] I. C. Sanchez and R. H. Lacomb, Macromolecules **11**, 1145 (1978). 62

[85] I. C. Sanchez and A. C. Balazs, Macromolecules **22**, 2325 (1989). 62

[86] L. P. MacMaster, Macromolecules **6**, 760 (1973). 62

[87] V. Brandani, Macromolecules **12**, 883 (1979). 62

[88] W. P. Polik and W. Burchard, Macromolecules **16**, 978 (1983). 63

[89] K. Devanand and J. C. Selser, Nature **343**, 739 (1990). 64

[90] D. Boils and M. L. Hair, J. Colloid Interface Sci. **157**, 19 (1993). 64

[91] O. V. Borisov and A. Halperin, Macromolecules **32**, 5097 (1999). 64, 70

[92] C. Qian, S. J. Mumby, and B. E. Eichinger, Macromolecules **24**, 1655 (1991). 71, 73

[93] K. Šolc and R. Koningsveld, J. Phys. Chem. **96**, 4056 (1992). 71, 73, 88, 95

[94] H. Schäfer-Soenen, R. Moerkerke, H. Berghmans, R. Koningsveld, K. Dusek, and K. Solc, Macromolecules **30**, 410 (1997). 71, 73, 88, 95

[95] B. Erman and P. J. Flory, Macromolecules **19**, 2342 (1986). 71, 71, 78, 81

[96] S. Bekiranov, R. Bruinsma, and P. Pincus, Europhys. Lett. **24**, 183 (1993). 71

[97] C. Jeppesen and K. Kremer, Europhys. Lett. **34**, 563 (1996). 71

[98] C. Williams, F. Brochard, and H. L. Frisch, Ann. Rev. Phys. Chem. **32**, 433 (1981). 71, 77, 81

[99] P.-G. de Gennes, J. Phys. Lett. (Paris) **39**, 1978 (1978). 71, 77, 81

[100] S. Alexander, Journal de Physique (France) **38**, 983 (1977). 72

[101] A. Halperin, M. Tirrell, and T. P. Lodge, Adv. Polym. Sci. **100**, 31 (1992). 72

[102] T. M. Birshtein and V. A. Pryamitsyn, Macromolecules **24**, 1554 (1991). 77

[103] V. A. Baulin and A. Halperin, Macromol. Theor. and Simul. **12**, 549 (2003). 79, 79, 88, 89, 103, 119

[104] I. M. Lifshits and A. Y. Grosberg, Sov. Phys. JETP **38**, 1198 (1974). 82

[105] I. M. Lifshits, A. Y. Grosberg, and A. R. Khokhlov, Rev. Mod. Phys. **50**, 683 (1978). 82

[106] S. T. Milner, Science **251**, 905 (1991). 83, 91

[107] E. B. Zhulina, O. V. Borisov, V. A. Pryamitsyn, and T. M. Birshtein, Macromolecules **24**, 140 (1991). 83, 91, 91, 93, 93, 104

[108] V. A. Baulin, E. B. Zhulina, and A. Halperin, J. Chem Phys. **119**, 10977 (2003). 83, 115

[109] M. Wagner, F. Brochard-Wyart, H. Hervet, and P.-G. de Gennes, Colloid Polym. Sci. **271**, 621 (1993). 88, 89, 95, 97

[110] P. Linse, Macromolecules **27**, 6404 (1994). 89

[111] M. Björling, Macrmolecules **25**, 3956 (1992). 89

[112] M. Svensson, P. Alexandritis, and P. Linse, Macromolecules **32**, 637 (1999). 89

[113] W. L. Mattice, S. Misra, and D. Napper, Europhys. Lett. **28**, 603 (1994). 89

[114] P. W. Zhu and D. H. Napper, J. Colloid Interface Sci. **164**, 489 (1994). 90, 118

[115] P. W. Zhu and D. H. Napper, Colloids Surfaces A **113**, 145 (1996). 90, 118

[116] A. Halperin, Eur. Phys. J. B **3**, 359 (1998). 90, 95, 100, 129

[117] E. M. Sevick, Macromolecules **31**, 3361 (1998). 90

[118] A. N. Semenov, Sov. Phys. JETP **61**, 733 (1985), translation of Z. Eksp. Teor. Fiz. 88, 1242 (1985). 91, 91, 92

[119] S. T. Milner, T. A. Witten, and M. E. Cates, Europhys. Lett. **5**, 413 (1988). 91, 93, 93

[120] A. M. Skvortsov, A. A. Gorbunov, V. A. Pavlushkov, E. B. Zhulina, O. V. Borisov, and V. A. Priamitsyn, Polymer Science USSR **30**, 1706 (1988). 91, 91, 104

[121] J. S. Hager, M. A. Anisimov, J. V. Sengers, and G. E. Gorodestskii, J. Chem. Phys. **117**, 5940 (2002). 99

[122] P. Pincus, Macromolecules **24**, 2912 (1991). 100, 103, 129

[123] J. C. Charmet and P.-G. de Gennes, J. Opt. Soc. Am. **73**, 1977 (1983). 101

[124] S. Safran, *Statistical Thermodynamics of Surfaces and Interfaces* (Addison-Wesley, New York, 1994). 103

[125] H. Yim, M. S. Kent, D. L. Huber, S. Satija, J. Majewski, and G. S. Smith, Macromolecules **36**, 5244 (2003). 119

[126] H. Yim, M. S. Kent, S. Mendez, S. S. Balamurugan, S. Balamurugan, G. P. Lopez, and S. Satija, submitted. 120

[127] H. Yim, M. S. Kent, S. Mendez, S. S. Balamurugan, S. Balamurugan, G. P. Lopez, and S. Satija, in preparation. 120

[128] T. Hu, Y. You, C. Pan, and C. Wu, J. Phys. Chem. B **106**, 6659 (2002). 120, 120

[129] C. Wu, Polymer **39**, 4609 (1998). 121, 121

List of Publications

1. Vladimir A. Baulin, Ekaterina B. Zhulina, Avi Halperin, "*Self-consistent field theory of brushes of neutral water-soluble polymers*", J. Chem. Phys., **119**(20), 10977-10989 (2003).

2. Vladimir A. Baulin, "*Self-assembled Aggregates in the Gravitational Field: Growth and Nematic Order*", J. Chem. Phys., **119**(5), 2874-2890 (2003).

3. Vladimir A. Baulin and Avi Halperin "*Signatures of a concentration dependent Flory χ parameter: swelling and collapse of coils and brushes*", Macromolecular Theory and Simulations **12**(8), 549-559 (2003), cond-mat/0206458.

4. Vladimir A. Baulin and Avi Halperin, "*Concentration dependence of the Flory χ parameter within two-state models*", Macromolecules, **35**(16), 6432-6438 (2002).

5. Vladimir A. Baulin, Elena Yu. Kramarenko, Alexei R. Khokhlov "*Polymer – surfactant complexes: solubilization of polymeric globule by surfactants*", Computational and Theoretical Polymer Science, **10**, 165-175 (2000).

6. Vladimir A. Baulin, Alexei R. Khokhlov, "*Nematic ordering of rigid rods in a gravitational field*", Physical Review E **60**(3), 2973-2977 (1999).

Abstract

The origin and signatures of the concentration dependent Flory χ_{eff}-parameter for neutral water-soluble polymers are studied. The three versions of two-state model proposed previously to explain the phase behavior of Poly(ethylene oxide) in water lead to $\chi_{eff}(\phi)$. This dependence can serve as a useful diagnostic of the performance of models: it allows to distinguish between different models and test involving parameters. The emergence of $\chi_{eff}(\phi)$ from alternative single-state models is also discussed. The macroscopic signatures of $\chi_{eff}(\phi)$ are illustrated on the example of swelling of isolated coils and planar brushes. The ϕ dependence of χ_{eff} in systems with uniform concentration gives rise to two main consequences: a shift in the crossover between Gaussian and self-avoidance regimes, and a possibility of a first-order collapse transition for isolated flexible coils. $\chi_{eff}(\phi)$ can lead to a vertical phase separation in polymer brushes involving coexistence of two phases of finite concentration. This approach is applied to the interpretation of indirect evidence that Poly(N-isopropylacrylamide) brushes exhibit this effect.

Résumé

Ce travail est consacré à l'étude d'origine et signatures de la dépendance en concentration ϕ du paramètre de Flory χ_{eff} pour les polymères neutres solubles dans l'eau. Les trois versions du modèle à deux états qui ont été proposés pour expliquer le comportement de phase de Poly(oxyéthylène) dans l'eau mènent à $\chi_{eff}(\phi)$. Cette dépendance peut servir à tester la qualité des modèles: elle permet de distinguer entre les différents modèles et juger de la pertinence des paramètres impliqués. L'apparition de $\chi_{eff}(\phi)$ à partir des modèles alternatifs à un seul état est aussi discutée. Les signatures macroscopiques de $\chi_{eff}(\phi)$ sont illustrées avec l'exemple du gonflement des chaînes isolées et des brosses planes. La dépendance de χ_{eff} avec ϕ dans les systèmes à concentration uniforme a deux conséquences principales: entraînement du déplacement du croisement entre les régimes Gaussien et auto-évitant, et la possibilité d'une transition de phase du premier ordre pour les chaînes flexibles isolées. $\chi_{eff}(\phi)$ peut provoquer une séparation verticale de phase dans des brosses polymères qui implique la coexistence de deux phases de concentration finie. Cette approche est appliquée à l'interprétation d'un ensemble des résultats expérimentaux qui suggère que cet effet pourrait exister avec les brosses de Poly(N-isopropylacrylamide).

Thèse préparée au Département de Recherche Fondamentale sur la Matière Condensée
Laboratoire Structure et Propriétés des Architectures Moléculaires
UMR 5819 CNRS–UJF–CEA Grenoble
2003